DUT

DURBAN UNIVERSITY OF TECHNOLOGY
INYUVESI YASETHEKWINI YEZOBUCHWEPHESHE
CREATIVE. DISTINCTIVE. IMPACTFUL.

DESIGN AND APPLICATION OF PASSIVE FILTERS FOR IMPROVED POWER QUALITY IN STAND-ALONE PV SYSTEM

By
Sandile Dlamini
Student Number: 21434128

A dissertation submitted in fulfilment of the requirements for the award of the degree of Master of Engineering in Electrical Power Engineering

Department of Electrical Power Engineering, Faculty of Engineering and the Built Environment

Supervisor: Dr. A.A. Adebiyi
Co-Supervisor: Prof. M. Kabeya

2024

Declaration

I affirm that this dissertation is entirely my own work, and I have appropriately referenced or cited every text. In addition, this work has not been previously published in any form for another degree at any other university.

The research was effectively supervised by Dr A.A. Adebiyi and Prof M Kabeya at the Durban University of Technology.

Submitted By

_____ 06/02/2024

Sandile Dlamini Date

Student Number: 21434128

Approved for final submission:

29/04/2024

sor Date

_____ 29/04/2024

Prof. K. Musasa: Co-supervisor Date

Dedication

I dedicate this study to God Almighty for granting me life, strength to persevere, and the intellect and fortitude to never give up. I also dedicate this study to my four ancestors. As the scarlet flash of red-wing blackbirds in the sky lifted my spirits, I felt a change in my heart from the heavy iron of sadness to the lighter weight of appreciation. I also dedicate this to my late child, Thembalami Dlamini, and my two African queens, Oyintando Dlamini and Nkanyezi Dlamini. They are the reason I push harder every day; they bring light into my life; they are my dream; they give me strength to keep going.

Acknowledgement

I acknowledge the contribution of my supervisor, Dr. A.A. Adebiyi (Dr. Shine). Thank you, sir, for all your kindness, effort, and assistance from the beginning of this journey up to the end. I appreciate you and my co-supervisor, Prof. M. Kabeya.

To Prof. E.E Ojo, thanks a lot for trusting me in this study and for your confidence in my ability. Also, Prof. I.E. Davidson, thank you for your support towards the DUT scholarship and for accepting to supervise my study at the beginning of the Master's degree and giving me the proper guidance.

I express my gratitude to all the people involved for their valuable contributions to this study. I would love to express my sincere gratitude to God and the Four Ancestors for giving me strength and the brain to keep on going. The Smart Grid Research Centre at the Durban University of Technology provided facility support for this study and is hereby acknowledged.

To all postgraduates who were studying towards their Master's and PhDs, thank you, Mr. K. W. Ntuli, Ms. L.B. Zulu, Ms. Z. Z. Lunga, Mr. U Ikitde, Ms. PB Mhlongo, and Dr. M.S.P. Mgongoma, for your support and encouragement.

To the Durban University of Technology, Directorate for Research and Postgraduate Support, and DUT scheme scholarship for the funding provided throughout the Master of Engineering to help me study without any problem-related financial challenges. I also want to thank the whole faculty of Engineering and the Built Environment, the Department of Electrical Power Engineering, and the DUT library for their support and training throughout the study.

To my mother, Miss Thokozani Mkhwanazi, and my late father, Mr. Thulani Dlamini, I would love to thank you both for everything. To my big brother, Mandlenkosi Victor Makhathini, thank you for paving the way to university for me by paying my registration fee at MUT, and to my uncle, Dr. Thamsanqa Patrick Mbonambi, I appreciate you for being the person I look up to and for paying for my registration fee at DUT. God bless you. Never stop by me to help people. To Gugulethu Princess Cele, thank you for everything throughout this process of studying from Day one. God bless you and my two daughters, Oyintando Dlamini and Nkanyezi Dlamini. I love you and I appreciate you; you are the reason I keep on going.

The author expresses gratitude to all individuals involved for their valuable contributions, with special acknowledgment to the following people: Mr. Tholinhlenhla Mkhwanazi, Mr. Njabulo Mkhwanazi, Mr. Sihle Mkhwanazi, Miss Thola Mkhwanazi, Mr. Musa Mkhize, Mr. Senzo Mkhize, Mr. Sithembiso Mkhize, Miss Nompumelelo Cecilia, Miss S.T. Msani, Mrs. S.J. Mkhize, Siyanda Lembede ka Dlamini, family, and friends.

Abstract

Harmonic components have developed in power systems due to the non-linear properties of the circuit components utilized in power electronics-based products and their rapid application. Power systems rely on fundamental quantities like sinusoidally varying voltage and current, which oscillate at a frequency of 50 Hz. The standard restrictions of IEEE-519-1992 were utilized as a benchmark in this study. To generate the best output, the total harmonic distortion (THD) should be decreased below the limit, even for certain individual harmonic numbers, and reflect the power factor output. Using the results of the simulation and projections for each mitigation strategy, the THD_I can be reduced below the IEEE-519 standard whilst also providing cost and electrical advantages. Analysed and modelled is the PV system, which comprises solar panels, a DC-DC converter, a DC-AC inverter, and a non-linear load.

Passive filters are an effective solution for improving power quality in standalone photovoltaic (PV) systems. This dissertation provides an overview of the design and application of passive filters for this purpose. Firstly, an introduction to PV systems and the power quality issues associated with them was preferred. Next, different types of passive filters, namely LC filters, LCL filters and LLCL filters, are discussed along with their advantages and disadvantages, and the design considerations for these filters, including the selection of filter components and the calculation of filter parameters. The application of passive filters in standalone PV systems was then discussed, including their implementation in DC-DC converters and Z-Source inverters and, the design of PWM controllers such as the constant boost control method and simple boost control method.

The analysis of the outcome of the engineered systems was conducted according to the IEEE standard and SANS 10142 Standard to protect the connected equipment within the off-grid network. The outcomes pertain to the single-phase stand-alone/off-grid photovoltaic system and the single-phase Z-Source inverter. The Z-Source inverter is equipped with two distinct methods for PWM control, namely the constant boost control method and the simple boost control method. All three designs incorporate three passive filters, namely the LC filter, the LCL filter and the LLCL filter. The results were obtained from the network consisting of three distinct designs. LLCL demonstrates superior performance as a passive filter, substantiating its position as the optimal choice. The optimal outcomes of a single-phase off-photovoltaic (PV) network can be achieved using LC, LCL and LLCL filters, with corresponding percentages of 2.99%, 2.45% and 1.71%

respectively. Unfiltered was 89.05%, which is not good for the equipment connected to the network.

The Z-Source showcases the capability of voltage amplification to an infinite level, rendering it highly effective in minimizing total harmonic distortion. This research investigation further demonstrated the efficacy of the Z-Source Inverter with Constant Control Boost Method and Simple Boost Control Method, achieving unfiltered total harmonic distortion levels of 38.85% and 44.96% respectively. The Z-Source inverter, when combined with the Constant Boost Control method and Simple Boost Control method, exhibits various filter configurations such as LC, LCL, and LLCL filters. In the context of the constant boost control and simple boost control methods, it is imperative to assess the total harmonic distortion percentage of voltage and current for LC, LCL, and LLCL configurations. The constant boost control voltage (LC, LCL, LLCL) and current total harmonic distortion (LC, LCL, LLCL) are measured at 4.177%, 2.655%, 1.951%, and 2.958%, 2.09%,1.465% correspondingly. The voltage-based boost control methods, namely LC, LCL and LLCL, exhibit total harmonic distortion levels of 2.345%, 1.920% and 0.211%, respectively. Similarly, the current-based boost control methods, LC, LCL and LLCL, demonstrate total harmonic distortion levels of 2.346%, 1.921%, 0.211%, and 2.346%, 1.921%, 0.211%, respectively.

Finally, the dissertation wrapped up by exploring the potential of passive filters for enhancing power quality in standalone PV systems. The thesis offers a comprehensive investigation of the design and implementation of passive filters in standalone PV systems, providing valuable insights for engineers and researchers in the field. It enhances understanding and utilization of these imperative devices.

Table of Content

Declaration ..... **i**

Dedication ..... **iii**

Acknowledgement ..... **iv**

Abstract ..... **vi**

List of Figures ..... **xii**

List of Tables ..... **xiv**

Publications list ..... **xv**

List of Acronyms ..... **xvi**

Chapter One: Introduction **1**

1.1 Introduction to the Research 1

1.2 Background 1

1.3 Motivation 3

1.4 Research Question 6

1.5 Aim and Objectives 6

1.6 Structure of Dissertation 6

Chapter Two: Literature Review **8**

2.1 Introduction 8

2.2 Photovoltaic System Two Main Structure of An Off-Grid and Grid-connected 8

2.3 Photovoltaic Cells 9

2.4 Off-Grid PV System Modelling 11

2.5 DC-DC Boost Converter Modelling 14

2.6 Z-Source Inverter 17

2.6.1 The Voltage Source Inverter 17

2.6.2 The Current Source Inverter 18

2.6.3 The classical single-phase Z-Source Inverter 19

2.6.4 The analysis of a ZSI circuit 21

2.6.5 The PWM control approach for ZSI 23

2.6.5.1 Simple Boost Control 23

2.6.5.2 Constant Boost Control 24

2.7 Harmonics 25

2.8 Harmonic Components in Stand-Alone PV Networks 27

2.9 Power Factor under Conditions with Sinusoids 27

2.10 Power Factor in Situations with Non-Sinusoidal Patterns 29

2.11 Different solution to the mitigation of harmonics within PV system 30

2.12 Kalman Filter 30

2.12.1 What the Kalman Filter Means in Mathematics 30

2.13 Harmonic Mitigation Filter Design Features 33

2.13.1 LLCL PASSIVE FILTERS DESIGN AND ANALYSIS 40

2.13.2 Implications of Filters 45

2.14 Conclusion 48

Chapter Three: Modelling and Simulation 50

3.1 Introduction 50

3.2 Literature Review 50

3.2 Design of Single-Phase Photovoltaic System 51

3.3 Design of a Single-phase Z-Source Inverter Circuit 52

3.4 The Design of PWM Control Techniques 53

3.5 The Selection of a Simulation Tool 54
3.6 Results of a Stand-Alone Single-Phase PV System 55
3.7 The Results of Single-Phase Z-Source Inverter PV System 55
3.8 Conclusion 57
Chapter Four: Result and Analysis 58
4.1 Introduction 58
4.1.1 The Design of the step-up Booster for the stand-alone PV system 58
4.1.2 The Universal Bridge inverter 59
4.1.3 The Photovoltaic system 60
4.1.4 Analysis of the effect of PV array Irradiance and Temperature on Power Quality/Total Harmonic Distortion 64
4.1.4 Designing of the passive filters 67
4.2 The Designed Stand-Alone/off-grid PV System with Passive filters 71
4.2.1 LC Filter Results for off-grid PV Systems 71
4.2.2 LCL Filter Results off-grid PV System 72
4.2.3 LLCL Filter Results for the off-grid PV System 73
4.3 Basic ZSI Design 75
4.3.1 The Design of an Inductor for ZSI 75
4.3.2 The Design of a Capacitor for ZSI 76
4.3.3 The Selection of a diode and Switching devices 77
4.4 The PWM Technique Schemes 78
4.4.1 Sinusoidal Pulse Width Modulation (SPWM) 78
4.4.2 The Constant Boost Control method (CBM) 81

4.4.3 The Simple Boost Control Method (SBC) 89

4.5 Comparison analysis of the LLCL Filter in the Single-phase off-grid PV System and Single-phase Z-Source inverter off-grid PV System 96

Chapter Five: Conclusion and Recommendation 98

5.1 Conclusion 98

5.2 Recommendation 100

References 101

Appendices 110

List of Figures

Figure 1. 1: Overview of South Africa Annual Direct Normal Irradiation (Wh/M2 /D) In 2022 4
Figure 1. 2: Major Building Blocks of Typical Solar Power System. 5

Figure 2. 1: PV System with co-ordinating components 9
Figure 2. 2: functioning of Solar cell [27] 10
Figure 2. 3: A PV cell model 11
Figure 2. 4: MATLAB/Simulink model 11
Figure 2. 5: Boost Converter for Dc/Dc Voltage 15
Figure 2. 6: A Single-Phase traditional VSI 17
Figure 2. 7: The Single-Phase Current Source Inverter 18
Figure 2. 8: The Classical Single-Phase Z-Source Inverter [60] 19
Figure 2. 9: The Non-Shoot-through state of a ZSI (mode 1 and 2) [60] 20
Figure 2. 10: The Shoot-through State of a ZSI (mode 3) [60] 21
Figure 2. 11: Single-Phase simple boost control 23
Figure 2. 12: Single -Phase Constant Boost Control Method 24
Figure 2. 14: Flow diagram for Kalman filter based on THD reduction [81] 33
Figure 2. 15: LCL filter modelling with inverter side and load side [88] 36
Figure 2. 16: Current inverter output [98] 40
Figure 2. 17: LLCL filter Frequency response [2] 41
Figure 2. 18: Input voltage of solar inverter [101] 42
Figure 2. 19: LLCL filter schematic illustration [101] 42
Figure 2. 20: Harmonic-induced simplified waveforms [106] 45
Figure 2. 21: LCL-LC FILTER 47
Figure 2. 22: The LCL - LC filter's vibrational annotations [121] 48

Figure 3. 1: The Single-Phase Stand-Alone PV System Block Diagram 51
Figure 3. 2: Single-Phase Z-Source Inverter Block Diagram 52
Figure 3. 3: Block Diagram design of PWM Control Techniques 53

Figure 4. 1: the output voltage of the step-up Booster, which is 400 $V_{DC.}$ 59
Figure 4. 2: Protection Configuration Of Pv System 62
Figure 4. 3: (A) Irradiance VS V_{PV}_Out .....
FIGURE 4.3: (B) Irradiance VS THD% 65
Figure 4. 4: (c) Irradiance VS PV Array output Current 66
Figure 4. 5 (A): Iac-Load Without a Filter 80
Figure 4.5 (B): Vac-Load Without a Filter 67
Figure 4. 6 (A): The Load Current With LC Filter 71
Figure 4. 7 : The Load Voltage With LC Filter 71

Figure 4. 8: The Load Current with LCL Filter 72
Figure 4. 9: The Load Voltage with LCL Filter 72
Figure 4. 10: The Load Current with LLCL Filter 73
Figure 4. 11: The Load Voltage with LLCL Filter 73
Figure 4. 12: Stand-Alone PV System with passive Designed filters and without passive filters 74
Figure 4. 13: The Designed Basic ZSI Diagram 77
Figure 4. 14: SPWM Control design 80
Figure 4. 15: The Positive and Negative Phase for Leg A, Leg B with V carrier at 90° 80
Figure 4. 16: The state of switching devices from S1, S2, S3 and S4 81
Figure 4. 17: Third harmonic injected harmonic single-phase fundamental waveform. 82
Figure 4. 18: THE Constant Boost PWM control method 83
Figure 4. 19: Unfiltered Harmonic at supplied voltage of 200 V and 0.65 Modulation index 84
Figure 4. 20: Filter waveform of load voltage at the Modulation index (0.65) 85
Figure 4. 21: The single-phase waveform for Simple Boost Control 89
Figure 4. 22: Simple boost control method 91
Figure 4. 23: Unfiltered waveform of simple boost control method 91
Figure 4. 24: Filtered Waveform of Simple Boost Control Method 92

List of Tables

Table 2. 1: THDI is affected by temperature and irradiance. 39

Table 3. 1: For collecting result of stand-Alone single-phase PV System 55
Table 3. 2: Single-phase Z-Source Inverter 56

Table 4. 1: The Parameter of DC-to-DC Boost Design 58
Table 4. 2: More details on solar parameter 60
Table 4. 3: Parameters of the Photovoltaic 61
Table 4. 4: Varying Irradiance and temperature parameters to analysis harmonics and power quality in the Stand-alone PV System. 64
Table 4. 5: Four switching devices state. 79
Table 4. 6: The switching state at active state, zero state, shoot-through state and output of voltage in different states. 82
Table 4. 7: Analysis of harmonic components and other causes of thd% 86
Table 4. 8: Truth table for switching state in the Simple boost control PMW Method 90
Table 4. 9: Analysis of harmonic components and other causes of thd% for simple boost control method 93

List of Publications

1. Dlamini, S., Davidson, IE and Adebiyi, AA. "Design and Application of the Passive Filters for Improved Power Quality in Stand-alone PV Systems." *2023 31st Southern African Universities Power Engineering Conference (SAUPEC)*. IEEE, 2023. DOI: 10.1109/SAUPEC57889.2023.10057777

List of Acronyms

PV	Photovoltaic
LC	Inductor-Capacitor
LCL	Inductor-Capacitor-Inductor
LLCL	Inductor-Inductor-Capacitor-Inductor
CAD	Computer Aided Design
IEEE	Institute Of Electrical Electronics Engineers
THD%	Total Harmonic Distortion in Percentage
THD_I%	Total Harmonic Distortion of Current in Percentage
THD_V%	Total Harmonic Distortion of Voltage in Percentage
MPPT	Maximum Power Point Tracking
AC	Alternating Current
DC	Direct Current
DC-DC	Direct Current to Direct Converter
DC-AC	Direct Current to Alternating Current Converter
MW	Megawatt
P+O	Perturbations And Observation
HC	Hill Climbing
RCC	Ripple Corelation Control
ANN	Artificial Neural Network
VSI	Voltage Source Inverter

CSI	Current Source Inverter
EMI	Electromagnetic Interference
MOSFET	Metal-Oxide-Semiconductor-Field-Effect-Transistor
IGBT	Insulated Gate Bipolar Transistor
ZSI	Impedance Source Inverter
CBC	Conanst Boost Control
SBC	Simple Boost Control
MBC	Maximum Boost Control
PWM	Pulse Width Modulation
PCC	Point Common Connection
LQE	Linear Quadratic Estimate
SANS 10142	South African National Standard (The Wiring Premises/ Part 1-2: Specific Requirement for Embedded Generation Installations Connected to The Low Voltage Distribution Network In South Africa)

Chapter One: Introduction

1.1 Introduction to the Research

This study proposes the application of passive filters to eliminate harmonic component in an off-grid photovoltaic (PV) system. Severe harmonic difficulties arise in standalone PV systems due to the extensive usage of power-electronic equipment and non-linear loads. Typically, a stand-alone photovoltaic (PV) system is engineered to function at a frequency of 50Hz. However, specific loads generate current and voltage signals that contain multiple integer values of the fundamental frequency of 50Hz. [1]. The term "electrical pollution" refers to higher frequencies in power systems, specifically known as power system harmonics. Therefore, harmonics interfere with the regular functioning of the equipment or the PV system. Consequently, there has been an increase in the frequency of LC and LCL-related projects discussed in literature and research on the renewable energy sector. Thus, this study uses different methods to examine the effectiveness of passive filters under various operating situations in stand-alone PV systems. It also introduces a novel passive filter architecture to enhance performance, power factor, and power quality.

1.2 Background

The concept of LC filters has been around for over a century, and their design has evolved over time. The earliest known work on LC filters dates to the 19th century when Michael Faraday and Joseph Henry independently discovered the principles of inductance and mutual inductance. However, the first systematic analysis of LC filters was carried out by Oliver Heaviside in the late 1800s. Heaviside was a British mathematician and physicist who is credited with developing the modern theory of electrical circuits [1, 2].

Heaviside's work on LC filters provided a theoretical foundation for the design of filter circuits, and his ideas were later refined by other scientists and engineers. In the early 20th century, LC filters were widely used in radio communication systems, and their design was further developed by pioneers such as Guglielmo Marconi, Reginald Fessenden and Edwin Armstrong [3].

Since then, LC filters have been extensively used in numerous electronic applications, including power supplies, audio systems and data communication networks. The design of LC filters continues to evolve, with modern techniques such as computer-aided design (CAD) and optimization algorithms being used to improve their performance and efficiency [4].

The LCL filter is a modification of the traditional LC filter and was developed by researchers in the field of power electronics. The exact origins of the LCL filter are not clear, as it has likely been developed independently by multiple researchers over time.

The mathematical equations for the LCL filter can be derived using standard circuit analysis techniques, such as Kirchhoff's laws and nodal analysis. The derivation of the LCL filter equations is a complex process that involves modelling the filter as a set of differential equations and solving them to obtain the transfer function of the filter.

Several researchers have contributed to the development and analysis of the LCL filter, including B. Singh and K. Al-Haddad in their paper "A Comparative Study of LCL and L Filter for Grid-Connected PV Inverters" published in the IEEE Transactions on Industrial Electronics in 2012, and H. Akagi, Y. Kanazawa, and A. Nabae in their paper "Instantaneous Reactive Power Compensators Comprising Switching Devices Without Energy Storage Components" published in the IEEE Transactions on Industry Applications in 1983 [5, 6].

The world's energy demand is steadily increasing, necessitating the development of alternative energy sources to meet future demands. Thus, as a result of escalating costs of fossil fuels and associated ecological apprehensions, renewable energy has emerged as a substantial electricity provider for both private and public structures. Solar energy is an environmentally friendly energy source that harnesses the power of sunshine and converts it into electrical power using photovoltaic (PV) panels [7, 8]. As a result, the use of photovoltaic systems as a renewable energy source derived from solar radiation is increasing. Many people prefer solar photovoltaic (PV) due to its notable benefits, such as the absence of fuel expenses, pollution, noise, and the need for minimal maintenance. Photovoltaic technology could be used as a grid-connected system or stand-alone system. The Off-Grid PV system generates electricity during daylight hours and stores it in a battery. The battery bank supplies the necessary energy for the load [9].

DC voltage is generated when solar irradiation hits the PV panel. The amount of voltage depends on the solar irradiation level that the PV panel receives and the climatic parameters. As a result, this study proposes to investigate the performance of the standalone PV system under varying temperatures and solar irradiation intensities. PV power generation technology is one of the most important types of research in renewable energy, which is significant in mitigating the global energy crisis. Furthermore, the standalone PV system can provide power for remote loads that do not have any access to power grids, as well as provide energy for local loads. However, this study is concerned with harmonic behaviour on a standalone PV system. The use of non-linear loads is

increasing every day, and highly nonlinear loads cause harmonics in power systems. This increasing use of non-linear loads has created more distortions in current and voltage waveforms [10, 11]. This study will discuss the problem of harmonics and design passive filters to mitigate the impact of the poor power quality. In addition, a comparative analysis of the designed filters will be conducted for optimal performance of the PV system.

Photovoltaic (PV) conversion of solar energy is gaining higher acceptance compared to other resources to generate electricity. The electrical resource of the sun is produced using either off-grid (Standalone) or grid-connected PV techniques. Off-grid PV generators are either used as stand-by alternative power or are employed in some other cases to produce all the power requirements of a facility, making the user of the standalone photovoltaic system completely independent from the utility company. However, there is a concerned with harmonic behaviour on a standalone photovoltaic system.

Non-linear loads are the primary cause of harmonics in a power system. The prevalence of non-linear loads is steadily increasing. The increasing popularity of non-linear loads has resulted in an escalation of distortions in current and voltage waveforms. This study explores the issue of harmonics in systems and examines how non-linear loads, such as Personal Computers, Printers, Fluorescent Lamps, Cell Phones, and battery chargers, can distort the waveforms of voltage/current and inject harmonics into the system [12].

1.3 Motivation

The world is currently experiencing the fourth industrial revolution, characterized by rapid growth in industrialization. This results in an increased demand for electricity and the burning of fossil fuels. In terms of energy in South Africa, there is a gap in demand and supply. To minimize this gap, which is disturbing the progress of the industrial sector, renewable energy sources like solar energy can be utilized. Amongst the available sources of renewable energy, photovoltaic is the most promising. Photovoltaic cells offer many advantages. It is a direct energy conversion in which there are no moving parts, no noise, and negligible wear and tear, with little or no maintenance required for proper operation [13].

Renewable energy systems are the future of electric power generation systems. In the near future, the demand for electric energy is expected to increase rapidly due to global population growth, and industry growth as well. This increase in energy demand requires electric utilities to increase their generation. Recent studies predict that the world's net electricity generation is expected to

rise from 24.4 trillion kilowatt-hours in 2015 to 33.3 trillion kilowatt-hours (an increase of 73.3%) in 2030 [14].

Currently, a large share of electricity is generated from fossil fuels, especially coal due to its low prices. However, the increasing use of fossil fuels accounts for a significant portion of environmental pollution and greenhouse gas emissions, which are considered the main reason behind global warming. South Africa needs to make a U-turn from using coal for energy generation to alternative energy sources which will never harm the environment. Looking at the top ten countries using renewable energy, Germany is number one and South Africa is ranked at number 15, although South Africa more sunlight than Germany.

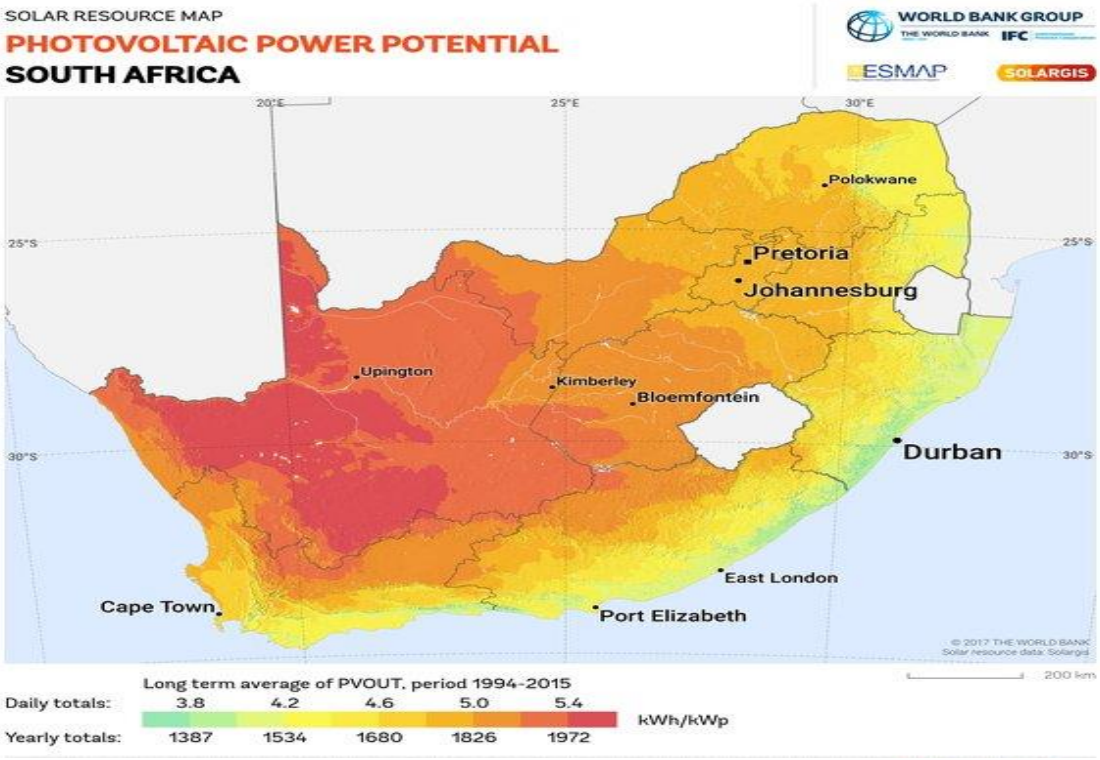

Figure 1. 1: Overview of South Africa's Annual Direct Normal Irradiation (Wh/M2 /D) In 2022 [15]

However, previous studies have shown that the use of power electronics devices (PV inverters, etc.) and non-linear loads on the distribution system results in power quality problems due to injected harmonic components, which cause significant issues in power systems. Therefore, this study is motivated to design and implement a passive filter to mitigate the impact of harmonics on a standalone PV system. The main drawback of a standalone structure is that the maximum available power is not always used, while maximum power point tracking (MPPT) control could be accomplished [15, 16]. On the other hand, grid-connected PV systems can transfer all maximum

available PV energy to the loads and grid simultaneously without any energy storage necessity [17, 18].

Power electronic equipment and non-linear loads are widely used in standalone PV systems, resulting in serious harmonic problems. In figure 1.2 shows a typical block diagram with different connections from a PV array that produces dc current, through the dc-to-dc converter which is coupled with the changer controller for the battery that is a bidirectional controller, than the dc to ac converter linked with the dc-to-dc converter, and the load is linked with inverter. The block diagram does not have a passive filter for the protection of the system from harmonics effects.

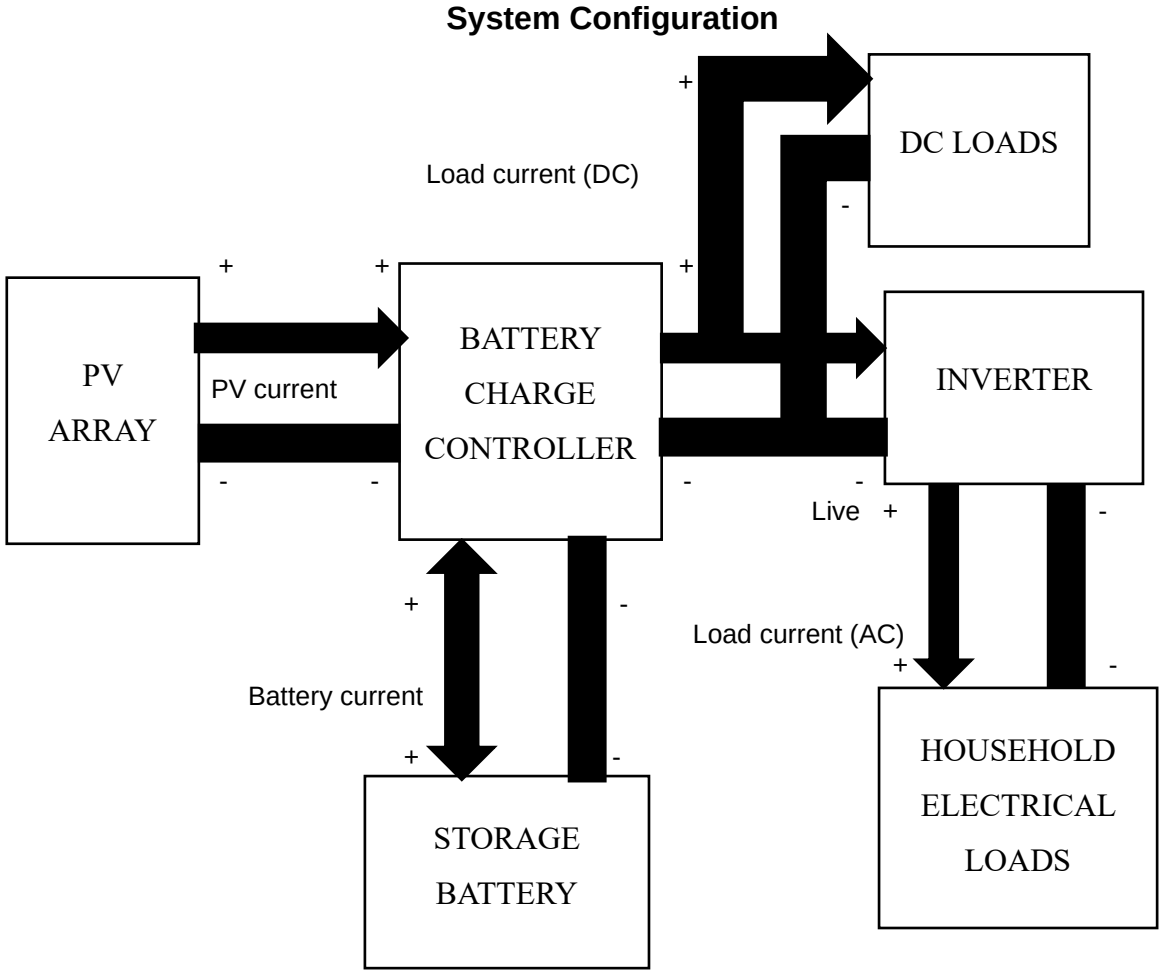

Figure 1. 2: Major building blocks of typical solar power systems

The above application or block diagram demonstrate the structure of an off-grid PV system without a filter. The standalone system comprises a PV module containing several PV cells connected in series to obtain the desired DC voltage. A DC/DC boost converter is used to generate a higher DC voltage. A DC/AC inverter is necessary to provide an AC output voltage.

1.4 Research Question

The research questions for the study are the following:

- How do different power filters (LC, LCL, and LLCL filter) perform in reducing total harmonic distortion in application of controlled (Z-Source inverter) and uncontrolled inverters (Single-phase PV system)?
- How do changings in the incoming solar Irradiance impact the performance of passive filters?

1.5 Aim and Objectives

Many studies have been conducted in analysing the various components that form a power system to develop appropriate harmonic models. This study aims to mitigate harmonic distortion on standalone PV systems during steady-state and changing operating conditions. The objective is to investigate the impact of harmonic distortion; analyse the effectiveness of the methods to mitigate the harmonic effect; and evaluate it against harmonic limits provided by IEEE standards, ensuring compliance with internationally recognized recommendations to operate equipment safely and reliably on the system.

This research on the harmonics behaviour effect on the standalone photovoltaic system aims to assess photovoltaic input voltage waveform and current waveform. It examines the characteristic using MATLAB. The objectives are:

- To determine a suitable method for representing off-grid for harmonic studies; and
- To develop the calculations method for determining the acceptable penetration level of photovoltaic systems.

1.6 Structure of Dissertation

Chapter One: This chapter provides an introduction and overview of the study, including the background, problem statement, motivation, aim, and objectives. It also discusses the research questions related to implementing a passive filter and different methods to reduce total harmonic distortion.

Chapter Two: A comprehensive analysis of the pertinent literature is conducted. The report provides background information on the worldwide and South African energy markets, specifically focusing on the deployment of solar PV. Additionally, it offers a description of the impact of harmonic distortion. Fundamentals of power system harmonic analysis and harmonics are discussed to present the key theoretical concepts fundamental to the topic. Harmonic analysis techniques using measurement and simulation are discussed and accompanied by a review of relevant case studies. Detailed modelling techniques and simulation tools are described. Finally, harmonic measurement and components of measurement systems are reviewed.

Chapter Three: Every component of the system model was described in the development of a simplified, aggregated off-grid PV model on MATLAB. The harmonic impedance of the simplified model is simulated at the MATLAB and alternatively open-circuited and short-circuited. The mechanisms of observed series and parallel resonances are identified. The simulations are repeated with a full model of the PV system and the results compared to those of the aggregated model. The impact of an equivalent non-linear load and harmonic injected by non-linear loads is assessed. Both the short-term and long-term behaviour of the harmonic signals. Methodologies and standards for the management of harmonic distortion are outlined.

Chapter Four: Results and Discussions - Analysis of the calculated results and simulated results. The chapter compares the results discussing the different measurements of harmonic behaviours on standalone photovoltaic systems. Analysis of the non-linear load and linear load harmonics on the off-grid system is made.

Chapter Five: Conclusions and recommendations - The study results are compared with the research objectives and conclusions are drawn. Recommendations are made for further related research.

Chapter Two: Literature Review

2.1 Introduction

Every piece of equipment, gadget, or electronic device needs some kind of energy to function. Due to the depletion of fossil fuel reserves, finding practical renewable energy sources that can reduce reliance on fossil fuels is essential. Solar energy is the source of energy from the sun which is part of renewable energy. Due to its endless supply and lack of pollution, it is a desirable energy source. The total solar energy incident on Earth exceeds the world's present and future energy needs by a wide margin. If solar energy is correctly utilized, it has the ability to meet all of the world's energy demands in the future [19]. Less than 5% of solar energy is now utilised globally, despite the energy potential that is at a human being disposal. Some countries are working to transition to solar energy from fossil fuels. Certain nations make up the G-20, which has taken the lead in promoting the use of renewable energy sources on a global scale. Germany is one of the G-20 nations that has shifted 38% of its energy requirements to solar energy and plans to totally phase out nuclear power and substitute it with solar energy by the year 2050 [19, 20]. Other nations could observe Germany and learn from it in terms of changing the energy sources that have an adverse impact on the environment.

2.2 Photovoltaic System Two Main Structure of An Off-Grid and Grid-connected

PV panels and a few ancillary parts make up photovoltaic (PV) generation systems that are required to convert the energy generated into a form that is easily usable by common loads like household appliances, industrial loads, and a variety of other loads. Currently, there are two main types of PV systems in use: standalone and grid-connected, with outputs ranging from a little wattage to several MW. To keep the energy that has been captured and release it when needed in the first scenario, an electric energy storage device is often required [21]. The usage of simple power converters, such as a battery charger and DC-AC converters that can power both DC and AC loads, is made possible by this design. While Maximum Power Pont Tracking (MPPT) control could be achieved, the fundamental disadvantage of a standalone construction is that the maximum amount of power is not always utilized [22]. On the other hand, grid-connected PV systems may deliver the whole amount of PV energy that is available to the loads and grid at once without the need for energy storage [23].

Configuration of the Photovoltaic System

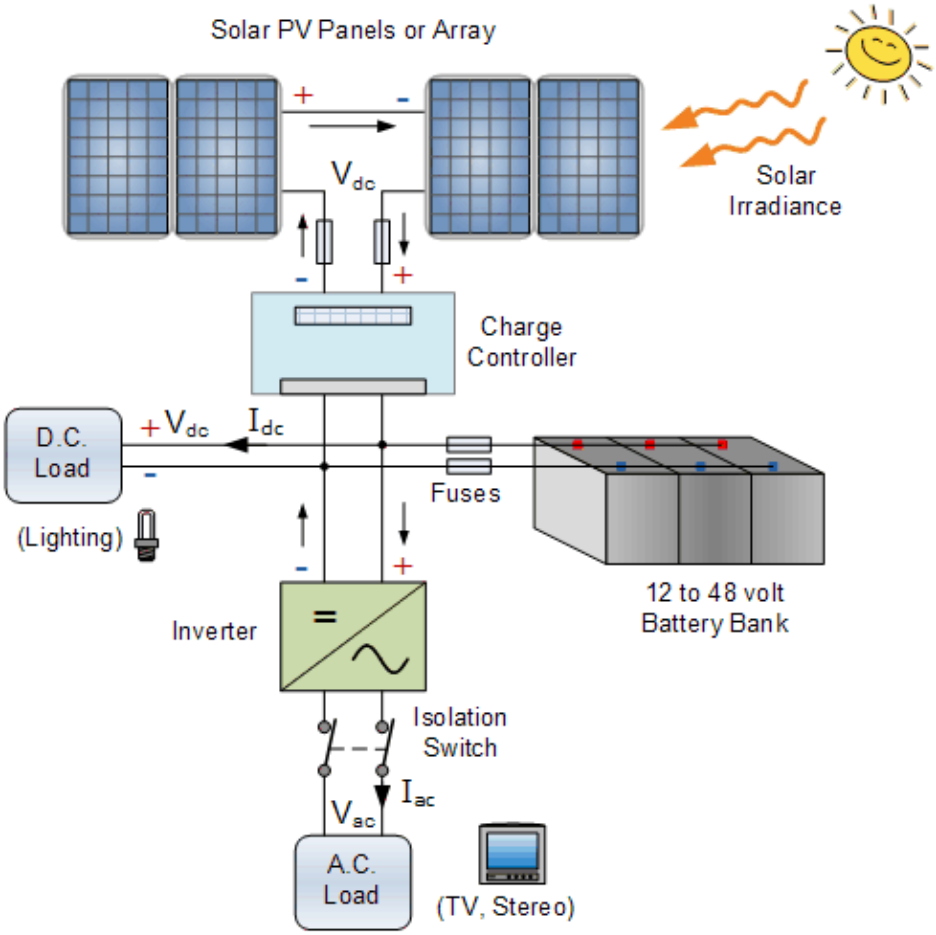

Figure 2. 1: PV System with co-ordinating components

A PV module with numerous photovoltaic cells linked in series to create the necessary DC output voltage makes up the standalone system. A higher DC voltage is delivered via a DC-to-DC boost converter. The only device that can generate an AC output voltage is a DC to AC converter [24].

2.3 Photovoltaic Cells

An engineering and natural miracle, a solar cell, also known as a PV cell, transforms incident photon energy into electrical energy. A separate cell unit may be connected to a frame module, also known as a solar panel. A solar photovoltaic board or module is made up of a group of solar cells that have been placed in a plane to make a single set [25]. Glass is typically used in PV modules to cover the semiconductor plate inside the housing while allowing light to pass through the panel [25]. According on the needs of the client, solar cells are typically linked together and placed in modules that are either parallel or in series. The parallel interface unit receives more current, but there are still issues, such as the possibility of shadow effects ceasing to exist (less

bright). Parallel strings (different combinations of cells) might result in very undesirable outcomes and even injury as a result of their enlightened cooperation and the reversal of dark cell inclinations [26].

The sun is a significant source of electromagnetic radiation, which travel across the universe. Such radiation can take on many different shapes, such as light, radio signals, and so on [11, 27], based on the light's wavelength at the time of emission. There is relatively little visible light in the sun's radiation that enters the atmosphere of the planet. In solar cells, this visible light is transformed into electrons. Different solar cell designs use light with different wavelengths. Solar cells produce energy using silicon-based semi-conductors. A movement of electrons, which are minuscule particles that represent electricity, is referred to as "electric current". Electric currents can move in either a direct current (DC), where the flow direction is constant, or an alternating current (AC), where the flow direction can fluctuate. The two layers of silicon in a typical solar cell are p-type at the bottom and n-type at the top. Energy is produced by a solar cell when sunlight strikes it. The silicon absorbs the electrons, which then move between the n and p layers and generates current. A metal contact is then used to let the electricity depart the solar cell [27, 28].

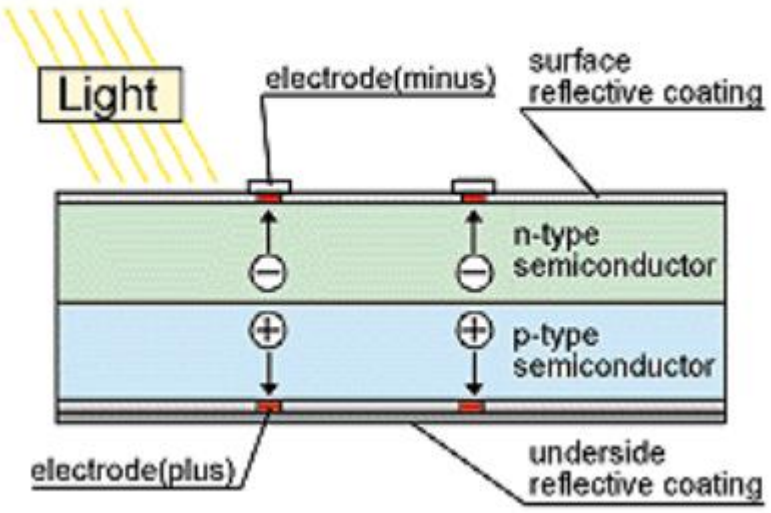

Figure 2. 2: Functioning of Solar cell [27]

2.4 Off-Grid PV System Modelling

A current source, a diode, a shunt resistor, R_{sh} , and a resistor,R_S, are used to construct the most basic model of a solar cell.

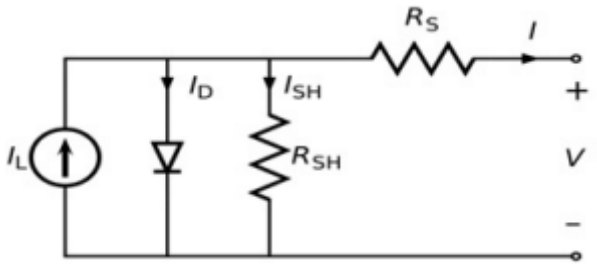

Figure 2. 3: A PV cell model

The model for PV cells in general has been created. There are three input values, two of which are crucial for defining how the device will operate and producing better output power [10, 29, 30].

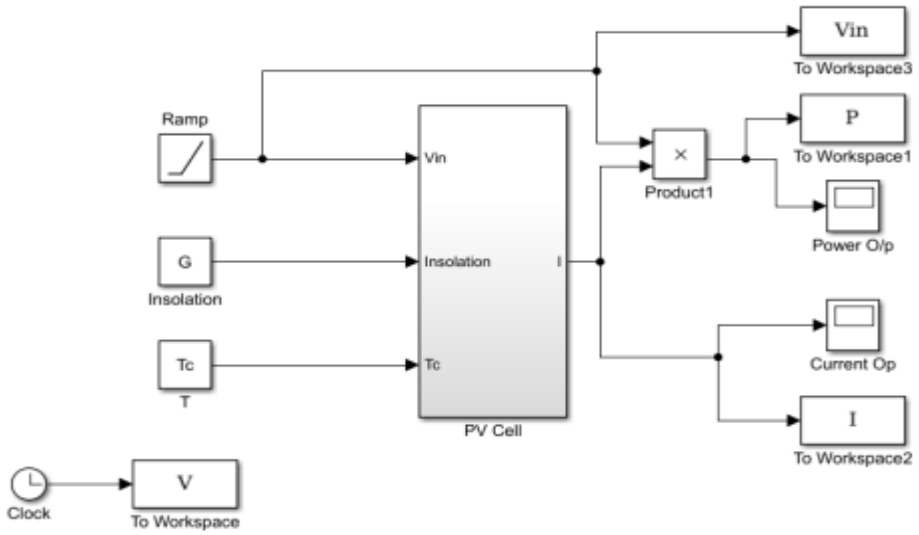

Figure 2. 4: The Subsystem of PV Network on MATLAB/Simulink model

The following equation is employed to generate the Photovoltaic cells of an output voltage (2.1):

$$V_c = \frac{cKT_o}{e} In \frac{I_{ph} + I_d - I_c}{I_c} \qquad (2.1)$$

c: With the aid of the V-I Characteristics model matching factor, any Photovoltaic cell's V-I curves are modified to represent actual values

e: charged electrons

K: J/K is units of Boltzmann's constant

I_C: Current drawn from a PV cell in amps

I_{ph}/I_L: Photovoltaic current, measured in amperes and dependent on temperature and irradiance

I_d: Diode's reverse saturation current, expressed in amps

T_O: operating temperature in Kelvin of the reference cell

The temperature, along with the sun's irradiation, affect how much power a PV array generates. Using a known temperature and known solar irradiation level, a PV array model is created [31]. The model has been improved and adjusted to take temperature and solar radiation fluctuations into account. The output voltage and photo current of a PV cell change when the surrounding temperature T_a varies. Similarly, variations in the sun's S_C solar irradiation have an impact on the photovoltaic current and operating temperature of PV cells [17, 31]. The coefficients C_{tv}, C_{ti}, C_{sv} and C_{si} ,which are given using the equations from 2.2 to 2.5, are used to describe the effects brought on by these changes.

$$C_{tv} = 1 + \alpha_t(T_a - T_n) \tag{2.2}$$

$$C_{ti} = 1 + \frac{\beta_t}{S_c}(T_n - T_a) \tag{2.3}$$

$$C_{sv} = 1 + \alpha_t \gamma_s (S_n - S_c) \tag{2.4}$$

$$C_{SI} = 1 + \frac{1}{S_s}(S_n - S_c) \tag{2.5}$$

Where, constants are indicating the slope of the changes, C_{tv}, C_{ti}, C_{sv} and C_{si} are correction factors in the PV cell voltages and photo current owing to changes in temperature and different solar irradiation factors respectively. The new values of photo current I_{phn} and PV cell voltages V_{cn} are computed as (2.5) and (2.6) for new temperature T_n and new solar irradiation, S_n, respectively,

using the correction factors supplied in (2.2), (2.3), (2.4) and (2.5). (2.7) where α, β and γ are factors indicating the slope of the variations:

$$V_{cn} = C_{tv} C_{sv} V_c \tag{2.6}$$

$$I_{phn} = C_{ti} C_{si} I_{ph} \tag{2.7}$$

In most cases, a PV cell's output voltage is very low. Individual PV cells are joined in series and parallel to create a PV module in order to enhance voltage magnitude and current rating respectively [31].

Solar irradiance has a significant impact on I_{ph}, which in turn has an impact on I_{sc}. Season, air mass, and time of day are the main factors that affect the intensity of solar radiation at a specific location. These factors also have an impact on other variables such as temperature, humidity, the tilt angle required for solar panels, shade, wind speed, and others. Furthermore, it is claimed that series and parallel resistances in a photovoltaic cell influence solar radiation [10, 32].

Temperature – The cell's temperature is impacted by environmental factors including wind speed, thermal dissipation, etc. Other aspects of the cell's characteristics start to change as its temperature rises. The relationship between solar brightness and the light current is shown in the following equation (2.8):

$$I_{ph} = \left[\left(K_i\left(T_c - T_{ref}\right)\right) + I_{sc}\right]\lambda \tag{2.8}$$

$I_{ph} -$ Photo Current

$K_i - I_{sh}$ Temperature Coefficient

$T_{ref} -$ Reference Temperature

$\lambda -$ Radiance (kw/m^2)

Secondly, equation (2.9) shows how the PV cell's saturation current fluctuates with cell temperature (2.10).

$$I_s = I_{RC}(\frac{T_c}{T_{ref}})^3 exp\left[\frac{qE_g(\frac{1}{T_{ref}} - \frac{1}{T_C})}{KA}\right] \quad (2.9)$$

$$I_{ph} = \frac{I_{sc}}{\left[\exp\left(\frac{qV_{oc}}{N_S K A T_C}\right) - 1\right]} \quad (2.10)$$

I_{rs} – Reverse Saturation Current above T_{ref}

A – Ideality factor, dependent on the PV technology

E_g – Band – gap energy of a Semiconductor

A PV cell voltage current mathematical model is depicted in the expression below.

$$I = I_{ph}N_p - I_s N_p\left[\exp\left(\frac{q(V+IR_s}{KT_c A}\right) - 1\right] - (\frac{V+IR_s}{R_{sh}}) \quad (2.11)$$

I_S– Cell Saturation of dark current

R_S – Series Resistance

R_{sh} – Shunt Resistance

K– Boltzmann's constant

A – Idealist Factor

T_C – Cell's working temperature

q – Electron Charge = 1.6*1019 C

2.5 DC-DC Boost Converter Modelling

Depending on the application, the output voltage from the PV module is increased using a step-up boost converter. Boost converter in step-up mode is shown in Figure 2.5 It is made up of a filter capacitor C, a diode D, a controlled switch S, a boost inductor L, and a load resistance R.

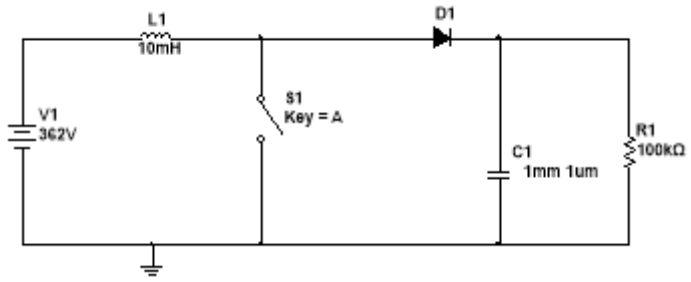

Figure 2. 5: Boost Converter for Dc/Dc Voltage

The equation below provides the boost converter's output voltage V_0 (2.12):

$$\frac{V_o}{V_{in}} = \frac{1}{1-d} \tag{2.12}$$

Where d is the converter that switch's the duty cycle. The inductor value is selected to ensure continuous current flow through the inductor. The voltage ripple ΔV is often selected to be 3% of the output voltage V_O, then current-ripple ΔI, typically designed towards 5% of a current output I_O [11, 33]. Using equations (2.13) and (2.14), the values of Capacitor C and Inductor L are selected.

$$L = \frac{V_{in}d}{8f_{sw}\Delta V} \tag{2.13}$$

$$C = \frac{I_o d}{f_{sw}\Delta V} \tag{2.14}$$

Where f_{sw} is the switching frequency of the dc/dc converter switches. The switches are regulated by pulse width modulation technology, and a single-phase bridge inverter circuit is utilized to convert the DC link voltage generated from the dc - dc converter into an AC output [33]. The inverter output is linked to the load.

The most advanced MPPT algorithm is the metaheuristic method. This is used to tackle the classification problem that PV systems experience as a result of determining out a maximum power point [34]. The efficiency of a Photovoltaic system might be decreased by errors and oscillations caused by the perturbations and observation (P+O) and hill climbing (HC) approaches [34, 35]. A new kind of adaptive HC was developed after the introduction of HC with a variable disturbance size that can only be altered during the tracking process. Other approaches have also been used,

including fractional open-circuit voltage to short-circuit current, ripple correlation control (RCC), current sweep strategy, and the linear current control approach [18, 36]. Current MPPT techniques are also accessible, including metaheuristics, fuzzy logic control and artificial neural networks (ANN). These techniques have been combined with P+O and HC to develop powerful MPPT strategies. To solve the optimization issues that PV systems encounter, it has been utilized to determine the maximum power point [34, 37, 38].

Furthermore, partial light shade from overhanging clouds can easily affect how well MPPT methods function, resulting in a 25% reduction in power delivery [39, 40]. Harmonics are generated in the output power signal by power fluctuations. By lowering harmonics that are generated in the DC/DA converter and DC/AC converter parts of a system, THD in a Photovoltaic system can be decreased. DC-DC converter topologies such as buck, boost, buck-boost, Cuk, single-ended primary-inductor converters and flyback converters have all been studied in detail [41]. These topologies perform the role of switching-mode-regulators, regulating along with transforming a DC value of an output into the desired stages of voltage [24]. This is strongly influenced by the PWM control signal's switching frequency [42]. All the DC-DC converter topologies that have been shown reduce the induced THD by maintaining the output DC voltage at specific values. Most popular of these topologies is the buck-boost converter because it effectively maintains the output DC signal at a specific level, lowering THD. Since the frequent switching of DC-AC converters and their unfavourably high degree of harmonic distortion is apparent, numerous research studies have been done in this area [43, 44].

The integration of PV panels into grids has been studied using a variety of inverters and control techniques [45]. These inverters' output signals can be single-phase or three-phase and have a range of magnitudes, but their typical frequencies are 50, 60 and 400 Hz. Three different inverter types exist: single-phase, three-phase, and multilayer [43, 45]. Using several passive and active filtrations may lead the PV system to reach the S-plane resonance zone if several inductors or capacitors are used, decreasing signal stability and adding bulk to the circuit [46]. Amongst other drawbacks, only a portion of the PV system can benefit from the strategies. The PV system becomes more complex when multiple strategies are often coupled to mitigate the accumulated THD. For these reasons, a straightforward filtering technique is required to get rid of undesirable harmonics which build up all over at the different phases or stages of Photovoltaic system, without complication within the system’s design structure, as other approaches do. Ideally, this technique can be applied at the system's very end just before the load.

2.6 Z-Source Inverter

The Z-Source inverter topology was first proposed by *Professor Fang Zheng Peng* in a paper titled "Z-source inverter", which was published in the IEEE Transactions on Industry Applications in May 2003 [47, 48]. Professor Peng was affiliated with the University of Tennessee when he proposed the Z-source inverter topology [49, 50]. The Z-source inverter has since gained much attention in the field of power electronics due to its unique features such as voltage buck-boost capability, improved reliability, and reduced harmonic distortion [51].

Voltage source inverters (VSI) and current source inverters (CSI) are both well-established topologies in power electronics that have been studied and used for many years.

The first published work on voltage source inverters dates to the late 1960s and early 1970s, in [52]. and [53]. On the other hand, current source inverters have also been studied for several decades. The earliest published work on CSI dates to the 1950s, in [28] and [54]. Hence, both VSI and CSI have a long history of research and development and have been used in various applications in power electronics.

2.6.1 The Voltage Source Inverter

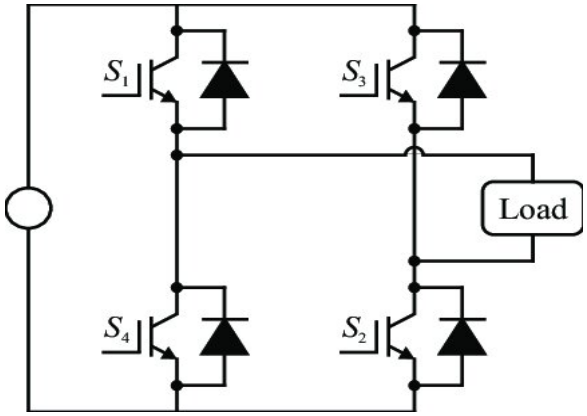

Figure 2. 6: A Single-Phase traditional VSI

Figure 2.6 illustrates the fundamental circuit of a single-phase voltage source on an inverter. When a direct current power supply is connected in parallel with a slightly larger capacitor, it generates a direct current voltage-source that supplies the primary inverting phase. A DC power source can be a battery, diode rectifier, fuel cell stack, as well as capacitor, depending on the application of a VSI [49]. A direct current (DC) source of power in a PV system application is a PV cell or an array of PV cells [55]. A bridge is made up of four electrically-controlled switching devices (IGBTs/MOSFETs), each of which contains a power transistor and an oppositely or free-wheeling

diode. This diode is capable of bi-directional current flow and uni-directional voltage blockage. Considering the general availability of VSIs in application conversion, it has theoretical and philosophical obstacles and restrictions [41, 52, 56].

A VSI's output voltage is restricted to values below or above the DC-link voltage, meaning that it either boosts or reduces the input voltage. When overloading is a priority, an extra dc-dc boost converter stage is required to provide the desired ac output, which increases the system's total expenses and reduces its efficiency [24, 33, 57].

The upper and lower switching devices of the same phase leg cannot be gated on at the same time as this would result in a shoot-through condition and damage to the VSI. In response to this issue, engineers have used 'dead time' to prevent upper and lower switching devices from switching on at the same time, but this causes greater waveform distortion and lowers the output power quality [54, 57].

2.6.2 The Current Source Inverter

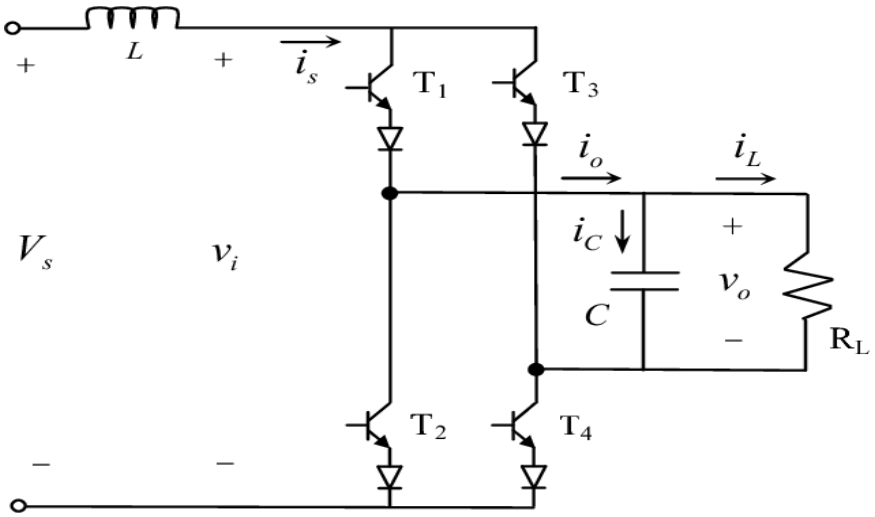

Figure 2. 7: The Single-Phase Current Source Inverter

Figure 2.6.2 depicts the fundamental circuit of a phase-phase current-source inverter. A DC power source is connected in series with a moderately big inductor to generate a DC source. Power switching devices having reverse block capabilities, such as a gate-turn-off thyristor (GTO), silicon-controlled switches (SCR), or power transistors with series diodes, are usually used in the switching devices (IGBTs/MOSFETs). These series diodes are capable of uni-directional current flow as well as bi-directional voltage blocking. A CSI contains theoretical and philosophical boundaries, as well as restrictions [58, 59].

The output voltage of the CSI is like that of a VSI, limited to values below (bucks) or above (boosts) the DC-link voltage. When overdrive is desired, an extra dc-dc boost converter stage is required to provide the desired ac output, which increases the overall expenses of the system and reduces its efficiency [59]. The most important details of the phrases ‘open circuit, inductor, (EMI) Electromagnetic Interference, switching, and open’ are that at least one upper switching device and one lower switching device must be gated on to prevent an open circuit in a DC inductor from developing. Engineers have devised 'overlap time' for safe current commutation in response to this issue, but it can cause greater waveform distortion and lower output power quality [59].

A current source inverter's main switching devices must block reverse voltage, which necessitates the use of a series diode in conjunction with high-speed and high-performance transistors such as insulated gate bipolar transistors (IGBT). This limits the use of low-cost, high-performance IGBT modules and intelligent power modules directly.

Aside from the concerns with VSIs and CSIs, each of these inverter topologies have certain shared shortcomings. VSIs and CSIs can only buck or boost the input voltage, they cannot both buck and boost. This means that the output voltage can either be larger than or less than the input voltage. The major circuitries of VSIs and CSIs are incompatible. The VSI's main circuit cannot be utilized for the CSI application, and vice-versa. Both VSIs and CSIs are susceptible to EMI noise, which undermines their dependability. Most of the disadvantages of VSIs and CSIs have been solved by Z-source inverters. This is why researchers are concentrating their efforts on Z-source inverters. Figure 2.8 depicts a basic schematic of a ZSI with a DC input (PV array, battery, fuel cell). Z-impedance connection (C1, C2, and L1, L2,) and a single-phase universal bridge (S1, S2, and S3, S4).

2.6.3 The classical single-phase Z-Source Inverter

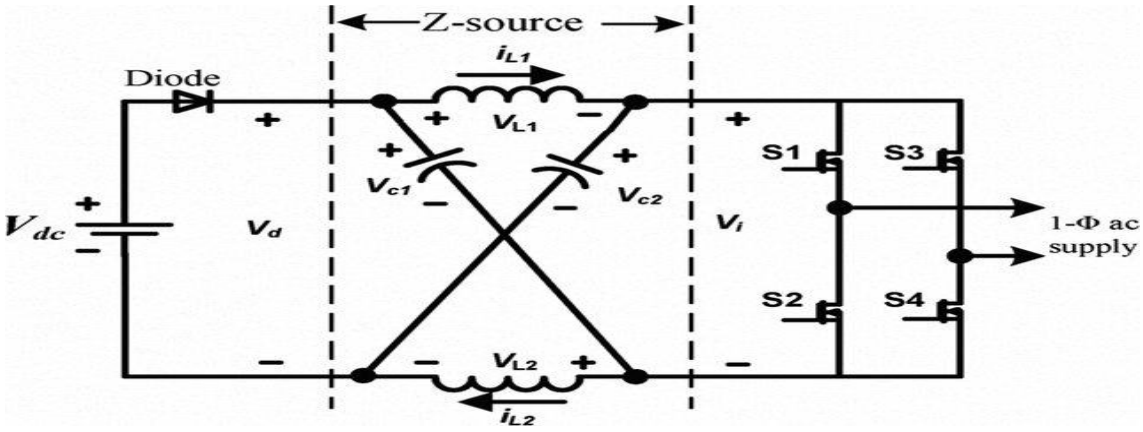

Figure 2. 8: The Classical Single-Phase Z-Source Inverter [60]

A z-source inverter is an advancement over the two previously described inverter topologies, namely the VSI and CSI. As previously stated, the ZSI overcomes most of the theoretical and psychological challenges and restrictions identified with both VSIs and CSIs. Regardless of the input voltage, the output ac voltage of a z-source inverter can potentially be any value ranging from zero to infinity. As a result, a z-source inverter is a buck-boost converter with a wide range of output voltages. Unlike typical VSIs and CSIs, this shoot-through situation is identical to the one stated before, which causes serious damage and unreliability in VSIs. As a result, a ZSI embraces a VSI's weakness and turns it into its strength.

The Z-Source Inverter couples the converter main circuit to the power supply, load or another converter through an impedance network, providing extra characteristics not inherent in standard voltage or current source converters [61]. The inclusion of two inductors and two capacitors in the Z-source network allows both switches on the same phase-leg to be ON at the same time, known as the shoot-through condition, and provides the inverter with boosting capacity without damaging the switching devices.

During the shoot-through condition, energy is transferred from capacitors to inductors, allowing ZSI to enhance voltage. In order to avoid the discharge of overcharged capacitors through the source, diode 'D' is required. The shoot-through state inside the zero-state time is employed not only to manage the average voltage, but also to achieve the buck-boost function.

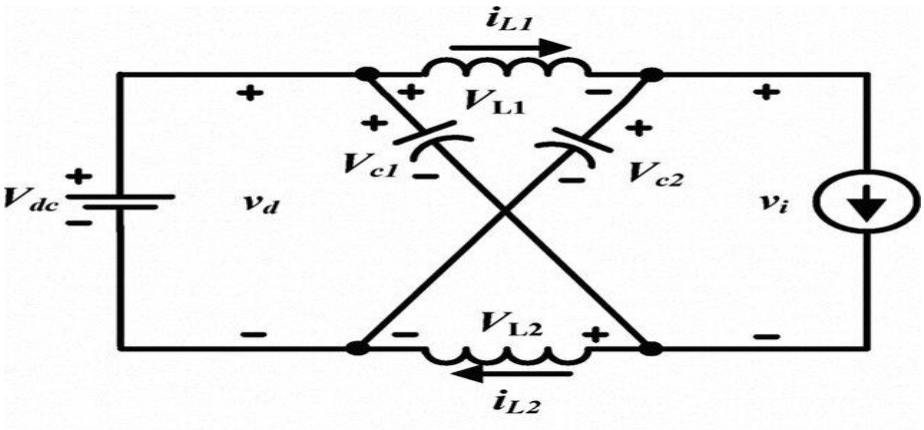

Figure 2. 9: The Non-Shoot-through state of a ZSI (mode 1 and 2) [60]

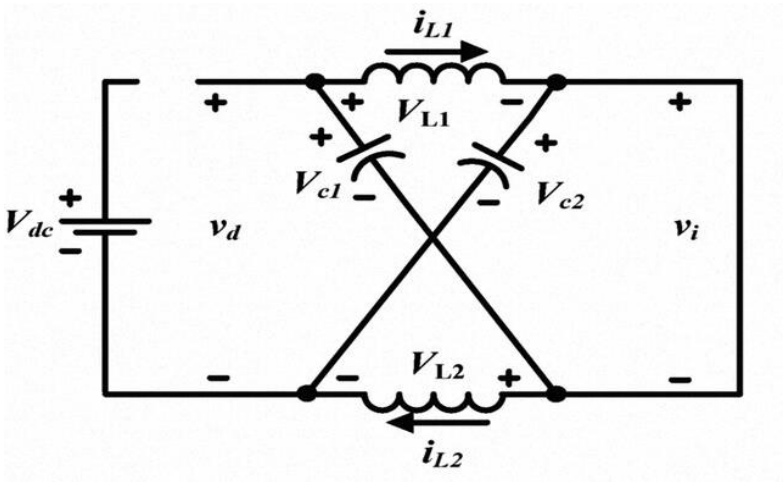

Figure 2. 10: The Shoot-through State of a ZSI (mode 3) [60]

The inverter bridge is represented as a current source when the ZSI is not in the shoot-through condition Figure 2.9 It is important to note that an inverter bridge is represented by a current source with finite current during any of the four active states, while an inverter bridge is represented by a current source with zero current (open) during any of the two zero states [60, 61]. In the shoot-through condition of a ZSI, the inverter bridge is represented by a short circuit, as shown in Figure 2.10

2.6.4 The analysis of a ZSI circuit

The impact of adding shoot-through within the zero states of a PWM switching cycle is investigated using a symmetric Z-source network with $L_1 = L_2 = L$ and $C_1 = C_2 = C$. Figures 2.9 and 2.10 depict the equivalent circuits of a Z-source inverter in the shoot-through and non-shoot-through modes. An analogous current source with a finite current during non-shoot-through active state and a zero current during shoot-through zero states can be used to treat the inverter side of a z-source network. Since Z-source is symmetric:

$$V_L = V_1 = V_2, \&... V_C = V_{C1} = V_{C2} \tag{2.15}$$

During non-shoot-through conditions, the 'T_{NS}' inverter circuit is represented by current source and dc source is coupled to the ac load, according to the equivalent circuit, Fig. 2.9.

$$\begin{cases} V_d = V_{dc} \\ V_L = V_{dc} - V_C \\ V_i = V_C - V_L = 2V_C - V_{dc} \end{cases} \tag{2.16}$$

Based on the equivalent circuit In Fig. 2.10, the inverter circuit is represented as a short circuit during the shoot-through state 'T_{ST}', and several relationships are:

$$\begin{cases} (\because v_i = 0) \\ V_C = v_L \\ v_d = V_C + v_L = 2V_C \end{cases} \tag{2.17}$$

where 'T' is the half-period of the carrier wave, 'T_{NS}' and 'T_{ST}' are the non-shoot-through and shoot-through times respectively, and T = 'T_{NS}' +'T_{ST}'. Applying volt-sec balance to the z-source inductor over one switching period

$$\int_0^T V_L dt = 0 \tag{2.18}$$

the voltage across Z-Source Capacitor can be obtained.

$$V_C = \left(\frac{T_{NS}}{T_{NS} - T_{ST}} \right) \times V_{dc} = \left(\frac{1 - T_{ST}/T}{1 - 2\left(T_{ST}/T\right)} \right) \times V_{dc} \tag{2.19}$$

Using (2.16) and (2.19), calculate the peak dc-link voltage across the inverter bridge:

$$\hat{v}_i = 2V_C - V_{dc} = \left(\frac{1}{1 - 2\left(T_S/T\right)} \right) \times V_{dc} = BV_{dc} \tag{2.20}$$

ZSI output peak phase voltage and applying (2.19),

$$\hat{v}_{ac} = m\left(\hat{v}_i/2\right) = m\left(BV_{dc}/2\right) = B\left(mV_{dc}/2\right) \tag{2.21}$$

Where 'B' is the boost factor, which is greater or equal to one and depends on the shoot-through state and modulation index 'm'. According to eqns. (2.19) and (2.20), the shoot through duty ratio is $d = \left(T_{ST}/T\right)$ and its operational range is $0 \le d < 0.5$, with $\hat{v}_i > 0$ as it is shown by equation (2.19) and (2.20), the capacitor and dc-link voltage are affected by the shoot-through duty ratio.

2.6.5 The PWM control approach for ZSI

In the context of single-phase inverters, the PWM control approach can be described as a way of creating an adequate PWM signal for switching the switching devices of a universal bridge such that a desired AC waveform is achieved at the output terminals of a ZSI [58, 60]. This section discusses three of the most prevalent PWM control algorithms in the literature: maximum boost control (MBC), constant boost control (CBC), and simple boost control (SBC) [47, 50, 52, 58, 60].

2.6.5.1 Simple Boost Control

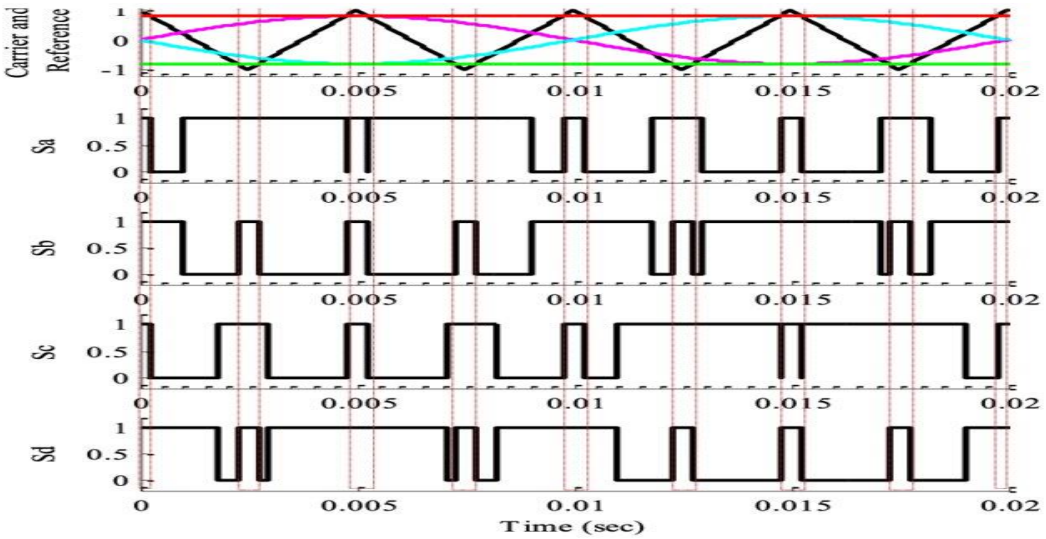

Figure 2. 11: Single-Phase simple boost control [47]

In Figure 2.11, a signal diagram of a Simple Boost Control method is shown. Two straight lines (V_p and V_n), a set of single-phase reference voltages (V_{an} and V_{bn}), and the triangular carrier wave ($V_{carrier}$) are used in a basic boost control. The two straight lines (V_p and V_n) are either equal, bigger, or less than a carrier wave. A ZSI is in a shoot-through state (mode 3) when a carrier wave is higher than V_p or less than V_n. Otherwise, it is in an active or zero state (mode 1 and mode 2).

A ZSI is in a shoot-through condition when a triangular waveform is bigger than an upper straight line or less than a bottom straight line. Otherwise, a ZSI functions similarly to a VSI, and the SBC approach functions similarly to the sine-PWM (SPWM) technique, which is a classic control technique used to regulate VSIs. This approach is the simplest. Nonetheless, the resulting voltage stress across the switching devices is very large due to the absence of certain usual zero states. The output voltage of the SBC approach is presented [47, 62-64].

2.6.5.2 Constant Boost Control

In Figure 2.12, a constant boost control signal diagram is shown. A constant boost control likewise employs two straight lines (V_p and V_n), a pair of single-phase reference voltages (V_{an} and V_{bn}) injected with a third harmonic signal, and a triangular carrier wave (Vcarrier). The two straight lines (V_p and V_n) are either equal, bigger, or less than a carrier wave. A ZSI is in a shoot-through state (mode 3) when a carrier wave is higher than V_p or less than V_n. Otherwise, it is in an active or zero state (mode 1 and mode 2). Consistent boost control minimizes the volume and cost of design components by maintaining a consistent shoot-through duty ratio [51]. Simultaneously, a higher voltage boost for any given modulation index is sought, and Constant Boost Control allows for lower voltage stress across the switches.

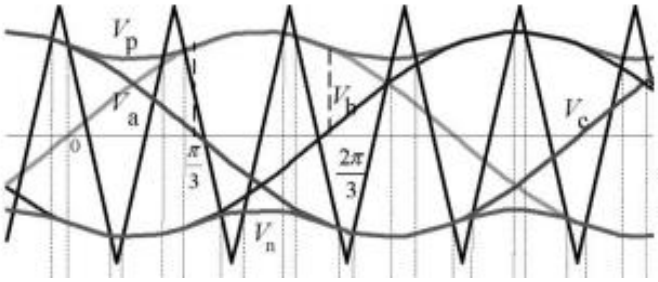

Figure 2. 12: Single -Phase Constant Boost Control Method [48]

A continuous boost control enables higher voltage gain (over SBC) whilst maintaining a consistent shoot-through and hence duty ratio. The sketch map of the maximum constant boost control with third harmonic injection is shown in Figure 2.12, CBC method output voltage [48, 50].

This method reduces the voltage stress across the switching devices whilst maintaining the necessary voltage gain, which is critical for the ZSI's efficient regulation. The maximum boost control does this by converting all standard zero states to shoot-through states [59].

This is done in a similar manner to basic boost control, with the exception of the absence of the two constant encircling lines. The modulation index range can also be extended via third harmonic

injection. Voltage stress can be reduced by converting all zero states to shoot-through states. However, this approach creates a low-frequency current ripple in the inductor current and capacitor voltage that is related to the output frequency. When the output frequency becomes very low, this increases the demand for passive components. As a result, the maximum boost control is appropriate for applications with a fixed or reasonably high output frequency [65, 66].

2.7 Harmonics

Non-linear system loads cause voltage and current harmonics. Circuits including power electronics components as well as other electrical loads with non-linear qualities frequently experience harmonic distortions [26, 67, 68]. IEEE standard 519-2014 states that a low voltage system must undergo harmonic analysis if the point of common connection (PCC) has more than 5% total harmonic distortion (THD) [68]. Harmonic distortion is at steady-state deviation of a voltage or a current waveform from the power line frequency's ideal sinusoidal wave. These harmonics are thought of as a synthesis of a large number of sine waves, or sine integrals, each of which has a different frequency. Total harmonic distortion (THD), a measurement of harmonic distortion in a waveform, is the ratio between the sum of the powers of all harmonic components and the power of the fundamental component. Fourier analysis of the deformed waveform yields the harmonic component's magnitude and frequency [69]. A percentage of the total harmonic distortion is used to define the distortion for current and voltage:

$$THD_I = 100 \times \frac{\sqrt{\sum_{n=2}^{\infty} I_n}}{I_1} = 100 \times \frac{\sqrt{I^2 - I^2{}_I}}{I_1} \tag{2.22}$$

$$THD_V = 100 \times \frac{\sqrt{V^2{}_2 + V^2{}_3 + V^2{}_4 + \cdots \ldots \ldots . V^2{}_n}}{V^2{}_1} \tag{2.23}$$

Using the total harmonic distortion equation for current and voltage to determine the distortion percentage. THDI remains a critical factor on off-grid solar systems, and it should be kept as low as possible. It is a typical technique for calculating the harmonic distortion in solar systems. THDI is defined as a harmonic component-to-fundamental component ratio expressed as a percentage of the fundamental component [70, 71]. Deterioration characterizes non-sinusoidal waves. Harmonic waveform distortion in voltage and current can harm or disrupt the power system and its users. Some non-linear loads that produce harmonics are as follows:

- Circuits for control,
- Converters for frequency,
- Chargers for batteries
- Compensators for static VAR,
- Motor drives with variable frequencies,
- Converters for direct current,
- Inverters,
- Electric transportation methods, converter DC/DC,
- Rectifier,
- Photovoltaic devices,
- Interruptible power sources (UPS),
- Switched electricity sources, and
- Induction stoves.

Even if non-linear loads are small, they cause sinusoidal waveform current and/or voltage distortion. Power system harmonics will cause the following damage [39, 71]:

- A rise in component losses in the stand-alone photovoltaic system,
- A failure of the di-electric insulating materials protecting power system components,
- An increase in the stand-alone photovoltaic system's voltage drops,
- Wrong readings at meters of the induction variety cause control circuits to have problems,
- Incorrect protective relay opening,
- Information loss and improper microprocessor operation,
- Communication device noise,
- A shift in the power factor,
- Overheating of electrical equipment, such as cables, AC/DC converters, inverters, six-pulse rectifiers, and inductive R-L loads,
- Reduced lifespan of inverters, wires and DC/DC boost converters found in off-grid systems,
- Switching components with false triggers include IGBT, MOSFET, gate turn-off thyristor (GTO) and thyristor, and
- Current, Voltage and Power measurement errors in stand-alone Photovoltaic systems.

2.8 Harmonic Components in Stand-Alone PV Networks

The efficiency of harmonic components has increased because of the solar system's expanding use of power electronics-based inverters. Voltage and current waveforms in the solar system are distorted due to the usage of non-linear converters and loads. Solar systems' current and voltage waveforms are distorted by non-linear circuit components and loads, even at low power levels. Harmonic components degrade the quality of energy delivered to loads and pose major issues for power systems. In power electronics devices, semi-conductor elements cause THD [46, 67].

Some power uses that were previously connected to the electrical grid, such as water pumps, communication stations, traffic lights, etc., are now powered by off-grid PV systems [72, 73]. As a result of the switching signals, a solar inverter's output voltage and current generally comprise a significant number of harmonic components. In addition to using a higher switching frequency, active or passive filters can be used to filter out high frequency harmonic material. The harmonic components in these results in problems with power quality. Harmonic components cause a variety of problems in power systems. They also endanger photovoltaic sources and converters. As a result, they must be reduced. Since their switching elements have non-linear characteristics, converters are a source of harmonics. Passive filters are highly recommended for reducing harmonic components in Photovoltaic solar systems. Types of passive filters are implemented to mitigate THD on an uncontrolled rectifier's input current, voltage and to improve the power quality. These results show that the designed passive filters have a basic structure and a relatively simple control, which has important advantages. Passive filters are fitted between the source and the load. They are therefore designed to destroy parts other than the fundamental component [74].

The use of passive filters in off-grid systems has many advantages, including their compact size; being inexpensive; and effective operation. These filters are used to cut down on low-rated radiation and harmonics produced by PWM inverters. They are also used to reduce harmonic components and improve power quality in off-grid power systems. Passive filters must be employed to keep the harmonic components within the restrictions defined in the standard.

2.9 Power Factor under Conditions with Sinusoids

The necessity to measure how well a load uses the electricity it takes from an AC power supply gave rise to the idea of power factor. Think about the optimum sinusoidal circumstance in the circuit below with the linear load, for instance.

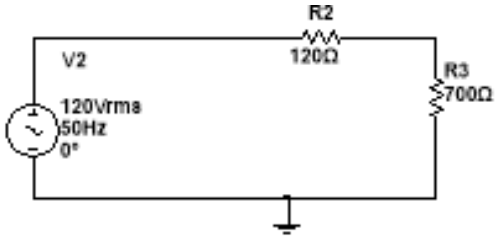

Figure 2.13 Sinusoidal Circuit of a Linear Load

The out voltage and current in the load respectively:

$$V_{(t)} = V_1 sin\ (\omega_\circ t + \delta_1) \tag{2.24}$$

$$i_{(t)} = I_1 sin(\omega_\circ t + \theta_1) \tag{2.25}$$

Where δ_1 and θ_1 are the respective phase angles and V_1 and I_1 are the 50 Hz voltage and current peak values. The ratio of average power to apparent power is known as the true power factor at the load [75].

$$pf_{true} = \frac{P_{avg}}{S} = \frac{P_{avg}}{V_{rms} I_{rms}} \tag{2.26}$$

For the purely sinusoidal

$$pf_{true} = pf_{disp} = \frac{P_{avg}}{\sqrt{P^2 + Q^2}} = \cos\ (\delta_1 - \theta_1) \tag{2.27}$$

Where $(\delta_1 - \theta_1)$ is referred to as the power factor angle and pf_{disp} is known as the displacement power factor. Since the real power factor and displacement power factor are equivalent, there is only one power factor in sinusoidal conditions. In a sinusoidal condition, the unity power factor is equivalent to zero reactive power Q, and low power factors are equivalent to high Q [75, 76]. Low power factors in sinusoidal systems can be fixed by adding shunt capacitors because most loads utilize reactive power.

2.10 Power Factor in Situations with Non-Sinusoidal Patterns

Consider non-sinusoidal conditions when harmonics are present in system voltages and currents, while some harmonics are brought on by non-linearity's in the system. Power electronic loads like diode bridge rectifiers and adjustable-speed drives generate harmonics. Due to the fact that harmonics are often the 3rd, 5th, and 7th multiples of 50 Hz, the significant harmonics research are interested in frequencies below the range of human hearing [76].

When steady-state harmonics are present, currents and voltages can be represented by a Fourier series with the following structure:

$$V_{(t)} = \sum_{k=1}^{\infty} V_k sin\,(k\omega_0 t + \delta_k) \tag{2.28}$$

$$i_{(t)} = \sum_{k=1}^{\infty} I_k\, sin(k\omega_0 t + \theta_k) \tag{2.29}$$

RMS values for the voltage and current:

$$V_{rms} = \sqrt{\sum_{k=1}^{\infty} \frac{V_k{}^2}{2}} = \sqrt{\sum_{k=1}^{\infty} V_{krms}{}^2} \tag{2.30}$$

$$I_{rms} = \sqrt{\sum_{k=1}^{\infty} \frac{I_k{}^2}{2}} = \sqrt{\sum_{k=1}^{\infty} I_{krms}{}^2} \tag{2.31}$$

$$P_{avg} = \sum_{k=1}^{\infty} V_{krms} I_{krms} cos(\delta_k - \theta_k) \tag{2.32}$$

Where the harmonics contribute, either positively or negatively, well to power average

$$pf = \frac{P_{avg1}}{V_{1rms}I_{1rms}} \times \frac{1}{\sqrt{1 + (^{THD}/_{100})^2}} = pf_{disp} \times pf_{dist} \tag{2.33}$$

The equations used above determine the true power factor and displacement power factor in the stand-alone system.

2.11 Different solution to the mitigation of harmonics within PV system

This section will discuss the types of filter design that are intended to reduce overall harmonic distortion. The easiest method is to employ passive filters made to block off the desired frequencies. A better tactic is to use active filters that inject compensation currents to counteract the harmonic effect. Hybrid filters are filters that incorporate both active and passive technology.

2.12 Kalman Filter

Based on a series of observed measurements taken over time, the Kalman filter is a technique that generates estimates of some unknown states or variables [77]. This approach is sometimes known as the linear quadratic estimate in statistics and control system theory (LQE). It bears the name of Rudolf Kalman, one of the original proponents of the theory [77]. Despite its difficulty in terms of comprehension and execution for people who are not familiar with estimate theory, the Kalman filter is a straightforward form that uses little computational power. Many different domains, such as object tracking, navigation, computer vision and others, have embraced the Kalman filter. Loud systems are typically managed with it. The Global Positioning System (GPS), a satellite-based navigation system that provides users with precise and accurate positioning information, is arguably the most well-known Kalman filter real-world application [77-79].

Based on the significant Kalman filter uses previously stated, this literature presents the use of the Kalman filter for THD reduction in PV system. However, one should first be familiar with the mathematical structure of the Kalman filter.

2.12.1 What the Kalman Filter Means in Mathematics

In linear dynamic systems, Kalman filters are used to estimate states based on the systems' representation in state space format. The system state is represented as a vector of real values, while the process model describes the evaluation of the state from the current time instance to the following one as follows:

$$X_j = AX_{j-1} + B\boldsymbol{u}_j + w_j \tag{2.34}$$

$\boldsymbol{A}$ Is the state transition matrix applied to the prior state vector, $\boldsymbol{B}$ is the input matrix gain applied to the control vector,u_j, and w_j is the process harmonic, where X_{j-1}, X_j are the state vectors at the current j and initial $j-1$ time occurrences. The relationship between the states and the measurements at the present step in time is expressed by an output equation in addition to the state equation (2.35), which is above[80]

$$z_j = HX_{j-1} + V_j \tag{2.35}$$

Where H it is a matrix gain of output, V_j is a measurement harmonic, and Z_j is the output vector on the current instance j. According to the system's knowledge, the primary function of the Kalman filter is to offer state estimation at the present time instance, the initial state estimation, and a number of measurements. Usually, two phases predict, and updates are used to do that. During the forecasting phase, the priori state estimate is created using the base model from the previous time step. The current time step's state is estimated [80, 81]. The state estimate is improved and corrected throughout the update phase by combining the most recent priori estimate with the most recent observational data. The posteriori state estimate is another name for this updating procedure. Below are the predictor equations:

$$\hat{X}_{j-} = A\hat{X}_{j-1} + B\boldsymbol{u}_{j-} \tag{2.36}$$

$$P_{j-} = AP_{j-1} + A^T Q \tag{2.37}$$

where $\hat{X}_{j-}$ and $\hat{X}_{j-1}$ are the most recent priori and posteriori estimates of the states; P_{j-} and P_{j-1} are the errors of a posteriori and priori transformation matrix; T denotes the matrix's transposition; and Q is the measurement harmonic linear correlation. This can be used as an adjustment factor to get the performance one wants. Equations for phase improvement were made as follows:

$$\hat{X}_j = \hat{X}_{j-1} + k_j(Z_j - HX_{j-}) \tag{2.38}$$

$$k_j = P_j H^T (R + H P_{j-} H^T)^{-1} \quad (2.39)$$

$$P_j = (1 - k_j H) P_{j-} \quad (2.40)$$

$$y = Z_j - H X_{j-} \quad (2.41)$$

Where I is the identity matrix; -1 an inverse matrix, y is a measurement of a residual; R is the process harmonic covariance, which can be utilized as a tuning parameter to perform its function; and k is the Kalman gain.

Figure 2.13 illustrates the suggested technique for reducing the accumulated THD and cleaning up the noisy current based on the Kalman filter. The required filtered current was expected to be represented by a single state in the state vector [82, 83]. The distorted current is one of the elements that make up the measurement vector at the same time. Depending on that phase transformation matrix, $\boldsymbol{A}$ will only contain one element, just like the other matrix in the predict and inform phases. The input vector $\boldsymbol{u}$ was set to zero because there is no outer input that could alter the expected phase or state [81, 84]. The THD reduction process flow-chart is displayed in Figure 2.13 as follows:

From the photovoltaic system's output, load the distorted current signal. The harmonics measurement that needs to be filtered is the distorted current.

Their levels can range from 0 to 1. Therefore, find the covariance matrices of the process R and measurement Harmonic Q. To get the required outcomes, they can be utilized to fine-tune the filtering performance.

Set the state, output measurement, residual, pre and posterior covariance errors, as well as the Kalman gain, to their initial values.

To the nth measurement, apply the nth distorted current sample.

Calculate the priori state estimate and priori covariance error using the predictor equations.

Correct the Kalman gain values using the predictor equations, and then calculate the posteriori state estimation, residual and posteriori covariance error.

Again, until the complete harmonic measurement (distorted current/voltage) has been recorded, repeat step 4 to 6.

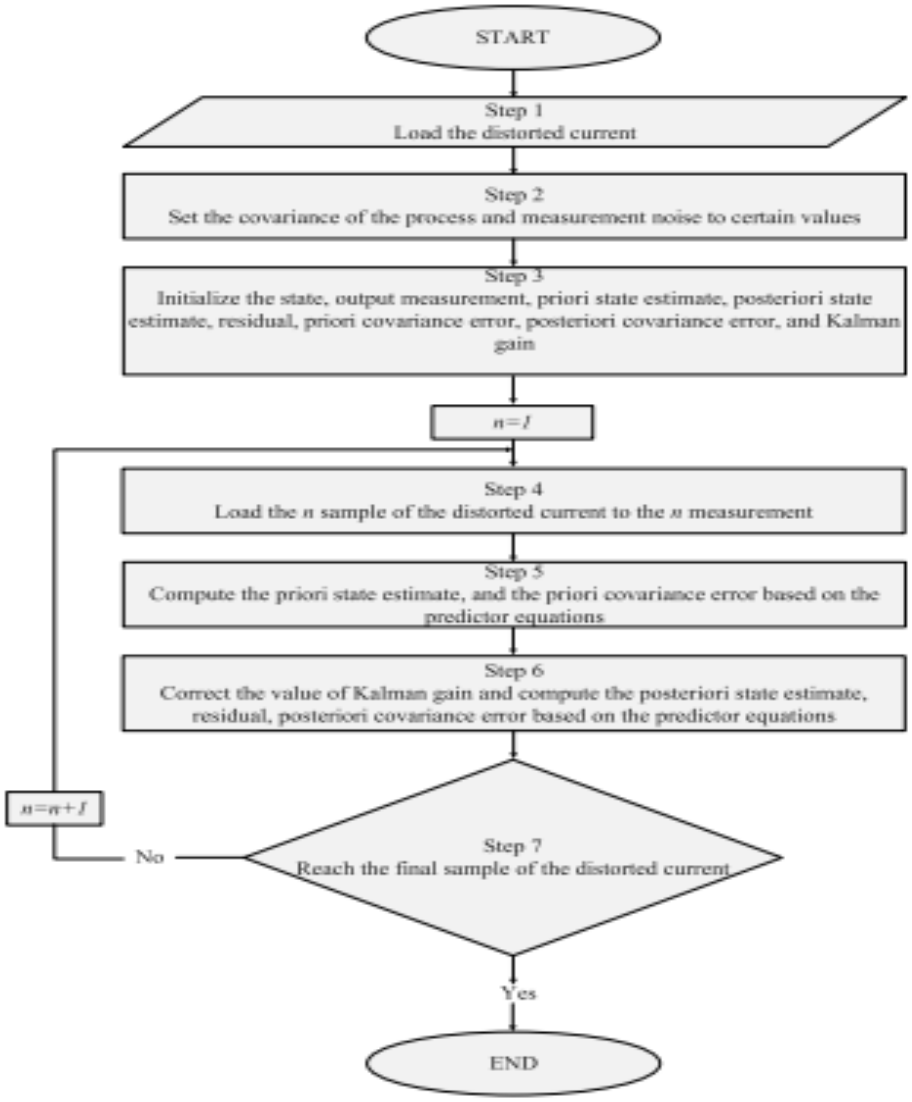

Figure 2. 13: Flow diagram for Kalman filter based on THD reduction [81]

The Kalman filtering method for lowering THD in PV systems: The distortion output current of a single-phase standalone PV system was determined again from readings as waveforms. The Kalman filtering technique was used to filter out harmonic current and mitigate the total harmonic distortion over time [25, 80, 82].

2.13 Harmonic Mitigation Filter Design Features

Due to the switching signals, the current and voltage outputs of an inverter typically include a significant amount of harmonic distortion. In addition to using a higher switching frequency to

reduce the harmonics, a filter can be used to filter out all high-frequency harmonics distortion. Filtration is formed and utilized to eliminate the high-frequency harmonics distortion from the output power converter. The passive filter is one method designed to reduce harmonics in a PV system. The effects of the LC filter, L filter and double-tuned filter design features on overall harmonic mitigation are compared in this research project. The initial findings from the off grid/standalone PV application with LCL along with $LLCL$ are designed using the LC filter [8, 21, 30].

The LC Low pass Filter is utilized to deliver an output voltage that is completely sinusoidal. In a standalone PV system, it is situated between the inverter and the load. It is anticipated that the voltage drop across the inductor will not exceed 3% of the inverter output voltage V_O when a second order LC filter with an inductance value L that eliminates all high order harmonics is used [85].

$$2\pi f_O L I_{Lmax} < 0.03\% \times V_O \tag{2.42}$$

The filter capacitance value C is then determined using the variables,$I_{L_{max}}$,V_O, and f. $I_{L_{max}}$ Is the maximum Root Mean Square load current, Vo is the inverter output V_{RMS} value, and f is the Load frequency of 50 Hz. The resonance relation is then used to calculate,C, as shown in equation (2.43):

$$C = \frac{1}{(2\pi f_O)^2 L} \tag{2.43}$$

at which f_o is the frequency cut off.

Equation represents the LC filter transfer function (2.44)

$$G_{tf} = \frac{V_{OUTPUT}}{V_{INPUT}} \tag{2.44}$$

V_{in} is the LC filter circuit's input voltage, and the output voltage generated by the PV through converters with an LC filter is V_{OUT}. The voltage - divider rule is used.

$$V_{OUT} = \frac{Z_{LOAD}}{1 + j\omega Z_{LOAD}} \tag{2.45}$$

$$V_{in} = \frac{Z_{LOAD}}{1 + j\omega Z_{LOAD} C} \tag{2.46}$$

$$G(j\omega) = \frac{1}{1 + LC(j\omega)^2 + j\omega \frac{L}{Z_{LOAD}}} \tag{2.47}$$

Z_{load} represents the impedance of the load connected to the off-grid PV generation system. The value for the LC filter is calculated using equation (2.48) where f_{sw} is the switching frequency of the converter. 5% of the rated current is the maximum ripple current limit [86].

$$L = \frac{V_{in}}{8 \times \Delta ripple f_{sw}} \tag{2.48}$$

The inductance L should be as low as possible due to its large capacity. The output impedance is likewise kept low with a low inductance L value. A key component in the design of a passive LC filter is the capacitor's appropriate size. The capacitor in the LC filter acts as a low resistance connection to ground, dampening harmonics. The quantity of reactive power absorbed by the LC filter determines the capacitor's rating [86]. To prevent excessive currents that could harm the switching devices, the capacitor should be tuned to offer a decent power factor at the fundamental frequency while remaining suitably low. Equation (2.49) involves determining a capacitor value popular for the LC filter in an off-grid PV system's LC filter [86, 87].

$$C = \frac{\alpha P}{2\pi f V^2} \tag{2.49}$$

α is a reactive power factor, which often falls below 5% [86]. P is a system rated power, ff_L is a line frequency and V is the system rated voltage. Equation gives LC filter's f_r resonant frequency (2.50):

$$f_r = \frac{1}{2\pi\sqrt{LC}} \tag{2.50}$$

The LC filter's resonance frequency is kept lower than the inverter switches' switching frequency. At a lower resonant frequency, high frequency harmonics are better dampened.

In the inverter topologies, a LCL filter is utilized in place of the L filter to mitigate harmonic current [86]. However, due to $LCL's$ capacity for resonance and capability for causing voltage harmonics, it demands a very rigorous approach to parameter availability and control [69]. To minimize fundamental component errors, Proportional-integral (PI) controllers are employed in LCL filters. Minimizing the efficiency of non-linear loads and mitigating harmonic distortion are critical in terms of power quality. Filters are circuits formed of inductor (L), capacitor (C) and, in some uncommon circumstances, resistance (R) components that are installed in the middle of the solar inverter along with the non-linear /linear load. They are designed to remove harmonic components that are not a part of the fundamental frequency [88, 89]. In comparison to an active filter, a passive LCL filter has several advantages, including stability assurance, null, void power draw, cost - effectiveness, and then conventionality. The passive LCL filter is especially important in reducing system harmonics for relatively high Standalone PV quality energy [90].

The following qualities must be present in an LCL filter:

- The chance of a drop across the filter is reduced;
- There must be a decrease in the energy collected; and
- A capacitance decreased the reactive power of the system.

The inverter side inductor's high value is required for ripple refraction. However, it does impose price, weight and size restrictions. A high-value capacitor is needed to tolerate the considerable ripple current. A high value, on the other hand, may degrade a power factor within a system. It is really challenging to develop an LCL filtration that satisfies all the requirements (standards). The low cost of the LCL filter is intended to eliminate harmonics in the system. This filter's design delivers a good stability margin, high dynamic responsiveness, and adequate reactive power compensation. The resistance is ignored in order to consider it in the worst-case scenario [88].

The overall power quality of the electricity generated by the off-grid PV system is enhanced and ensured by these devices/passive filters. This is the LCL principal diagram in Figure 2.14.

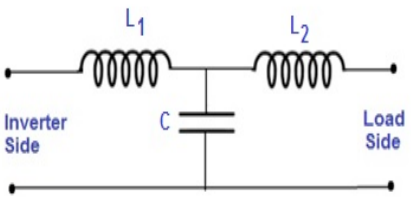

Figure 2. 14: LCL filter modelling with inverter side and load side [88]

A solar inverter is connected in a load with a LCL filtration between, which filters the harmonics component the solar inverter produces. A passive LCL filter is utilized in Standalone power systems to reduce harmonics and improve power quality. This filtration works by altering the L-C passive elements to remove harmonic components from the load side. It is necessary to employ the *LCL* filter to maintain the harmonic components within the boundaries stated in the standard, thus the *LCL* filter must be utilized [90].

The Transfer function of the *LCL* filter is defined in equation (2.51):

$$G(jw) = \frac{1 + Z_{load} jwC}{L_1 L_2 C(jw)^3 + (L_1 + L_2) Z_{load} C(jw)^2 + (L_1 + L_2) jw} \tag{2.51}$$

Z_{load} represents the load's impedance when it is connected to an off-grid solar power system. To prevent resonance issues, the resonance frequency needs to fall between the following frequency ranges:

$$10 f_L < f_{res} < 0.5 f_{sw} \tag{2.52}$$

f_L Is the load frequency

f_{sw} Is the switching frequency

f_{res} Is the resonance frequency

The resonance frequency of LCL filter is defined in equation (2.53):

$$f_{res} = \frac{1}{2\pi} \times \sqrt{\frac{L_1 + L_2}{L_1 L_2 C}} \tag{2.53}$$

Reactive power absorbed by capacitor is defined in equation (2.54):

$$Q_C = \frac{3{V_{rated}}^2}{X_C} = \frac{3{V_{rated}}^2}{\frac{1}{\omega C}} = 3(2\pi f) C {V_{rated}}^2 \leq \alpha P_{rated} \tag{2.54}$$

Below is an equation that provides the magnitude of the capacitor used in the LCL Filter (2.55):

$$C = \frac{\alpha P_{rated}}{3(2\pi f){V^2}_{rated}} \tag{2.55}$$

In applications, a third-order $LLCL$ filter is less in size. This filter still has a resonance frequency issue, though. Equation is used to determine the THD_i value, which rises at low switching frequencies any time a little amount of filter inductance is used at the inverter output L_1 (2.56). The value of the inductor L_1 on the inverter side is determined by the maximum permitted current ripple. A maximum of 20% of the current evaluated range should be the current ripple. (condition1)

$$L_1 = \frac{V_{DC}}{4 \times f_{sw} \times \Delta I_{ppmax}} \tag{2.56}$$

The maximum voltage drop across the inductor determines the total inductance ($L_1 + L_2$). The maximum map is limited to 10% of the rated voltage (condition 2).

$$V_{L1+L2} = (I)(X_{L1+L2}) \tag{2.57}$$

$$=(\mathrm{I})\ (2\pi f(L_1 + L_2)) \tag{2.58}$$

$$(\mathrm{I})\ (2\pi f(L_1 + L_2)) = 10\%\ of\ V \tag{2.59}$$

$$(\frac{S}{V})\big(2\pi f(L_1 + L_2)\big) = 10\%\ of\ V \tag{2.60}$$

$$L_1 + L_2 = \frac{0.1\ \times {V^2}_{rated}}{(s)(2\pi f)} \tag{2.61}$$

$$L_2 = \frac{0.1\ \times {V^2}_{rated}}{(s)(2\pi f)} - L_1 \tag{2.62}$$

A design methodology for an LCL passive filter for load-intersected solar inverters, as well as a thorough investigation of harmonic component mitigation. Between the source and the load, passive LCL filters are positioned with the intention of obliterating any additional components. Risks associated with these filters include serial and parallel resonance. For each harmonic component, resonance conditions must be computed separately. Using passive dampening techniques, precautions can be taken to reduce this danger [32, 91]. Harmonics are unwanted

network magnitudes because they have an impact on every component of the system. As a result, filter circuits must be set up immediately to eliminate harmonics. The electrical network has filters installed for this purpose. The usage of filters that are band pass and high pass is common. By balancing the system's capacitive and inductive impedances, resonance develops in the circuit. As a result, the power system cannot fully utilize ohmic character.

To ascertain how harmonics affect the system waveform and what kinds of problems will be rectified, simulations are done. As a result, in this research project, a passive LCL filter was used to reduce harmonics in power systems [32, 91, 92]. Higher order harmonics can have an impact on the entire system. These effects have a negative impact on the functionality of the energized electrical system. The performance within a designed passive LCL filter was evaluated using the MATLAB/Simulink program. Harmonics from non-linear loads must not oscillate with the power system. Resonance features of each harmonic component must be determined independently [93, 94]. A power system will resonate with any component when harmonics are introduced from harmonic sources [95].

Table 2. 1: THDI is affected by temperature and irradiance

Temperature (^{O}C)	Irradiance (W/m^2)	Total Harmonic Distortion for Current (THD_I)
15	1050	6,780
12	950	6,620
35	1200	7,24
20	880	6,77
22	1150	7,012
10	960	6,797
25	1000	7,083
20	1200	7,250
10	900	6,74

The use of a passive LCL filter to reduce harmonics and a standalone Photovoltaic configuration power quality should be improved.The THD_I has been well reduced from 91,52% to 6,778% [96]. Moreover, it is in used non-linear load systems, which meet the standards for current. The LCL filter design and performance analysis were carried out in this study [96, 97]. As a result, it has been discovered that the LCL filter performs well. Harmonics have numerous negative effects on power systems, including voltage waveform distortions, decreased system efficiency, and increased system losses. Single and three phase converters are important harmonic components in

energy systems. Several precautions can be taken to reduce them. These checks and balances are as follows:

- Expanded section with neutral conductors;
- Making use of K −factor transformers;
- Employing LCL filtration; and
- Employing high-pulse converters.

The total harmonic distortion of current was reduced with an LCL filtration device, and the THD_I value being reduced to less than 5%. Efficiency increased as system losses decreased. The output current waveform of a solar inverter is shown below:

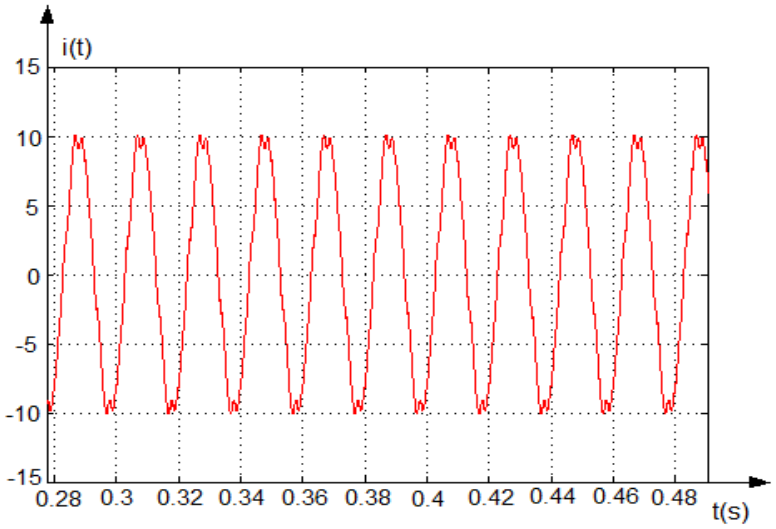

Figure 2. 15: Current inverter output [98]

When the total harmonic distortion exceeds the limits set forth in standards, LCL filters are employed to minimize the harmonic contents of the input current of controlled and uncontrolled rectifiers. Inductance current ripple, total filter impedance, reactive power produced by the capacitor, LCL filter resonance state, and a third order transfer function are some benefits and drawbacks of LCL filters [98].

2.13.1 LLCL PASSIVE FILTERS DESIGN AND ANALYSIS

This section discusses filters to enhance the quality of the power in PV stand-alone structures. The $LLCL$ filter has been extensively used in numerous renewable energy applications because of the tremendous global growth of renewable energy over the past ten years. Power electronic

components such as thyristors, diodes, MOSFETs and IGBTs generate harmonic currents that cause critical power quality issues in PV systems [2, 99].

In order to avoid facing high total harmonic distortion penalties levied by the utility operator, PV system operators may be forced to install larger, more expensive filters or even unplug their PV system from the grid when there is a high total harmonic distortion concentration. By using these non-linear components, the system's harmonic performance is increased. Moreover, the most important harmonic sources in an off-grid power system are rectifiers, inverters and DC/DC converters. This issue manifests itself near the resonance frequency. The frequency response of the LLCL filter is seen in Figure 2.16 [100].

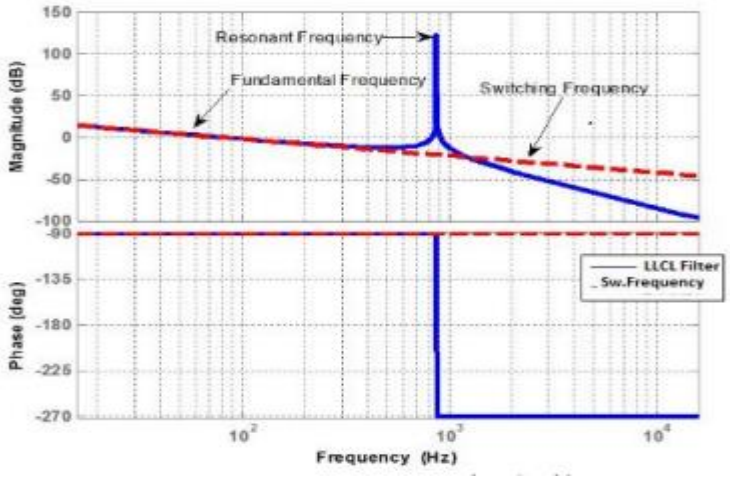

Figure 2. 16: LLCL filter Frequency response [2]

Harmonic levels can be adjusted by altering the current or voltage at one or more frequencies. Designs are generally created to maximize the effectiveness of harmonic components. The use of filters is motivated by both technical and economic factors. Its goal is to reduce the economic and technological costs associated with the damaging effects of harmonics on filters.

The $LLCL$ Passive filters are circuits composed of capacitors C_f, inductors L_1, inductors L_2 and inductors L_f that are installed between the loads and the solar converter [101]. As a result, they are intended to reduce harmonic components that exist outside of the fundamental frequency. Compared to an active filter, the passive LLCL filter has a number of benefits, including stability assurance, zero power consumption, low cost, and traditional design. Figure 2.17depicts the input voltage of a solar inverter.

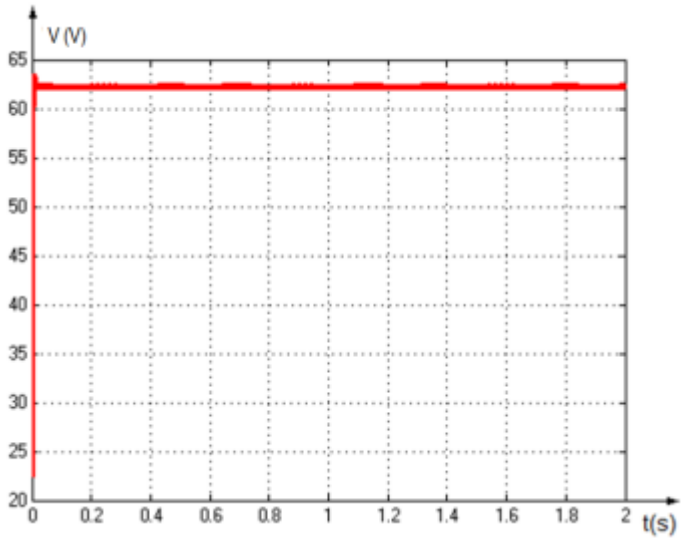

Figure 2. 17: Input voltage of solar inverter [101]

Regarding the load side of renewable energy sources such as wind and solar power, etc, passive LLCL-filters are typically utilized. The energy output of an off-grid PV system is enhanced and guaranteed by these technologies. The LLCL filter's schematic diagram is shown in Figure 2.18

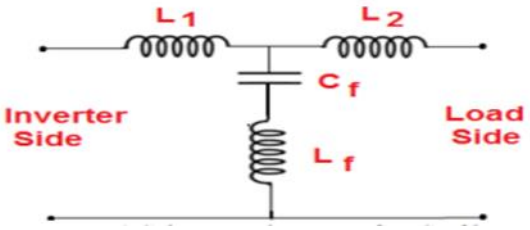

Figure 2. 18: LLCL filter schematic illustration [101]

For standalone PV systems, a passive LLCL harmonic filter should be properly constructed. When designing a passive LLCL filter, it is important to consider the solar system's authorized total harmonic distortion; the amount of reactive power needed in the system; the volume of harmonics produced by outside sources; the other loads in the system; and the schematic diagram of the solar system's output. Working values for the filter as well as the impedance altering for effective harmonics can be taken into consideration (frequency, temperature, voltage). A filter's fundamental frequency, also referred to as the reactive power it offers, determines its value. The amount of basic reactive power supplied by the capacitors is the same. The harmonic load should thus be located as near to the filter as viable [102, 103].

The harmonic current and voltage rise to exceptionally high peaks if the resonance event occurs in or close to one of these harmonic components. Therefore, altering the filter will change the resonance frequency. It is a helpful technique for enhancing the quality of power produced by an

off-grid PV system for an inductive $R-L$ load. The $LLCL$ filter circuit is made up of a capacitor C f, an inductance L_1 on the inverter output, and an inductance L_2 on the load side. Below is a equation of the $LLCL$ filter's transfer function:

$$G_{LOAD}(jw) = \frac{L_f C_f S^2 + 1}{\left[L_1 L_2 C_f + (L_1 + L_2) C_f\right] S^3 + (L_1 + L_2) S} \tag{2.63}$$

The $LLCL$ filter's frequency response should be selected from the range described in the equation (2.64). Whenever this range is selected within the off-grid solar system, there is no resonance.

$$10 f_L < f_{res} < 0.5 f_{sw} \tag{2.64}$$

f_L Is the load frequency.

f_{sw} Is the switching frequency.

f_{res} Is the resonance frequency.

The resonance frequency of the $LLCL$ filter is defined in equation (2.65):

$$f_{res} = \frac{1}{2\pi \times \sqrt{(\frac{L_1 L_2}{L_1 + L_2} + L_f) C_f}} \tag{2.65}$$

One could perhaps mitigate more harmonics by increasing, C_f. Yet the entire filter system's efficiency is decreased due to the higher reactive power and increased current demand from L_1. The equation below defines the reactive power absorbed by the capacitor (2.66):

$$Q_C = \frac{3{V_{rated}}^2}{X_C} = \frac{3{V_{rated}}^2}{\frac{1}{\omega C}} = 3(2\pi f) C {V_{rated}}^2 \leq \alpha P_{rated} \tag{2.66}$$

Under which Q_C stands for the amount of reactive power that the capacitor consumes. The effective phase voltage rated is V_{rated}. This is the rate at which reactive power builds up. The normal selection is as follows:

$$\alpha < 5\% \tag{2.67}$$

Three inductors and one capacitor are used in the $LLCL$ filter. The design's capacitor shunt component further lowers the switching frequency. The C_f value for the $LLCL$ filter is determined using the reactive power, Q_C, used by the filter under rated conditions (2.67). The C_f valuation for the $LLCL$ filter is determined through Eq. (2.68).

$$C = \frac{\alpha P_{rated}}{(3)(2\pi f) \times V^2{}_{rated}} \tag{2.68}$$

The current ripple is taken into consideration when designing the LLCL filter's inductors. Switching losses are decreased when low ripple current values are used. The amount of an inductor, on other hand, appears to be growing. The following equation defines the value of L_1 in the LLCL filter (2.69):

$$L_1 = \frac{V_{in}}{8 I_H f_{res}} \tag{2.69}$$

Where V_{in} is the inverter's input voltage and the ripple current, I_H, should not exceed 5% of the rated current. Equation (2.67) and (2.69) identifies the relevance of L_2 (2.70):

$$L_2 = \frac{L_1}{\alpha} \tag{2.70}$$

In this equation, α is the inductance ratio factor. For low- and medium-power applications, this coefficient is set to be bigger than 1. Between the source and the load, passive $LLCL$ filters are implemented with the goal of removing extraneous parts from the fundamental component. These filters include drawbacks such as fixed filtering frequencies, parallel and series resonance, and huge volume.

$$L_f = \frac{1}{C_f f^2{}_{sw}} \tag{2.71}$$

Harmonic orders of magnitude are undesirable in the system, even though they affect all parts of the system. As a result, it is an electronic circuit. High-pass and band-pass filters are often used.

2.13.2 Implications of Filters

Passive filters have been employed in a wide range of devices. Nevertheless, employing passive filtering has several disadvantages [13, 104], namely:

- Those same filters are so constrictive that they do not acclimatize to changes in the system. Once installed, the size or optimization frequency cannot be easily changed.
- If the expected operating conditions change, the filter could become detuned, resulting in distortions. Furthermore, unless there is online monitoring, this risk cannot be easily tracked.
- The source impedance of the filter is important when designing an optimal filter since the filter needs to have a lower impedance than the source. As a result, there is reactive power over-compensation and an unrealistically huge filter with a low source impedance.

THD_v detrimental impacts include interruptions, battery heating, cable warming, and inefficient electrical energy use. Electronic components or circuitry that convert direct current to alternating current are known as converters [105]. Solar inverters' output voltage waveforms contain harmonic components since they are not sinusoidal. In low and medium power applications, square wave output voltage is acceptable, whereas sinusoidal waveforms are required in high power applications. [105]. Systems for power distribution can survive persistent fundamental frequency currents and voltages. Even so, the presence of non-linear loads causes massive harmonic current distortions, resulting in current and voltage distortion.

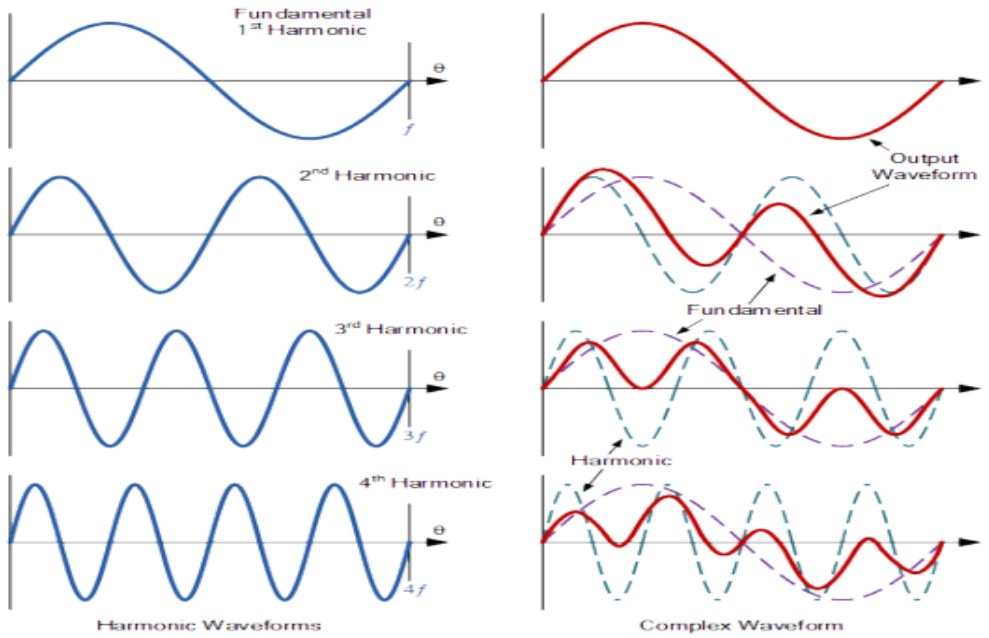

Figure 2. 19: Harmonic-induced simplified waveforms [106]

The above-depicted red waveforms are real waveform shapes that are appropriate to apply to the harmonic content that is being supplied to the frequency response. The first harmonics waveform is also known as the basic waveform. As can be seen in the column on the left, the second harmonic has a frequency that is twice as high as the core principle; the third harmonic has a frequency that is three times as high as the core principle; and the fourth harmonic has a frequency that is four times as high as the core principle. In the column on the right, complex wave configuration caused by the interaction of both the harmonic and fundamental waveforms on varied harmonic frequencies is being shown. It is noted that the shape of the extracellular and intracellular waveform is determined by the phase relationship between both the fundamental or base frequency and the multiple harmonic frequency distribution, as well as their number and amplitude. As can be seen, a complex wave is mostly made up of harmonics, each of which has a unique peak value and phase angle.

Boost converter inverters are an essential component of the vast majority of Photovoltaic network implemented for stand-alone and grid-connected technologies [107, 108]. The alternating current (AC) output produced by such power converters employs a sinusoidal pulse width modulation (PWM) technique, which results in high-speed switching of semiconductor materials and generates harmonics and high switching losses. To mitigate the PWM carrier, a low-cost passive filter is inserted between the inverter and the load or grid.

IEEE standards require harmonic content of power signal to be low than 5%. Previously, on the AC side of PWM converters, first-order passive L type filters have been employed to mitigate switching harmonics. Moreover, due to its inherent large size, the L filter is limited in low switching frequency applications [108]. A higher order LC or LCL filter gives more harmonics subversion at lower switching frequencies and a reduced overall filter size. As it can produce high frequency harmonic modulation with the same inductance value, the LCL filter is more desirable than the L filter [109]. On the other hand, these higher order filters result in a resonance between the converter and the grid or load demand that needs to be dampened using either active filters or a load [110, 111] or passive filters [112]. Active damping techniques are flexible because they use a smart control scheme to suppress the resonance. However, they remain restricted through their significant expense, and development is significant, with the inclusion of further sensors. The cost of passive damping systems is lower, less complicated and more trustable [100, 113].

The $LCL - LC$ filter, a revolutionary high-order power filter, is recommended at Figure 2.20 towards further lowering on a load-side inductor L_2 and establishing a rate of decrease of -60dB

at extreme frequency. The $L_f - C_f$ series resonant circuit is connected in parallel with an additional capacitor C_d as opposed to the $LLCL$ filter. It has been proposed to use an additional capacitor linked in parallel to the $LLCL$ filter's $L_f - C_f$ series resonant circuit [114, 115]. The $LCL - LC$ filter, in contrast to the $LLCL$ filter, can maintain almost zero impedance at the operating frequency and can significantly attenuate the current harmonics nearby the operating frequency, with the decrease rate reaching $-60dB$ on frequency range. This enables a load inductor L_2 to be reduced even further. The basic parameter selection process and, additionally, a proposed $LCL - LC$ filter characteristic configuration, are provided. It is apparent that the $LCL - LC$ filter's load-side inductor L_2 is determined primarily by harmonic components. Since the modulation rate at high frequency of the $LCL - LC$ filter is superior to that of the $LLCL$ filter, the constraint of the $LCL - LC$ filter is in fact comparatively less significant than that of the $LLCL$ filter. This is because the amplification rate at high frequency of the $LCL - LC$ filter is considerably larger than that of the $LLCL$ filter. [5, 116, 117].

The harmonic current peak value at the operating frequency in an LCL-LC filter is nearly equal to zero. It establishes that the damping resistor has no effect on the provided filter's potential to bypass switching current harmonics [116, 118, 119]. The LCL-LC filter's second/third switching frequency of the harmonics currently have smaller amplitudes than the trap filters. This demonstrates that the provided filter attenuates high-frequency harmonics more quickly than a trap filter [120].

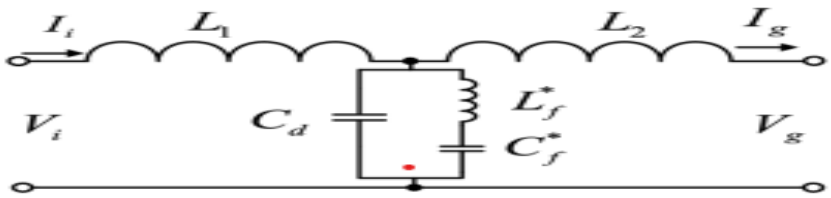

Figure 2. 20: LCL-LC FILTER

As shown in Figure 2.20, the $LCL - LC$ filter is a five-order circuit. The $LCL - LC\ filtertation$ developed after the LCL filter, bringing together the $LLCL$ and LCL filters' benefits. An LCL-LC filter's transfer function between converters' voltage and load-side current is depicted in (1). As shown in Figure 2.21 a calibration the $LCL - LC$filter's graphs could be acquired. To fully utilize the generally pro peaks of f1, f2 and f3, the LCL-LC filter can really be constructed with comparatively little passive components, massively decreasing system heaviness, amplitude, as well as expense.

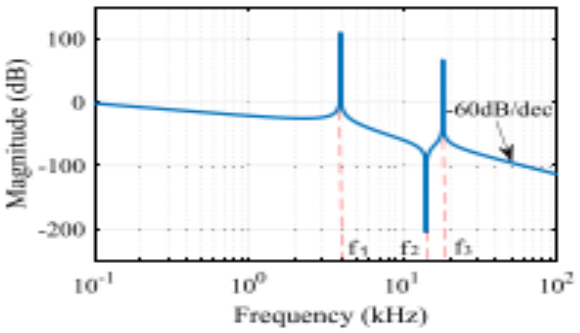

Figure 2. 21: The LCL - LC filter's vibrational annotations [121]

One of the biggest problems with power lines is harmonics, which arise from the widespread use of power electronics in daily life and their consequent growth in magnitude. Harmonics are another factor that must be considered in the renewable energy supply, notably in the PV array system [121, 122].

Harmonics are mostly produced by non-linear loads, including IT loads, UPS systems, variable speed drives, and others. Harmonics are created by drawing current from the natural world, or a reverse phenomenon like a wave. If the total harmonics generated exceed the IEC and IEEE 519 standard limit, there is a serious risk of interference. Harmonic levels that are too high risk shortening [122, 123].

Studies on the harmonics in the PV array will therefore clearly be needed to provide the methodology for harmonics mitigation that is in line with the new approach of contemporary harmonic sources [124, 125]. There are several methods in lowering the harmonic distortions, subject to financial constraints, and research on the type of load's viability that also analyzes the load profile, also the most commonly used reducing strategies for total harmonic distortion [12, 27, 55, 126, 127].

2.14 Conclusion

Electric utility companies and their customers are increasingly concerned about the quality of the electricity they supply. As current industrial technology advances, so does the use of renewable energy sources. However, non-linear loads from renewable energy sources, such as solar and photovoltaic energy introduce harmonic distortions into the power system and make electrical equipment less safe to operate. As a result, mitigating these harmonics is critical. This research

examines the effect of photovoltaic (PV) systems on the quality of power in distribution networks. Harmonics are primarily produced by power converters in a PV system. This research looks at the PV distribution system and discusses a method for reducing harmonics.

The effect of harmonics is demonstrated using a test distribution system in conjunction with a MATLAB-built PV system. To reduce the impact of harmonics, the filters are sized and placed using MATLAB tools. Much of the literature has concentrated on the design of the filter for mainstream. There are few supply voltage converters and multiple inverter filter configurations. The solutions that this study suggests can help with the challenges, with an LCL and LLCL passive bandpass filter for a pulse generator frequency modulation inverter used in loading conditions. Due to its ability to provide high-frequency harmonic attenuation and its inclusion of values like the L filter, the LCL filter is considered to be more desirable than the L filter. A LC filter (second-order) is used to prevent distortion in PV renewable energy.

The LC filter is outperformed by LCL and LLCL filter. Even though the filter has a low output Load at high frequencies, high frequency harmonics cannot be suppressed since the capacitor is linked in parallel with the coil. As a result of the switching signals, the output current and voltage of a converter typically contain a high number of harmonic components. In addition to selecting a significantly greater frequency deviation to mitigate frequency response, utilizing filter, the spectral harmonic component can be removed. One method for reducing harmonics in a system is to use a passive filter. The LCL and LLCL filtration will be designed on MATLAB in this study. The filter's effects on total harmonic mitigation will be compared. To design the LLCL filter, early findings from the standalone PV system with LCL filter are taken as a guide. In addition, passive LCL and LLCL filters would be designed and implemented to mitigate harmonics in the standalone system and non-linear loads.

In terms of performance and reliability, this chapter compared single-phase ZSIs to single-phase VSIs and CSIs. Thereafter, the fundamental design ideas of a single-phase ZSI, passive filters, and PWM control approaches were highlighted. Their fundamental concepts serve as the foundation for the construction of Chapter 4. The third chapter addresses the methodological strategy that was employed to attain the research study's objectives.

Chapter Three: Modelling and Simulation

3.1 Introduction

This chapter describes the methodological strategy employed in this research study to achieve the aims and objectives described in Chapter 1. As stated earlier in Chapter 1, the purpose of this research study is to investigate the performance response of a Harmonics components and analysis the inverter in different PWM control techniques are applied to it while varying the input variables, and to apply what was learned from the previous study to create a new inverter architecture that outperforms a traditional Z-source inverter for a single-phase PV system.

The literature review focused on the background theory and design principles of a stand-alone PV system, single-phase passive filters, inverter operation and PWM control techniques.

This research is based on harmonics. Moreover, research on different types of the PWM control techniques believed that there can also be a study which can improve the waveform within the Stand-alone photovoltaic system.

A structured approach was used for achieving the aforementioned goal, which included the following steps:

- Reviewing of Literature;
- Design of Single-phase Photovoltaic system;
- Design of Passive filters for Stand-alone PV system;
- Design of Single-phase Z-inverter;
- Design of PWM Control Techniques;
- Result collection and Analysis of results of UI and ZSI; and
- Conclusion.

3.2 Literature Review

The review of literature focused on the background theory and design concepts of a stand-alone system with a Universal Bridge, Z-source inverters, single-phase filters, and PWM control approaches. Regarding inherent operational dependability and output power quality, ZSIs were compared to classic inverter topologies (VSI and CSI). Particular attention was devoted to various uses already in the business and future directions of ZSIs, thereby justifying the need for this dissertation.

The calculations for the step-up booster will be presented in Chapter 4 (4.1.1), while specific formulas about this topic were discussed in Chapter 2. In Chapter 4 (4.1.2.1), the analysis of Solar Panel protection will be conducted, specifically focusing on the technical aspects of connecting the Solar Panels with electrical safety. The protection strategy employed was based on zone protection, wherein 29 parallel solar panels and 8 series solar panels are utilized. Consequently, the protection measures will be implemented for each individual line consisting of 8 series solar panels. However, implementing the protective measures on 4 series solar panels may result in a significant increase in costs. The consideration of Maximum PowerPoint Tracking (MPPT) was undertaken for the purpose of future design, as this system can be effectively implemented.

3.2 Design of Single-Phase Photovoltaic System

The stand-alone PV system design encompassed various specifications: The system is designed to operate with a DC voltage input of 290 V. The switching frequency is set at 10 kHz. The solar irradiance can vary within the range of 0 Wm^2 to 2000 Wm^2. The temperature range for operation is between $0°C$ to $100°C$. The power rating of the system is 2000 W.

The selected power rating of 2000 W is relatively low, as it has been chosen with the intention of accommodating future considerations for the potential implementation of a practical prototype of a stand-alone photovoltaic (PV) system. During the implementation phase of the prototype program, the achievement of this power rating will be achievable without incurring excessive costs as it will necessitate the utilization of low-power-rated components. The circuitry of a stand-alone photovoltaic (PV) system comprises four primary stages, as depicted in the block diagram illustrated in Figure 3.1.

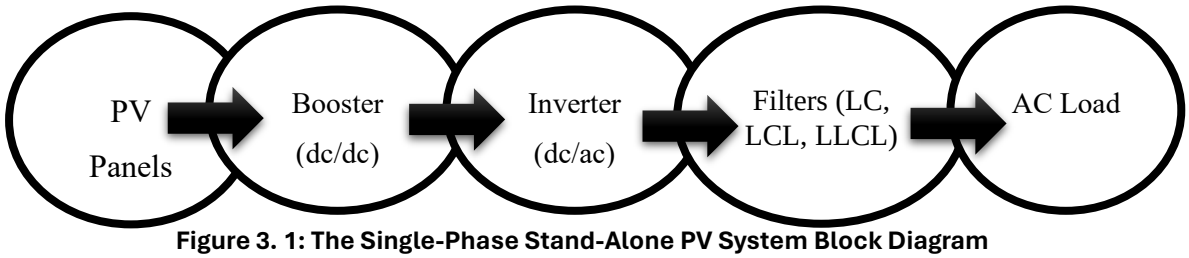

Figure 3. 1: The Single-Phase Stand-Alone PV System Block Diagram

The design of the Photovoltaic Panels was successfully accomplished in Section 4.1.2 of Chapter 4. Similarly, the design of the Booster was achieved in Section 4.1.1. The inverter, on the other hand, was extensively discussed in Chapter 2 of the thesis. Lastly, the design of filters was comprehensively covered in section 4.1.4.1. An extensive literature review derived the equations employed in a Stand-Alone Photovoltaic (PV) system.

3.3 Design of a Single-phase Z-Source Inverter Circuit

The ZSI Circuit Design is characterized by a specified input voltage range of 200 V to 500 V. All remaining parameters were held constant in accordance with the single-phase Photovoltaic system described in section (3.2). A research study was conducted with an input voltage range of 200V to 500V, which was determined based on the findings of reference publications reviewed during the literature investigations.

Moreover, the utilization of a voltage range spanning from 200 V to 500 V effectively emulates a practical scenario encountered in renewable energy systems, wherein the characteristic direct current (DC) output voltages of devices like photovoltaic cells or arrays tend to be relatively low. In each design of PWM control techniques, a solitary triangular carrier wave is used. Figure 3.2 displays the block diagram of the Impedance Source Inverter (ZSI) design, which encompasses a total of six primary steps within the block diagram.

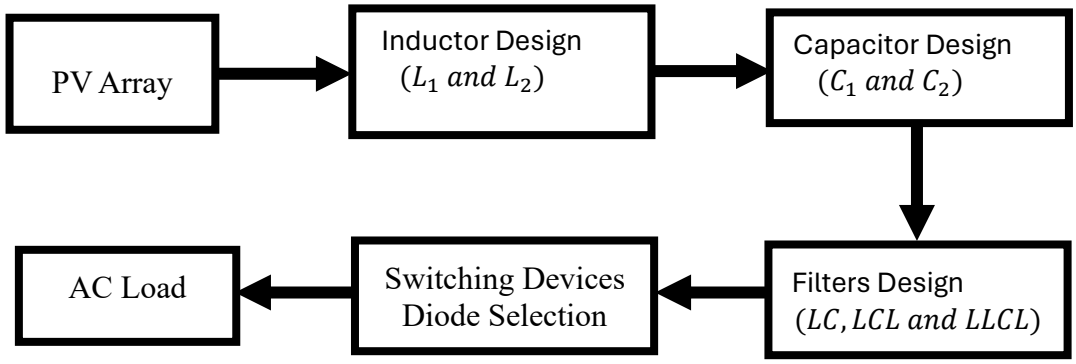

Figure 3. 2: SINGLE-PHASE Z-SOURCE INVERTER BLOCK DIAGRAM

The design of the Impedance Source inverter (ZSI) was successfully accomplished in Section 4.3. It is structured into six distinct components, with the initial and final components being discussed in Figure 3.1. The design of the inductor was successfully accomplished using the methodology outlined in Section 4.3.1, while the design of the capacitor was successfully achieved using the methodology outlined in Section 4.3.2. The process of selecting the appropriate switching devices and power diode was successfully accomplished in Section 4.3.3. The equations developed in the ZSI circuit design were derived from a comprehensive literature review. The design process as depicted in Figure 3.3 led to the complete development of a circuit design, specifically illustrated, accommodating a 2kW load with passive filters. For further reference, Appendix A1 to A7 provides additional insights into the designed circuit incorporating passive filters.

3.4 The Design of PWM Control Techniques

During the process of conducting a comprehensive literature review, it has been observed that there exist two predominant Pulse Width Modulation (PWM) control techniques, which have been frequently outlined. It is worth noting that several other PWM control techniques have also been reported, often deriving their foundations from these primary techniques. Therefore, this research study incorporates two PWM Control Techniques, namely Constant Boost Control (CBC) Pulse Modulation Width (PWM) and Simple Boost Control (SBC) Pulse Modulation Width techniques [65, 77]. Figure 3.3 depicts a comprehensive block diagram illustrating the fundamental components of the two Pulse Width Modulation (PWM) Control Techniques.

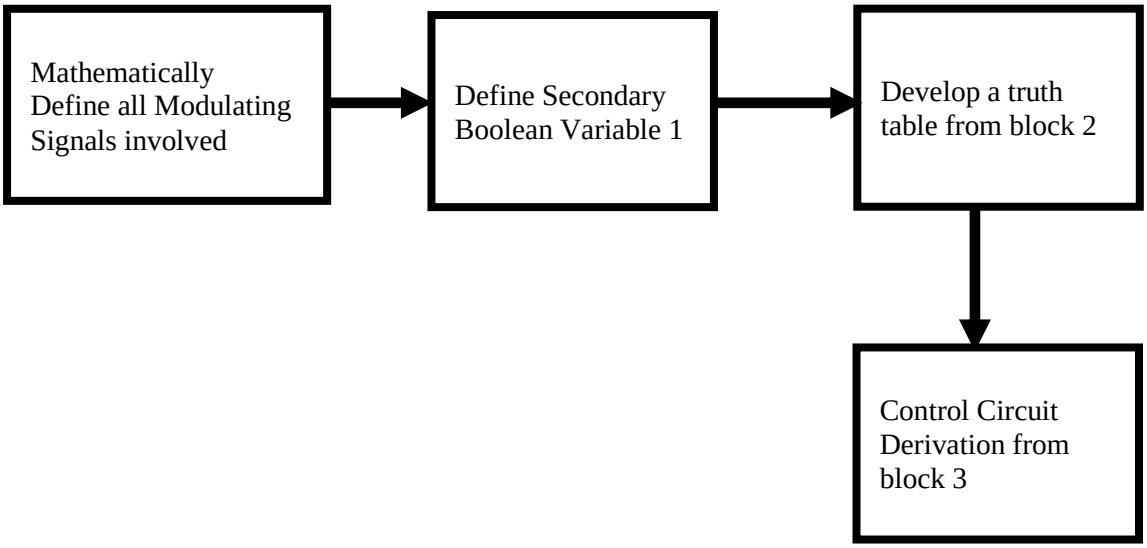

Figure 3. 3: BLOCK Diagram design of PWM Control Techniques

The first block in Figure 3.3 presents the mathematical definition of modulation signals for PWM control techniques. The proposed system consists of a fundamental single-phase reference waveform, Vac, which is injected with a third harmonic component, $V_{ac\text{-}3rd\text{-}injected}$. Additionally, a triangular carrier waveform is utilized, along with two constant voltages that envelope the fundamental reference waveform. These components are employed in a constant boost pulse width modulation (PWM) technique. The proposed system consists of a fundamental single-phase reference waveform, a triangular carrier waveform and two constant voltage (V-constant) signals that envelop the fundamental reference waveform. These components are essential for implementing simple boost PWM control techniques.

The second block formulates secondary variables that serve as function-modulating signals for each PWM control technique. The secondary variables are of a Boolean data type, where a value

of 0 represents false and a value of 1 represents true when assigned a value less than or greater than zero, respectively. The primary objective of secondary variables is to establish the correlations amongst various modulating signals throughout a specified duration with respect to the fundamental reference signals Vac and Vac-3rd-injected. By observing the secondary variable's state at a specific moment, one can accurately determine the sequence of modulating signals from the maximum to the minimum at that time instant.

3.5 The Selection of a Simulation Tool

Upon the successful completion of the proper design of a stand-alone single-phase photovoltaic circuit, Z-Source Inverter and PWM Control Technique, the subsequent step entailed the vital challenge of selecting an appropriate software tool for the implementation of the designed components.

Three software packages were considered, namely Power Sim (PSIM), Proteus Professional and MATLAB. The software's suitability was determined by evaluating its usability, analysing its ability to handle harmonic distortion percentages, and assessing its flexibility in displaying results. This includes the capability to export graphical results to an editor window for editing, with the aim of enhancing the image quality of figures in the thesis.

MATLAB possesses the inherent capability to model all designed circuits within the thesis. Conversely, the other two mentioned software also possess similar capabilities, albeit with certain limitations. Notably, these software programs lack the ability to plot harmonic magnitude or phase against frequency, and they do not support the exportation of graphical results as picture files. In contrast, MATLAB excels in all of the functionalities. The limitations pose a hindrance to the data collection process for the purpose of reporting in the thesis.

However, MATLAB, in contrast, leverages the limitations of Power Sim (PSIM) and Proteus Professional, transforming them into advantageous features that align with the suitability of this research study. In addition to the facts, it has been observed that the study of Literature exhibits a tendency towards favouring MATLAB as the preferred software platform for the execution of various research projects within its domain. The software chosen for the modelling of all circuits in this research study is MATLAB.

3.6 Results of a Stand-Alone Single-Phase PV System

After the successful implementation of a Stand-Alone single-phase PV System (SASPPVS) in MATLAB, simulation results were obtained. The data collection process involved utilizing a simulated SASPPVS prototype to gather information for each passive filter. A representative table is presented below for reference.

Table 3. 1: for collecting result of stand-Alone single-phase PV System

Changing of PV Array Irradiance at a constant Temperature of 25 degrees												
Irradiance	0	10	50	100	200	500	800	900	1000	1200	1500	2000
THD%	0	-	-	-	-	-	-	-	-	-	-	-
$V_{PV\ OUT}$	0	-	-	-	-	-	-	-	-	-	-	-
$I_{PV\ OUT}$	0	-	-	-	-	-	-	-	-	-	-	-
Changing of PV Array Temperature at a constant Irradiance of 1000 watts per square meter												
Temperature	0	5	15	20	25	30	35	40	50	60	70	100
THD%	-	-	-	-	-	-	-	-	-	-	-	-
$V_{PV\ OUT}$	-	-	-	-	-	-	-	-	-	-	-	-
$I_{PV\ OUT}$	-	-	-	-	-	-	-	-	-	-	-	-

In Table 3.1, the tool is used for the purpose of gathering outcomes within the context of this research investigation. In the first case: The alteration of photovoltaic (PV) array irradiance is observed under different conditions and a constant temperature of 25 degrees Celsius. In the second case: The alteration in the temperature of the photovoltaic (PV) array is being investigated under the condition of a constant irradiance level of 1000 watts per square meter.

These methods have resulted in the derivation of solutions and the analysis of total harmonic distortion, as well as the voltage and current characteristics under various conditions. A graphical representation has been made and explained in the vicinity of the aforementioned table of results on Excel, supported by MATLAB, incorporating certain outcome parameters.

3.7 The Results of Single-Phase Z-Source Inverter PV System

The Z-Source Inverter and PWM Control techniques were effectively implemented in MATLAB, and the simulation yielded the desired results. The tabular representation provided herein was used to gather actual data from a simulated prototype of a Z-Source Inverter, pertaining to the execution of two distinct Pulse Width Modulation (PWM) control methods.

Table 3. 2: Single-phase Z-Source Inverter

Varying the Modulation index and Input Voltage to analysis harmonic components								
V_{IN}	200	300	400	500	200	300	400	500
M	0.65	0.65	0.65	0.65	0.75	0.75	0.75	0.75
V_{Stress}	-	-	-	-	-	-	-	-
$V_{DC-LINK}$	-	-	-	-	-	-	-	-
$THD\%$	-	-	-	-	-	-	-	-
$THD_v\%\ with\ LC\ Filter$	-	-	-	-	-	-	-	-
$THD_I\%\ with\ LC\ Filter$	-	-	-	-	-	-	-	-
$THDv\%\ with\ LCL\ Filter$	-	-	-	-	-	-	-	-
$THD_I\%\ with\ LCL\ Filter$	-	-	-	-	-	-	-	-
$THDv\%\ with\ LLCL\ Filter$	-	-	-	-	-	-	-	-
$THD_I\%\ with\ LLCL\ Filter$	-	-	-	-	-	-	-	-
Table 3.2: Continues below from 0.85 to 0.95 of Modulation index and Input Voltage								
V_{IN}	200	300	400	500	200	300	400	500
M	0.85	0.85	0.85	0.85	0.95	0.95	0.95	0.95
V_{Stress}	-	-	-	-	-	-	-	-
$V_{DC-LINK}$	-	-	-	-	-	-	-	-
$THD\%$	-	-	-	-	-	-	-	-
$THDv\%\ with\ LC\ Filter$	-	-	-	-	-	-	-	-
$THD_I\%\ with\ LC\ Filter$	-	-	-	-	-	-	-	-
$THDv\%\ with\ LCL\ Filter$	-	-	-	-	-	-	-	-
$THD_I\%\ with\ LCL\ Filter$	-	-	-	-	-	-	-	-
$THDv\%\ with\ LLCL\ Filter$	-	-	-	-	-	-	-	-
$THD_I\%\ with\ LLCL\ Filter$	-	-	-	-	-	-	-	-

Table 3.2, presented above, serves as the instrument used for the collection of data outcomes within the context of this research investigation. In the given table, the second and third columns consist of two primary input variables, namely input voltage and modulation index. Additionally, there are four performance parameters associated with the Z-Source Inverter, which are presented as follows: The voltage stress experienced across the switches, the DC-link voltage, the unfiltered total harmonic distortion, and the filtered total harmonic distortion are the key technical variables under consideration.

As per the specifications outlined in Section 3.3, the decision to choose a voltage input ranging from 200 V to 500 V was made based on the observation that the majority of input voltages established in relevant research publications lie within this range. The modulation index range of 0.65 to 0.95 has been meticulously chosen to include all defined PWM control techniques within this interval. The control techniques of Carrier-Based Control (CBC) and Space-Based Control (SBC) exhibit distinct operational ranges for the modulation index. To conduct an analysis of the harmonics distortion within the system or circuit, the following variables are used to ascertain and gather the outcomes: The LC, LCL and LLCL Filters are commonly used in various applications.

In this context, we consider the utilization of these filters in conjunction with a CBC and SBC fundamental waveform. Specifically, focus is on the input voltage of 200V and a modulation index of 0.65, as detailed in sections 4.4.2 and 4.4.3. It is worth noting that the sections provide comprehensive information regarding the application of these filters. Another section where the invertor was simulated without a filter, was provided as frame of reference.

3.8 Conclusion

This section evaluated the extent to which the stated aims and objectives of the entire research study have been achieved. In accordance with the contents of Chapter 2, Chapter 3, and Chapter 4, which pertain to the design of a Stand-alone or off-grid Single-Phase Photovoltaic System and Z-Source Inverter, it is noteworthy to mention that the research study conducted in this regard has been effectively accomplished.

Chapter Four: Result and Analysis

4.1 Introduction

The purpose this chapter is model and Simulate LC, LCL and LLCL filter to be applied on the Z-Source inverter and single-phase PV system. The techniques and methodology that will be used in this chapter were discussed in chapter 2 and chapter 3 respectively. The single-phase PV system circuit is constructed with and without a filter, with the solar array connected to a step-up booster and the booster connected to an AC load through a Universal Bridge inverter. This study will look at the harmonic behaviour of an Off-grid photovoltaic system.

After some time, the necessity for designing the Z-source inverter (ZSI) with totally different PWM control methods that had been developed and applied to the ZSI system became apparent. Each PWM control approach scheme's outcomes are discussed and described in detail. Amongst the essential performance characteristics investigated are the percentage of total harmonic distortion, voltage stress across the switch, modulation index, DC-link voltage, voltage gain, and boost factor.

4.1.1 The Design of the step-up Booster for the stand-alone PV system

The DC-DC boost converter was designed in accordance with the step-by-step procedure outlined in the table 4.1, which summarizes the design. At an output voltage of 400 V, output power of 2kw and a switching frequency of 10 kHz, and input voltage of 290.33 V, the maximum current and voltage ripples were calculated to be 20% and 2%, respectively.

Table 4. 1: The Parameter of DC-to-DC Boost Design

Parameters	Formulas	Calculated values
Output Current ($I_{out(booster)}$)	$I_{out(booster)} = \frac{P_{out}}{V_{out(booster)}}$	The output current at full load = 5 A
Output Load **(R)**	$R = \frac{V_{out(booster)}}{I_{out(booster)}}$	At full Power load: 80 Ω
Nominal duty ratio **($D_{(booster)}$)**	$D_{(booster)} = 1 - \frac{V_{in(booster)}}{V_{out(booster)}}$	At full Power load: 0.275
Minimum capacitor **($C_{(booster)}$)**	$C_{(booster)} = \frac{V_{out(booster)} \times D_{(booster)}}{R \times \Delta V_{(booster)} \times f_{sw}}$	At full Power: 2.371 mF
Minimum inductor **($L_{(booster)}$)**	$L_{(booster)} = \frac{D_{(booster)} \times \left(1 - D_{(boost)}\right)^2 R}{2 f_{sw}}$	At full power: 0.578 mH

The booster design variables are critical for operation in the 600 W to 10-kilowatt power range. The step-up booster output voltage of 400 V is shown in the graph below, supporting the voltage used in the booster output voltage.

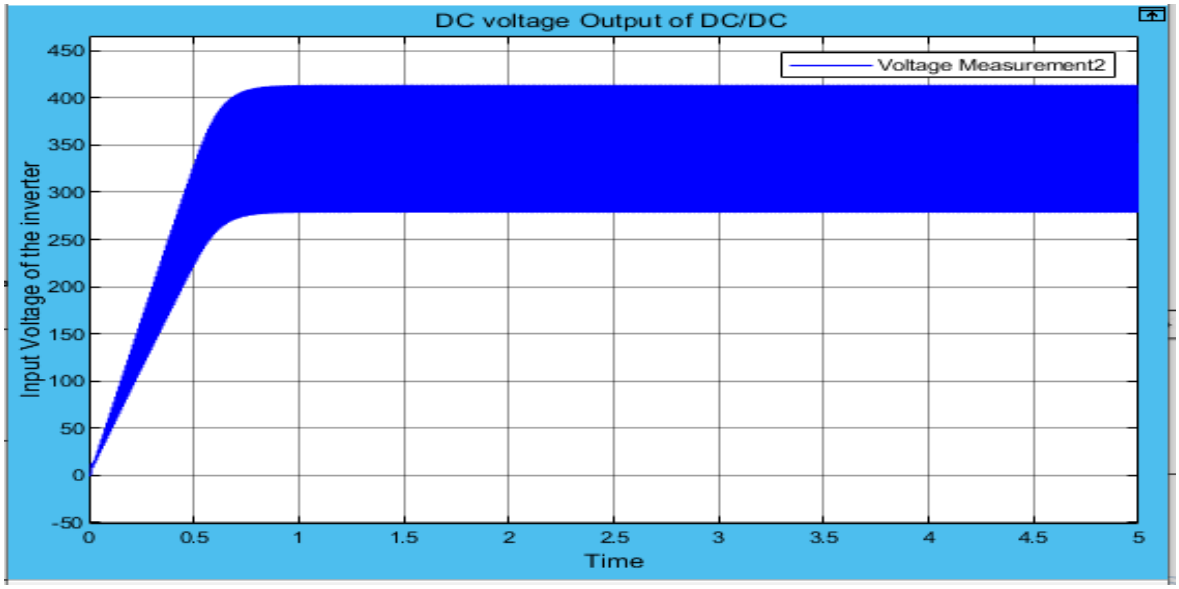

Figure 4. 1: Output voltage of the step-up Booster, which is 400 V_{DC}.

In Figure 4.1, the output voltage for the step-up booster is illustrated and it shows that it starts from 0.5 seconds because the Parameter of the Pulse Generator, which is Pulse Width (% of period) 5%, tells that the graph will not start from 0 or from rest. Pulse type determines the computational technique used. Time-based is recommended for use with a variable step solver, while sample-based is recommended for a fixed solver or within a discrete portion of a model using a variable step solver.

4.1.2 The Universal Bridge inverter

The Universal Bridge inverter (also known as a Full-Bridge inverter) is used to convert DC power into AC power with high efficiency. The switch that been used it the MOSFET/diode. The inverter is linked with a booster which sends 400 Vdc into the inverter. Inverters are also the cause of harmonics. In this case, the inverter was just selected due to the fact that it does not have more effect on the system regarding harmonics. It is fixed because the aim was to analysis harmonics, power quality, and the relationship between voltage and current. This inverter is for a single-phase PV system, but PWM is also considered, and some of the controllers and inverters were also designed in the following manuscript.

4.1.3 The Photovoltaic system

To support the input voltage from a photovoltaic system, their strings are linked in parallel, with series connected modules per string. The DC-to-DC booster's input voltage is 290.33 V, made up of 29 parallel strings and 8 series-connected modules per string. In the figure below, all the values within the Photovoltaic system are shown, which is supported by the equations in Literature Review. The table 4.2 below gives more details on the Photovoltaic system that has been selected for use in this thesis.

PV Module A10J-S72-175

Manufacturer: A 10 Green Technology	CSI Approved: Yes
Model Number: A10J-S72-175	CSI Model Number: A10J-S72-175
Production Status: unknown	Description: 175 Monocrystalline Module

Table 4. 2: More details on solar PV parameter

Electrical	**Values**
Power at STC (W)	175
Power at PTC (W)	151.2
Bifacial	No
Power Density at STC (W/m^2)	134.615
Power Density at PTC (W/m^2)	116.308
V_{mp}: Voltage at Maximum Power (V)	36.63
I_{mp}: Current at maximum Power (A)	4.78
V_{op}: Open Circuit Voltage (V)	43.99
I_{sc}: Short Circuit Current	5.17
Nominal Operating Cell Temperature	49.9
Open Circuit Voltage Temperature Coefficient (% / $°C$)	-0.362
Short Circuit Current Temperature Coefficient (% / $°C$)	0.042
Maximum Power Temperature Coefficient (% / $°C$)	-0.507
Mechanical	**Values**
Cell Type	Mono
Length (mm)	1576.0
Width (mm)	825.0
Module (m^2)	1.3

Table 4.2 located above provides further information on the type of solar that was utilized in this thesis. The possible acquisition of this solar type is the goal of picking it, and the eventual implementation of this design is a possibility in the future. The cost is manageable when

considering potential applications. When looking at the electrical and mechanical components, one notices that every parameter is necessary for this photovoltaic system. Many separate solar cells are joined together to form a larger unit called a module. Modules are contained in housings that are slanted at the proper angle to maximize solar energy collection. The produced current is collected by each module's two terminals and transmitted to the solar power management system.

The efficiency of a photovoltaic module may be measured as the ratio of the amount of electrical power that is discharged from the terminals to the amount of power that is generated by the sun's rays striking the module's surface. One thousand watts per square meter is the standard figure that is used to indicate solar radiation. The proportion of solar energy that is transformed into useable power is what determines a solar panel's level of efficiency, given that each square meter is exposed to 1,000 watts of sunshine. A photovoltaic module has a life expectancy of around 30 years on average.

Monocrystalline, polycrystalline, and thin film solar modules are most popular. *Monocrystalline* silicon: These dark blue, nearly black modules have silicon crystals facing the same direction, and blunted cells. They create 18-21% electricity in perpendicular light. *Polycrystalline silicon*: Silicon crystals facing opposite directions make these nearly iridescent blue modules. They use sunlight better throughout the day, but are less efficient (15-17%) when struck perpendicularly. Double-faced panels generate 10-15% more power than single-faced panels because the rear collects sunlight. Solar parks use fewer panels to provide the same output, saving space. 3SUN HJT panels survive over 30 years, unlike other solar modules. In conclusion, selecting the Monocrystalline lies in the fact of its efficiency, cost, and performance. The aim of the project is for it to be implemented in future and compare it with MATLAB results.

Table 4. 3: Parameters of the Photovoltaic

Characteristics	Settings
Input Voltage	Number of Panels in series × Open Ciruit Voltage : 6.6 × 43.99 = 290.334
Input Power	Total Number of parallel × series and produect of Maximum Power : (29× 8)(213.15)= 49450.8
Input Temperature	25 ° C
In Irradance	1000 W/m^2
Protection Configuration of Solar Panels	29 paralell and 8 series

The results of the simulation have been determined based on the characteristics and settings of the photovoltaic system or module, which are shown in Table 4.2 above.

4.1.3.1 Protection Configuration of Solar Panels

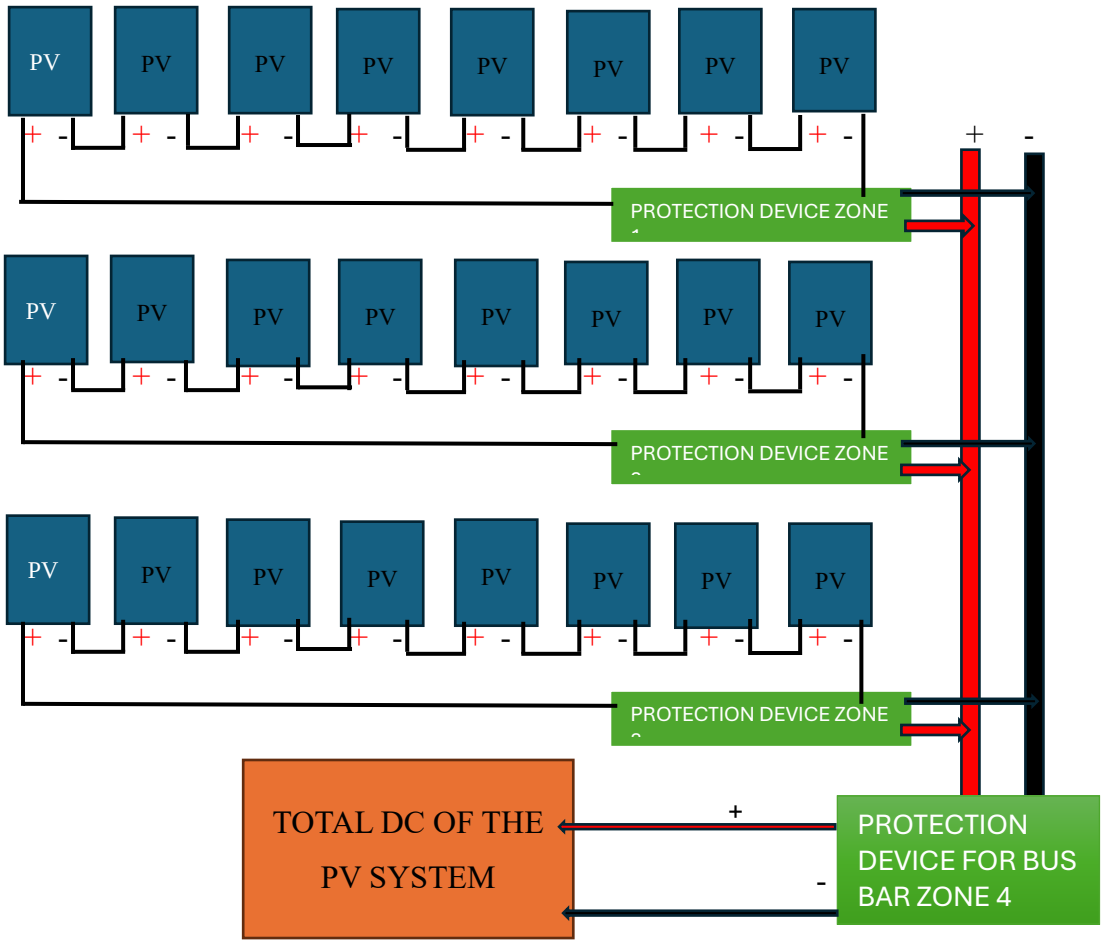

Figure 4. 2: Protection Configuration of PV System

Figure 4.2 demonstrates how to connect PV Arrays in series and parallel, as well as the many protection configurations that may be used for PV Arrays. The protection is then included in the zone protection mechanism, which may be a relay or a set of breakers with rated currents. PV Arrays are protected from the beginning of the first line to the very end of the third line when they are connected in series at the end by zones 1, 2 and 3. This principle may be used for a variety of PV Arrays to generate the necessary dc Voltage. The second option, which is the one that should be used more often, is to link four PV arrays in a single line and then connect another four PV arrays in the same line. This method uses more wire conductors, but it is the superior option. If there is a problem with line one of the PV Array or Solar planes, the protective zone 1 should shut off the supply of PV array in line one. Meanwhile, lines two and three should continue to function normally inside the PV System without encountering any challenges. Figure 4.2, the purpose is to illustrate how to accomplish the 29 parallel threads and 8 series connected modules per string that

is described in Section 4.1.3 on the design of a photovoltaic system. If sufficient finances are made available, the proposed system may be designed.

4.1.3.2 Maximum Power Point Tracking

This is a technique that is implemented in photovoltaic (PV) systems, with the purpose of maximizing the amount of energy that can be extracted from solar panels. In a photovoltaic (PV) system that is not linked to the utility grid, known as an off-grid PV system, the maximum power point tracking (MPPT) function is very vital to the system's ability to operate at its highest level of efficiency and effectiveness. Understanding the Maximum Power Point (MPP), Solar panels produce the most power at a certain operating point.

The operating point depends on solar irradiation, temperature, and load conditions. Solar panels provide the greatest electricity at their maximum power point (MPP). *Controller MPPT*: The maximum power point (MPP) of solar panels is monitored in real time by an MPPT controller. By monitoring the panels' output voltage and current, it changes the operating conditions to bring the system up to or near the MPP.

The Perturb and Observe Algorithm (P and O): Off-grid PV systems use this MPPT approach most often. The MPPT controller will periodically change the solar panels' operational voltage or current and measure the power produced. The controller compares power output at various operational points to determine the operating conditions needed to reach the MPP. This helps the controller find an MPP.

Voltage and Current Adjustment: Based on P and O algorithm analysis, the MPPT controller adjusts solar panel voltage and current. A DC-DC converter matches the panel voltage to the battery bank in an off-grid arrangement.

Continuous Tracking: The Maximum Power Point Tracking (MPPT) controller monitors solar panel output and adjusts operating conditions as needed. Real-time tracking ensures that the system will operate at the MPP regardless of environmental conditions like sun irradiance or temperature.

The following are some of the advantages of employing MPPT in an off-grid PV system:

- ***Enhanced Energy Harvest*:** MPPT allows the system to capture the maximum possible power from the solar panels, resulting in increased overall efficiency and enhanced energy harvest.

- ***Improved Environmental Adaptation*:** MPPT controllers can adapt the working settings of solar panels to accommodate variations in solar irradiation and temperature. This versatility guarantees that the system performs optimally in a variety of environments.
- ***Optimal Battery Charging*:** By keeping the solar panels at the MPP, MPPT controllers can charge the battery bank in the off-grid system effectively. This helps to optimize the capacity use of the battery and extend its life-span.

Overall, MPPT is a key technology for improving the performance and efficiency of off-grid PV systems by continuously watching and changing the working conditions in order to get the most power from the solar panels.

4.1.4 Analysis of the effect of PV array Irradiance and Temperature on Power Quality/Total Harmonic Distortion

The PV system was modelled in MATLAB/Simulink, and the simulation results revealed that the THD value increased due to the low radiation intensity. Power quality is regarded as an important criterion for the design of any electric power-producing system. As a result, it is vital to identify and assess the elements that are causing the decline in power quality. The table below provides more understanding on what happens to power quality and harmonics when irradiance and temperature are being varied on the Photovoltaic System.

Table 4. 4: Varying Irradiance and temperature parameters to analysis harmonics and power quality in the Stand-alone PV System

Changing of PV Array Irradiance at a constant Temperature of 25 degrees												
Irradiance	0	10	50	100	200	500	800	900	1000	1200	1500	2000
THD%	0	89.12	89.12	89.12	89.12	89.05	89.05	89.05	89.05	89.05	89.05	89.05
$V_{PV\ OUT}$	0	12.07	57.07	113.2	224.2	282	287.7	289.1	290.4	292.6	295.3	298.8
$I_{PV\ OUT}$	0	2.28	11.37	22.68	43.69	0.0028	0.0029	0.0029	0.0029	0.0029	0.003	0.003
Changing of PV Array Temperature at a constant Irradiance of 1000 watts per square meter												
Temperature	0	5	15	20	25	30	35	40	50	60	70	100
THD%	89.05	89.05	89.05	89.05	89.05	89.05	89.05	89.05	89.05	89.05	89.05	89.05
$V_{PV\ OUT}$	311.3	306.1	300.8	295.6	290.4	285.2	279.9	274.7	264.1	253.6	243	211
$I_{PV\ OUT}$	0.003	0.003	0.003	0.003	0.003	0.003	0.003	0.003	0.003	0.003	0.002	0.002

Table 4.4: provides an analysis of the Power Quality by varying PV Array Irradiance and Temperature. The Power Quality under different conditions whereby there is no filter in the System. The aim is to analyse Harmonics and the relationship between voltage and Current. The best irradiance level to use for a PV array depends on several factors, including the type of solar

panels, their specifications, and the desired output of the system. In general, PV array or Solar panels are rated based on their performance under standard test conditions, which typically assume an irradiance level of 1000 Wm^2. However, in real-world conditions, the actual irradiance can vary significantly depending on factors such as time of day, weather conditions, geographic location and shading. The relationship between Voltage and Current when the irradiance is being varied demonstrates that Voltage and Current are directly proportional to the irradiance, but when at initial irradiance, it influences harmonics in the system because it increases harmonics from 10 Wm^2 to 200 Wm^2. Thereafter, harmonics from 200 Wm^2 to 2000 Wm^2 decreases and harmonics from 500 Wm^2 to 2000 Wm^2 there plateau.

When the temperature is being varied it shows that the harmonics do not increase or decrease but are constant. Voltage and Current within the system are inversely proportional to the temperature when the temperature is varied from 0 to 100 degrees Celsius. It was operating at 1000 Wm^2 as shown in the table above. In terms of suitable operating temperatures, most solar panels perform well within a range of approximately 25 to 35 Degrees Celsius (77 to 95 degrees Fahrenheit). Higher temperatures can cause reduction in power output and overall system efficiency, while lower temperature also has a negative impact on the system.

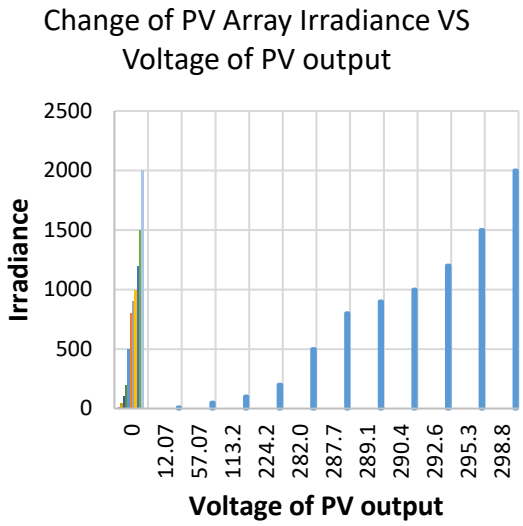

Figure 4. 3: (a) Irradiance VS V_{PV}_OUT

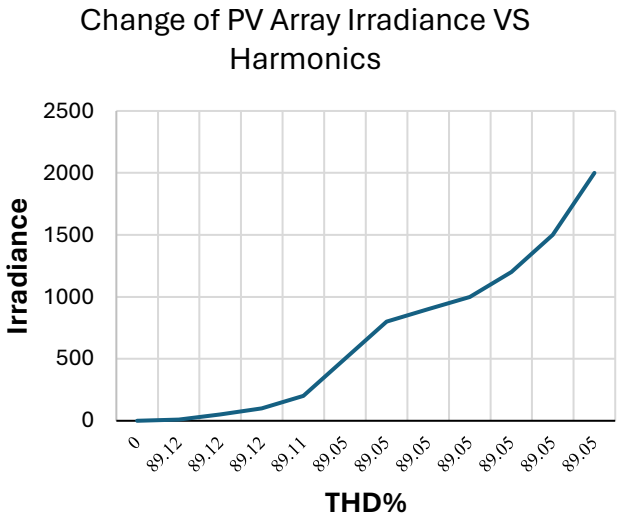

FIGURE 4.3: (b) Irradiance VS THD%

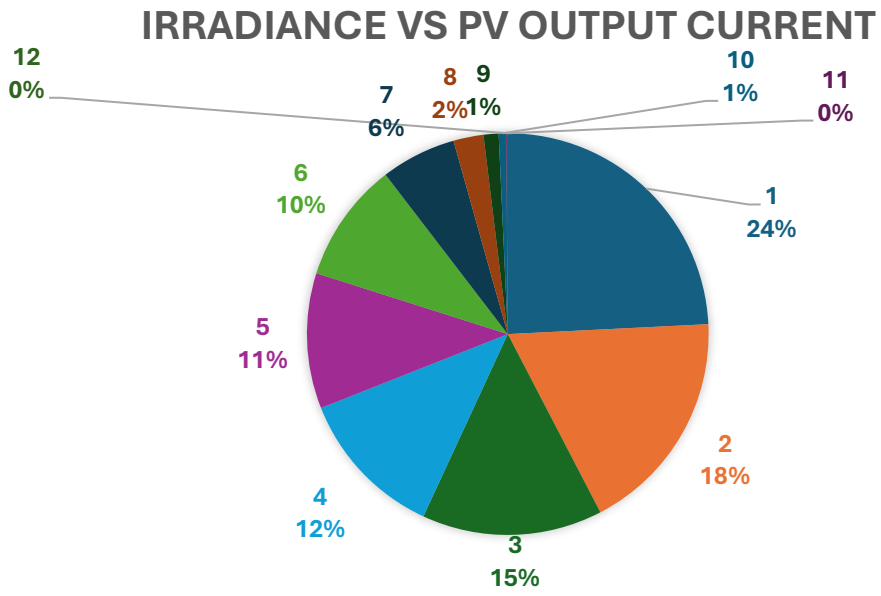

Figure 4. 4: (c) Irradiance VS PV Array output Current

The Photovoltaic Array out depends on the irradiance level, as Figure 4.3 (a) demonstrated by the bar graph. The graph's purpose is to analyse the performance of a stand-alone PV system with and without a filter at different levels of PV irradiance. The goal is to determine the effectiveness of total harmonic distortion and analyse the power quality within the system. The graph ranges from 0 W/m2 to 200 W/m2. Figure 4.3 (a) supports the statement made above that when the Irradiance is varied, the voltage and current are directly proportional to Irradiance in Wm^2.

The results at 1000 Wm^2 to 800 Wm^2, mostly used in different designs with a constant 25°C temperature, support the design standard of the stand-alone PV System without filter. Figure 4.3 (b) demonstrates the relationships between PV Irradiance and Total harmonic Distortion. When Irradiance is at rest (zero Wm^2), no power is being produced. After lower levels of irradiance, which is 10 Wm^2, it started to show high harmonic since there is no filter, at 89.12 % of THD. Up until 200 Wm^2 of Irradiance, THD is constant at 89.12%. when irradiance at 500 Wm^2 shows a decrease in total harmonic distortion with 7 %. It becomes 89.05%, which is constant towards 2000 Wm^2 without a filter, and shows the need for mitigation of Total Harmonic Distortion to meet IEEE 519 and IEC 61000-3-2 to ensure acceptable levels of total harmonic distortion in the system.

Figure 4.3 (c) shows the relationship between Irradiance and current. PV irradiance at lower levels from 10 Wm^2 to 200 Wm^2 gives an idea that the current is directly proportional to Irradiance. 500 Wm^2 to 2000 Wm^2 begins to be inversely proportional to the current. The amount of 24% on the pie-chart shows the level of irradiance at 2000Wm^2, and from number 1 to 12 demonstrates the PV Irradiance in the form of a percentage for each irradiance level (Wm^2) in the pie-chart.

4.1.4.1 The Irradiance level of 1000Wm^2 and Temperature of 25°C

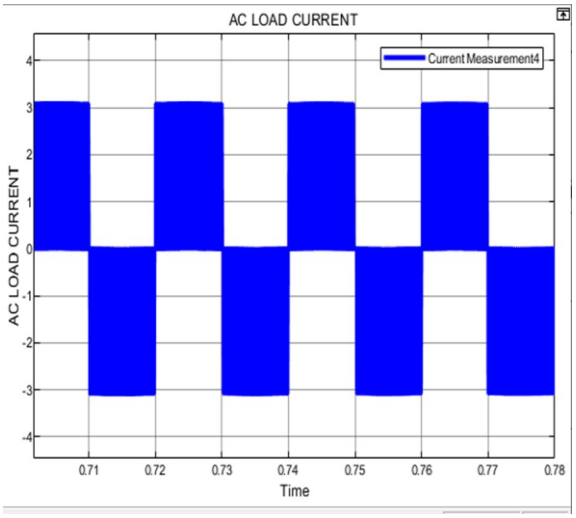

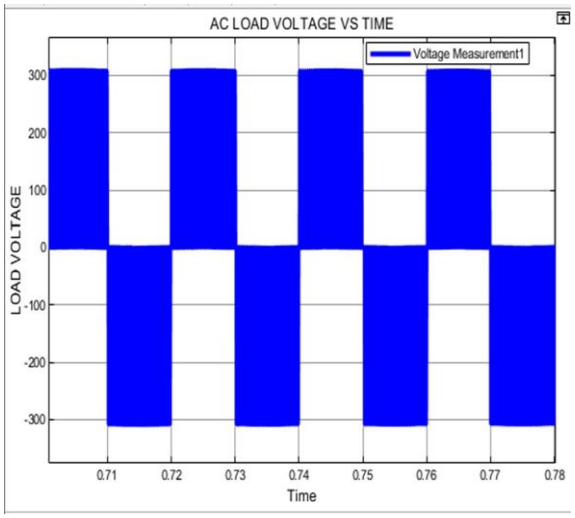

Figure 4. 5 (a): Iac-Load Without a Filter **Figure 4.5 (b): Vac-Load Without a Filter**

The total harmonic distortion of Current and Voltage waveforms is shown in Figure 4.5 (a) and Figure 4.5 (b) respectively. The measured total harmonics for current and voltage within system at 1000 Wm^2 and 25 °C is 89.05% respectively. Figure 4.4 makes it abundantly clear that the PWM inverter spectrum reveals harmonic components at the switching frequency. The IEEE limits are being violated by this very high value of THD. Hence, a passive filter is required at the inverter output to reduce the number of total harmonic distortions.

4.1.4 Designing of the passive filters

It is imperative that challenges brought on by current and voltage harmonics be avoided for reasons relating to safety. This will ensure that these challenges do not influence other loads that are connected to the same off-grid system. Input filters, such as the basic LC, LCL and the LLCL combination structure, are frequently utilized in stand-alone PWM inverter applications. This is done in order to reduce the amplitude of current and voltage harmonics.

4.1.4.1 Design of LC Filter, LCL Filter, and LLCL Filter

The equations that will be used in this section was presented in Chapter 2 and the following parameters are designed for a single-phase PV network:

Calculation of Filters
Data: supply frequency of 50 Hz, Power of 10 kW, Voltage of 230 V and switching frequency of 20 000 Hz,$V_{DC}\ of\ 400\ V$.

$$10f_{supply} < f_{rec} < 0.5f_{switching\ frequency} \quad (2.52)$$
$$(10)(50) < f_{rec} < (0.5)\ (20000)$$
$$500 < f_{rec} < 10\ 000$$

4.1.4.1.1 The Designing of a LC Filter for inductor and Capacitor

$$L_1 = \frac{V_{DC}}{4 \times f_{rec} \times \Delta I_{ripple}}$$
$$L_1 = \frac{400}{4 \times 5000 \times 2.46}$$

$$\underline{L_1 = 8.13\ mH}$$

$$C = \frac{\alpha P}{2\pi f_{supply} V^2}$$

$$C = \frac{0.05 \times 10000}{2\pi \times 50 \times 230^2}$$

$$\underline{C = 30.086\ uF}$$

$$f_{rec} = \frac{1}{2\pi\sqrt{LC}}$$

$$f_{rec} = \frac{1}{2\pi \times \sqrt{8.13 \times 10^{-3} \times 6.017 \times 10^{-6}}}$$

$$\underline{f_{rec} = 719.59\ Hz}$$

4.1.4.1.2 Designing of the LCL Filter

The value of L_1 for the LC filter is equal the value $L_1$of LCL filter. Condition 1. The maximum voltage drop across the inductor determines the total inductance ($L_1 + L_2$). The maximum is limited to 10% of the rated voltage, that is condition 2.

$$V_{L_1+L_2} = I \times X_{L_1+L_2}$$

$$V_{L_1+L_2} = \frac{P}{V} \times 2\pi f_{L_1+L_2}$$

$$10\%\ of\ V_{L_1+L_2} = \frac{P}{V} \times 2\pi f_{L_1+L_2}$$

$$L_1 + L_2 = \frac{0.1 \times V}{\frac{P}{V} \times 2\pi f}$$

$$L_2 = \frac{0.1 \times V^2}{P \times 2\pi f} - L_1$$

$$L_2 = \frac{0.1 \times 230^2}{10000 \times 2\pi \times 50} - 8.13 \times 10^{-3}$$

$$\underline{L_2 = 1.684\ mH}$$

$$C = \frac{\alpha P}{3 \times 2\pi f \times V^2}$$

$$C = \frac{0.05 \times 10000}{3 \times 2\pi \times 50 \times 230^2}$$

$$\underline{C = 10.028\ uF}$$

$$f_{rec} = \frac{1}{2\pi} \times \sqrt{\frac{L_1 + L_2}{L_1 \times L_2 \times C}}$$

$$f_{rec} = \frac{1}{2\pi} \times \sqrt{\frac{8.13 \times 10^{-3} + 1.684 \times 10^{-3}}{8.13 \times 10^{-3} \times 1.684 \times 10^{-3} \times 10.028 \times 10^{-6}}}$$

$$f_{rec} = 1345.611\ Hz$$

4.1.4.1.3 Designing of the LLCL Filter

$$L_1 = \frac{V_{DC}}{8\Delta I_{PPmax} f_{sw}}$$

$$L_1 = \frac{400}{8 \times 2.46 \times 5000}$$

$$\underline{L_1 = 4.065\ mH}$$

$$L_2 = \frac{L_1}{\alpha}$$

$$L_2 = \frac{4.065 \times 10^{-3}}{1.5}$$

$$\underline{L_2 = 2.71\ uF}$$

$$C_f = \frac{\alpha P}{3 \times 2\pi f \times V^2}$$

$$\underline{C_f = 300.86 \times 10^{-6}}$$

$$L_f = \frac{1}{C_f \times {f_{sw}}^2}$$

$$\underline{L_f = 0.133\ mH}$$

$$f_{res} = \frac{1}{2\pi \times \sqrt{(\frac{L_1 \times L_2}{L_1 + L_2} + L_f) C_f}}$$

$$\underline{f_{res} = 656.336\ Hz}$$

4.2 The Designed Stand-Alone/off-grid PV System with Passive filters

When compared to active filters and other filters, passive filters are far more effective. However, this is dependent upon the passive filter being developed. The findings shown in Figure 4.5 on current and voltage Total Harmonic Distortion are for the planned system of a PV Array that does not have a filter. This section displays more results from the many filters that may be selected, including the LC Filter, LCL Filter and LLCL Filter. The scale that is being utilized ranges from 0.7 to 0.95 in terms of time expressed in seconds. This method makes it simple to evaluate the outcome in each different circumstance. The LC Filter, the LCL Filter and LLCL Filter were designed so that the total harmonic distortion in percentage of each filter could be determined by passing current and voltage waveforms through the filters.

4.2.1 LC Filter Results for off-grid PV Systems

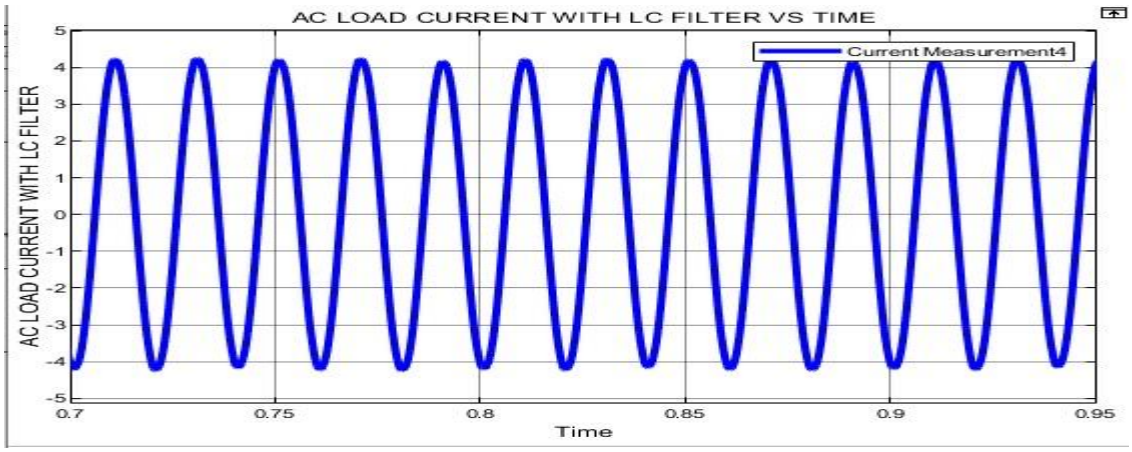

Figure 4. 6 : The Load Current with LC Filter

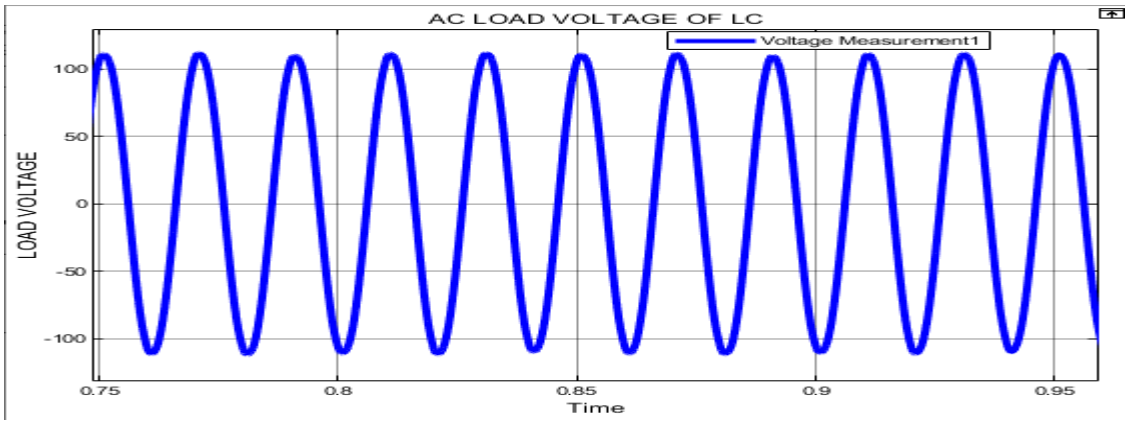

Figure 4. 7 : The Load Voltage with LC Filter

Figure 4.6 and Figure 4.7 show graphical waveforms of AC Load output Current and AC load voltage respectively, which meet the standard of harmonic limit with the help of the LC Filter in the Stand-Alone PV System. When the THD_I% and THD_V% values of an solar inverter output are higher than standard, an LC filter is utilized to reduce THD_I% and THD_V% to be less than 5%. There are a few drawbacks associated with LC filters, the most notable of which are the current ripple on inductances, the overall impedance of the filter, and the reactive power created by the capacitor. Current harmonic components are reduced by the LC filter from 89.05% to 2.95%, while voltage harmonic components are reduced from 89.05% to 2.99. These findings demonstrate an increase in power quality and the safeguarding of linked devices. The 3% and 5% tolerances for current and voltage were both met.

4.2.2 LCL Filter Results off-grid PV System

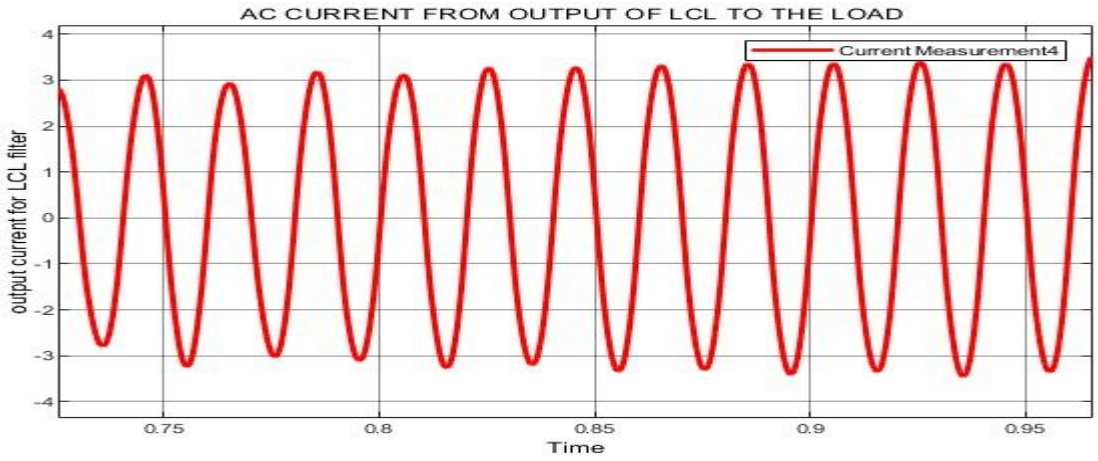

Figure 4. 8: The Load Current with LCL Filter

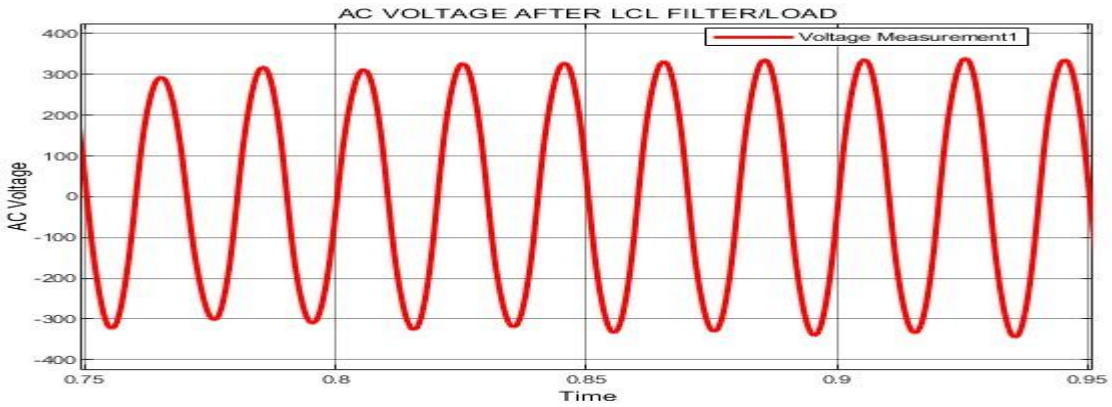

Figure 4. 9: The Load Voltage with LCL Filter

There is a clear relationship between voltage and current, as shown in Figures 4.8 and 4.9. The harmonic component limits for both current and voltage were within the range specified by the IEEE. The LCL Filter reduced the current and voltage harmonic components by 89.05% and 89.05% respectively, bringing them down to 2.45% and 2.45%.

4.2.3 LLCL Filter Results for the off-grid PV System

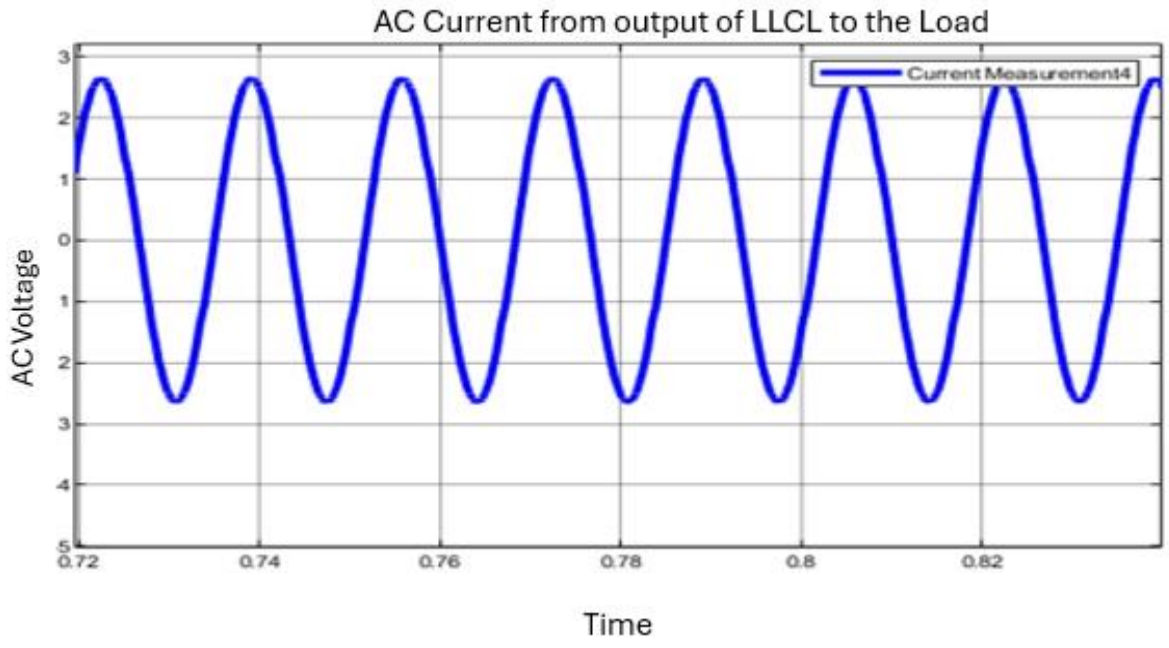

Figure 4. 10: The Load Current with LLCL Filter

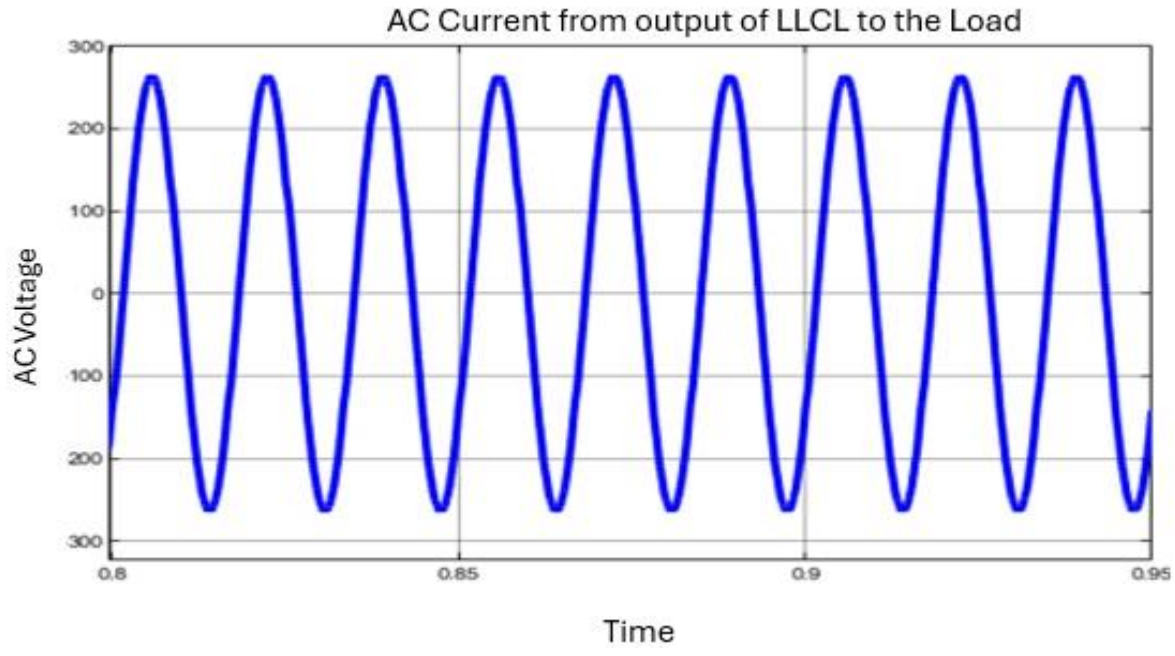

Figure 4. 11: The Load Voltage with LLCL Filter

Figure 4, and figure 4.11 display a considerable enhancement in power quality, which influences the power factor to the optimal level and provides enough protection for the devices connected to the Designed Off-Grid PV System. Current is proportional to voltage, but may be safely handled by lower-rated components. Total harmonic distortion of current and voltage are equal to 89.05, both very high, and are dropping to 1.68 and 1.71 percent respectively. The horizontal bar graph shows the results of total harmonic distortion in the Sand-alone PV system with and without passive filters.

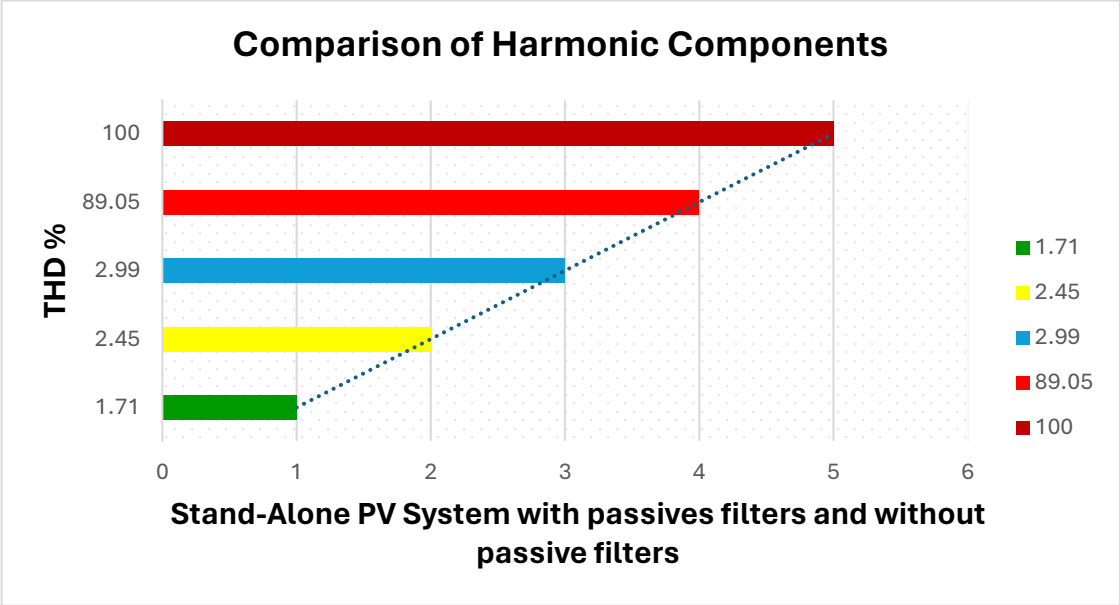

Figure 4. 12: Stand-Alone PV System with passive Designed filters and without passive filters

Figure 4.12 demonstrates different scenarios of Total harmonic distortion, different colours: stronger Red at 100% of THD%, Normal Red at 89.05% of THD%, Orange at 2.99% of THD%, Yellow at 2.45% of THD%, and Green at 1.71 of THD%.

- **Stronger Red:** shows that the total harmonic distortion is 100%, with the result that no piece of equipment will work at the level of 100% of total harmonic distortion.
- **Normal Red:** indicates that the proposed system has a total harmonic distortion of 89.05% despite the absence of a passive filter. This demonstrates the requirement for harmonic migration in an off-grid PV system.
- **Orange**: shows that the total harmonic distortion of the LC passive filter in the off-grid system is less than 2.99%, as required by the IEEE Standard for THD%.
- **Yellow:** a total harmonic distortion of 2.45% is demonstrated in the bar graph for the LCL passive filter in the off-grid system in order to establish compliance with the IEEE

standard and the LCL filter standard. Produces a result that is superior to that of the LC filter, while the LC filter is the less cost-effective option.

- **Green:** a total harmonic distortion of 1.71 % is demonstrated in the bar graph, which has perfect performance out of all the above passive filters.

The presence of harmonics causes overloading of a consumer's electrical system, a rise in terminal voltage, flickering, and increased heating of neutral conductors. All these issues are caused by the presence of harmonics. Therefore, it is essential to determine the causes of harmonic production along with the nature of its effect in the performance of off-grid photovoltaic (PV) systems. This is necessary to ensure satisfactory operation, design of component ratings, protection settings, and optimization of controllers that are present in off-grid PV systems.

Harmonics are normally produced if there is a non-linear nature present in the features. The amount of harmonic distortion in currents and voltages brought about by off-grid PV systems has been the topic of discussion in several international standards. Harmonics of an undesired nature are produced in greater quantities by PV inverters when they are allowed to function under conditions of poor solar insulation and low power levels. The following section of Z-Source inverter with three different techniques. The aim is to analyse total harmonic distortion for better harmonic performance.

4.3 Basic ZSI Design

In a broader context, the ZSI circuit can be analysed into three fundamental components: the inductor design, the capacitor design, and the power diode design, alongside the detailed selection of power electronic switching devices. In a practical design situation, it is often impossible to obtain an exact component rating that complies precisely with the design calculations, especially when working with standard component values. The upcoming sub-sections define the three sections of ZSI design, wherein the designed values establish the minimum threshold for the designed components.

4.3.1 The Design of an Inductor for ZSI

Calculating a minimum inductance requirement for a Z- impedance system, occasionally referred to by the terms $L_{1\,min}$ and $L_{2\,min}$, is an important part of the inductor design process. Calculating the average inductor current I_L, the current ripple ΔI, and the DC-link voltage $V_{DC-link}$ are the initial steps in achieving the goal of creating a design with the least possible amount of inductance. The equations (4.1) and (4.2) below are used to record a ripple current.

$$I_L = \frac{P}{V_{IN}} \tag{4.1}$$

After determining I_L, the ripple current ΔI may be calculated by first determining the maximum and minimum currents in the circuit. The following is a demonstration of how to calculate the maximum peak-to-peak current using equations (4.2) [29, 128]:

$$I_{maximum} = I_L + 30\%$$

$$I_{minimum} = I_L - 30\% \tag{4.2}$$

$$\therefore \Delta I = I_{maximum} - I_{minimum}$$

It is of absolute importance to prepare for the worst-case scenario in design as doing so increases the design's stability and reliability [18]. As a result, a boost factor B of 5 has been decided upon as the maximum value. In theory, so long as the ZSI runs within the boost factor range of 1 to 5, all the calculated elements, including the capacitor, the inductor, and the switching devices, will be able to effectively endure the stresses that are applied to them. A shoot-through time T_0 may now be calculated using equation (4.3). As a result, equation (4.4) is used to determine the minimum inductance requirement $L_{minimum}$ [29].

$$\frac{1}{1 - 2(^{T_0}/_{T})} =\leq B \tag{4.3}$$

$$L_{min} = \frac{V_{DC-link}(max) \times T_0}{\Delta I} \text{ ... Whereby, } V_{DC-link}(max) = \text{B} \times V_{in} \tag{4.4}$$

4.3.2 The Design of a Capacitor for ZSI

Calculating the minimum capacitance required for a Z- impedance system, also known as C_{1min} and C_{2min}, is an important step in the development method of designing a capacitor. To achieve a design with the smallest amount of capacitance, one must first determine an average inductor current (which has already been determined by 4.1), a shoot-through time (which was previously determined by 4.3), and the capacitor ripple voltage ΔV_C. The ripple in the voltage is calculated using equation (4.5), and the minimal capacitance is required to calculate applying equation (4.6) [58] [63, 128]:

$$\Delta V_C = V_{DC-link} \times 3\% \tag{4.5}$$

$$\therefore C_{minimum} = \frac{I_L \times T_0}{\Delta V_C} \tag{4.6}$$

4.3.3 The Selection of a diode and Switching devices

The maximum voltage that can be applied across the diode, as well as the power electronic switches that are equal to the peak DC-link and the inductor current were calculated during the establishment of the inductor. As a result, the maximum single-phase voltage and load current may be calculated using the equations (4.7 and 4.8) below. Therefore, the maximum current that flows through the switches happens when the power transfer is at its maximum, and can be found by using the formula (4.9) [58]:

$$V_{L(max)} = V_{RMS} \times \sqrt{2} \tag{4.7}$$

$$I_{load} = \frac{P}{cos\emptyset \times V_{L(max)}} \text{ At unity power factor} \tag{4.8}$$

$$\therefore I_{switch} = \frac{1}{2} \times I_{LOAD} + \frac{2}{3} \times I_L \tag{4.9}$$

In general, the switching devices to be selected, along with a diode, will have current and voltage ratings that are greater than the calculated values by a margin of at least 25% in order to ensure a safe working environment [57, 129]. The fundamental flow diagram of the z-source inverter may be seen in Figure 4.13. A PV Array-power supply, a Z-impedance system, a single-phase H-bridge, a single-phase filter, and a set of single-phase terminals to which a single-phase load is attached are illustrated in Figure 4.13 as the five primary blocks that make up a ZSI.

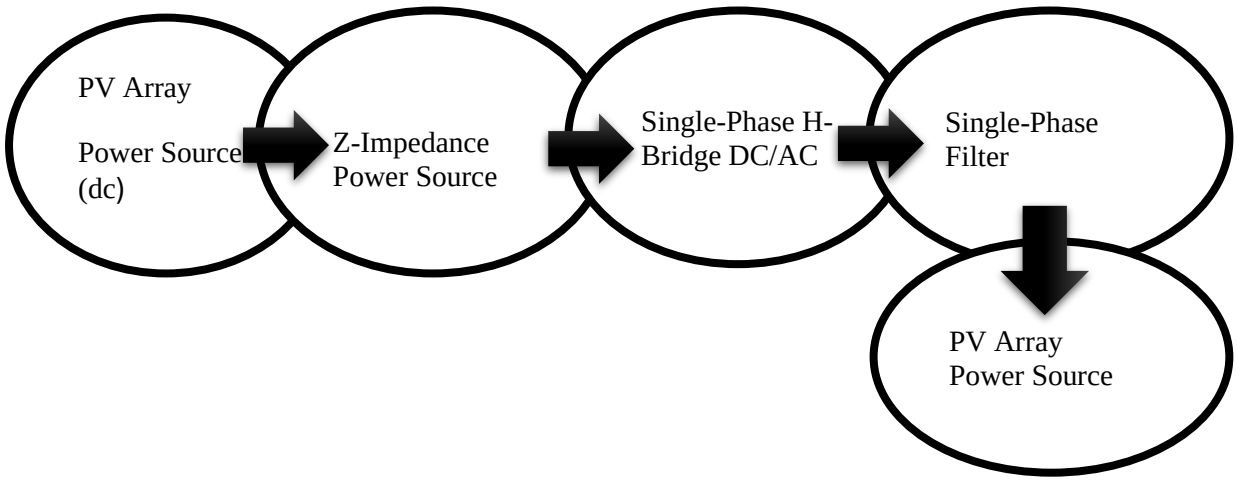

Figure 4. 13: The Designed Basic ZSI Diagram

4.4 The PWM Technique Schemes

The next sub-sections will present detailed design of several PWM control schemes and the analysis of crucial performance characteristics for each PWM control scheme. Following the tabulation of the findings, a subsequent discussion of those outcomes follows. The primary focus of this discussion is to highlight the interrelationships between the essential performance characteristics, and it supports these correlations using theoretical equations that were developed as part of the Chapter 2 literature study.

4.4.1 Sinusoidal Pulse Width Modulation (SPWM)

Controlling voltage source inverters (VSIs) and current source inverters (CSIs) often involves the application of a method known as sinusoidal pulse width modulation (SPWM). It is a method of modulation that generates a series of pulses of changing widths to approximate the appearance of a sinusoidal waveform. SPWM is applied in a voltage source inverter to manage the switching of power devices (such as insulated gate bipolar transistors, or IGBTs) to transform a DC voltage into an AC voltage with a changeable frequency. The amplitude and frequency of the output voltage may both be changed by altering the width of the pulses being produced [58].

As a result, it is solely discussed in this dissertation for the purpose of acting as a reference for other PWM approaches (CBC and SBC) regarding performance. Equation (4.10) is a basic frequency voltage waveform for a single-phase DC-AC converter, which is why it is referred to as a single-phase ZSI. This waveform should be the primary focus of all single-phase DC-AC converters.

$$V_{ac} = V_m \sin(wt) \tag{4.10}$$

The traditional v-source PWM inverter contains an equation that calculates the output peak phase voltage as follows:

$$V_{acp} = M_{SPWM} \frac{V_{dc}}{2} \tag{4.11}$$

M is the modulation index of the PWMV waveform and V_{acp} is the output peak phase voltage of ZSI. A comparison between a fundamental wave and a triangular carrier wave serves as the foundation for the sine PWM control approach. The control PWM signal is strong for the switching devices in the upper level (S1, S3). (1) A triangular carrier wave V-carrier is greater than a

fundamental wave Vac and is low (0) when a triangular carrier wave is lower than a fundamental wave. Whenever a triangular carrier wave is higher than a fundamental wave, the value is 1. The control PWM signal for lower switching devices (S2, S4) is high if a fundamental wave is lower than a triangular carrier wave V-carrier, and it is low whenever the fundamental wave is bigger than the triangular carrier wave [130].

A and B are two variables that are all functions of time. When these functions are sent via a Boolean operator, they may determine which of V_A and V_B is bigger than $V_{carrier}$.

$$A = V_a - V_{carrier} \tag{4.12}$$

$$B = V_b - V_{carrier} \tag{4.13}$$

The intended switching pattern of the PWM generator controlling a ZSI may be totally determined by combining the above-mentioned secondary variables A and B with switching states (S1 - S4). The switching behaviour of the PWM controller is essential for generating the required single-phase signal. The table below is a truth table that shows the states of each switching device at all the possible secondary variable states.

Table 4. 5: Show four switching devices states

Phase Leg A		
A	S_1	S_2
0	0	1
1	1	0
Phase Leg B		
B	S_3	S_4
0	1	0
1	0	1

The above truth table can be used as a basis for deriving the four Boolean equations that define the switching behaviour of four switching devices that are connected across the single-phase legs of a single-phase ZSI. The Sum of Product (SOP) technique is utilized to generate the equations that, when combined, provide the SPWM control PWM generator flow diagram shown in Figure 4.1. The following equations are included in the list:

$$S_1 = A\ (upper\ switch) \tag{4.14}$$

$$S_2 = \bar{A}\ (lower\ switch) \tag{4.15}$$

$$S_3 = B\ (upper\ switch) \tag{4.16}$$

$$S_4 = \bar{B}\ (lower\ switch) \tag{4.17}$$

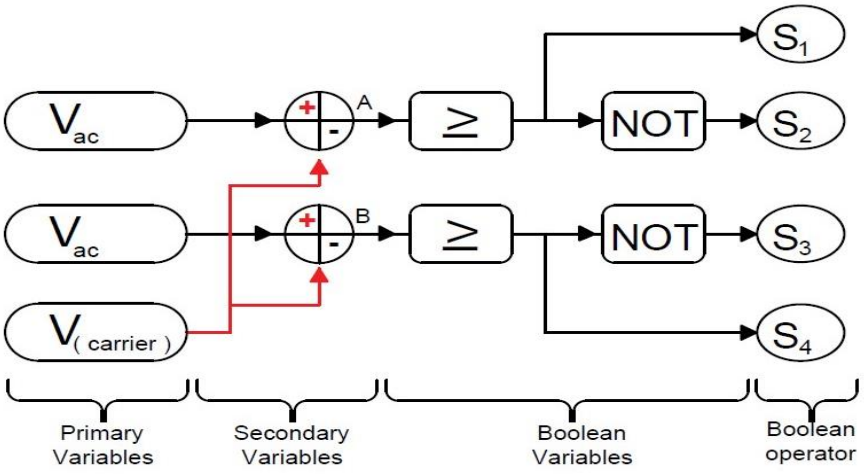

Figure 4. 14: SPWM Control design

Figure 4.14 illustrates the SPWM method used by the PWM Generator applied to switching devices. In this approach, S_1 and S_2 make up Lag A, whose behaviour is provided by equations 4.14 and 4.15 respectively. S_3 and S_4 make up Lag B, whose behaviour is supplied by equations 4.16 and 4.17 respectively.

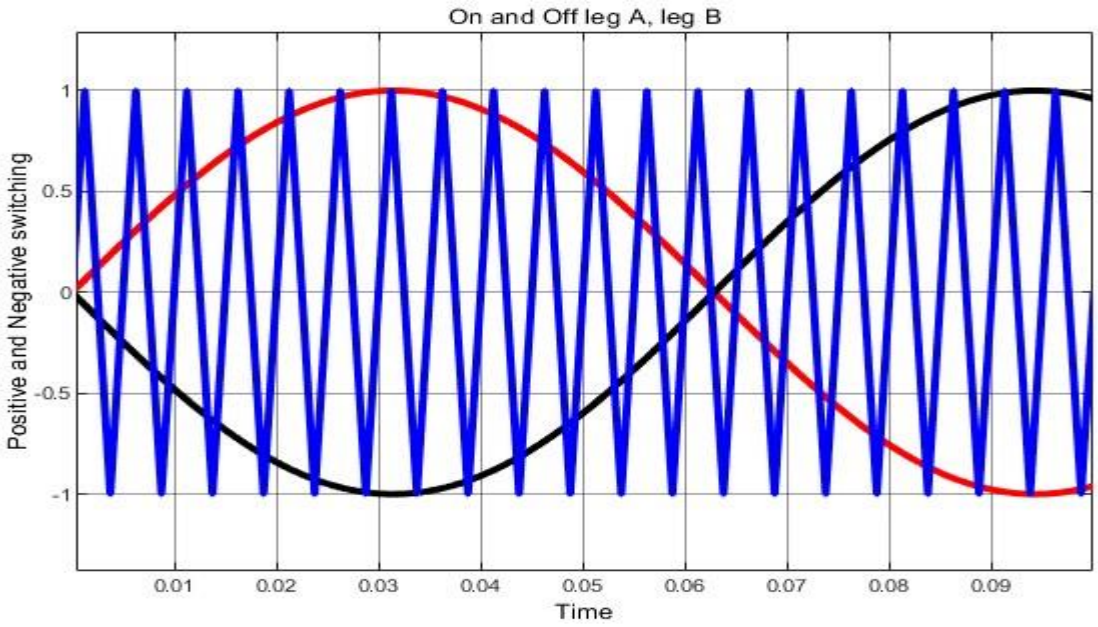

Figure 4. 15: The Positive and Negative Phase for Leg A, Leg B with V carrier at 90°

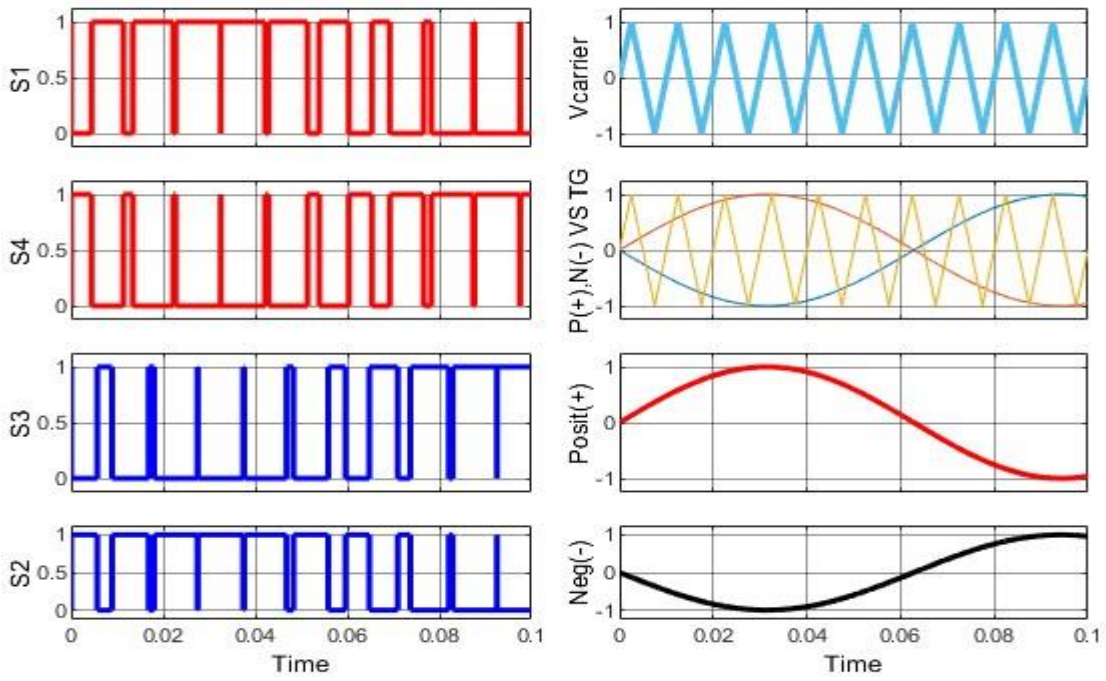

Figure 4. 16: The state of switching devices from S1, S2, S3 and S4

Figure 4.15 shows the positive phase with red colour and negative phase with block colour. The V carrier characteristic of the triangle generator is blue in colour. Figure 4.16 show the behaviour of switching devices where S_1 and S_4 are red in colour, S_2 and S_3 are blue in colour they make Leg A and Leg B.

4.4.2 The Constant Boost Control method (CBM)

The design of the constant boost technique is quite like the design of the simple boost method. The only difference is in the waveform of the reference voltage. In Section 4.4.1, the modulating signals V_{AC} and $V_{carrier}$ for the SPWM control method were defined. The constant boost PWM control method and the simple boost PWM control method both add two extra straight lines that envelope the fundamental single-phase signal of both positive and negative peak (see to Chapter 2 for more information). It is also possible that switching states will assist, given that ZSI inverters include active states, zero states and shot through states. For the CBC approach, the reference signal is injected with a magnitude of 16% to generate a third harmonic injected harmonic single-phase fundamental waveform [57, 60, 63]. Figure 4.17 shows the third harmonic of a single-phase fundamental waveform:

$$V_{ac(single\ phase-injected)} = V_{AB} + V_{(3rd\ harmonic)} \tag{4.18}$$

$$V_{ac(single\ phase-injected)} = 1.156\sin(wt) + 0.167\sin(3wt) \quad (4.19)$$

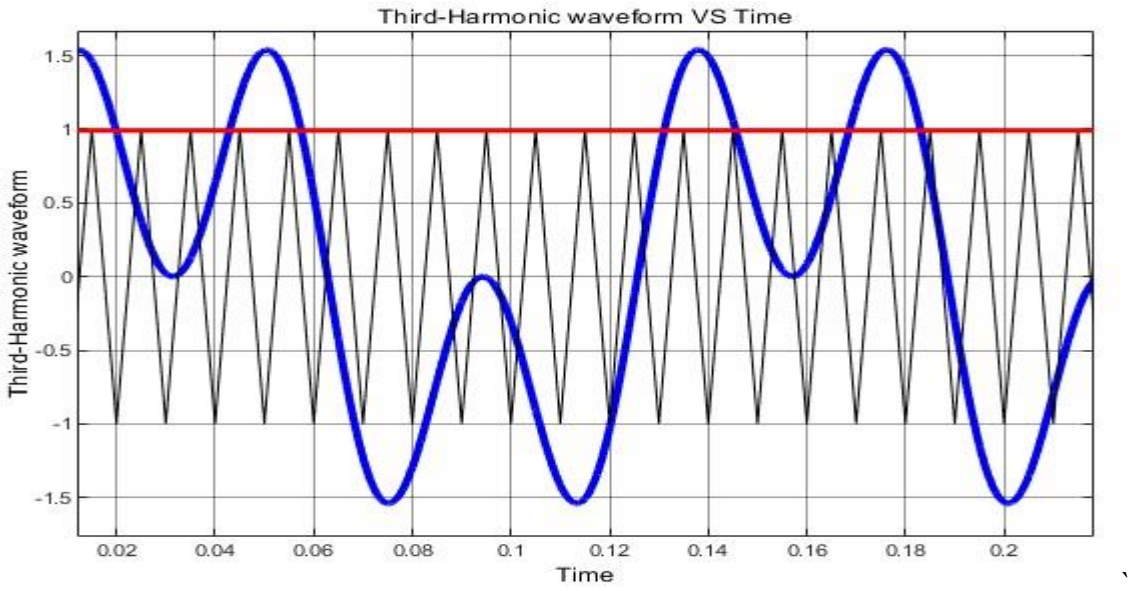

Figure 4. 17:Third harmonic injected harmonic single-phase fundamental waveform

Figure 4.17 is given by equation (4.19), which helps to design the control method for the constant boost PWM Generator. The variables to be designed in the system Vac and V carrier have been mentioned in the SPWM method. Below are some variables designed to have output into switches to boost the voltage, control power factor, analysis harmonic components within the system and improvement of power quality. The state of switches in the table below shows the active states, zero states and shoot-through state.

Table 4. 6: The switching state at active state, zero state, shoot-through state and output of voltage in different states

SWITCHING STATES	S_1	S_2	S_3	S_4	**OUTPUT VOLTAGE**
Active States-(1)	1	0	0	1	Finite Voltage
	0	1	1	0	
Zero States-(0)	1	0	1	0	Zero
	0	1	0	1	
Shoot-through state	1	1	**impossible**	**impossible**	Zero
	impossible	**impossible**	1	1	
	1	1	1	1	

Table 4.6, Completely describes logic of constant boost PWM control method. The states that have been marked with a shoot-through state, impossible states, refer to situations that are impossible according to mathematics. A situation where Vcarrier is more than $V_{constant}$ but less than Vac is an example of a state that cannot occur in a realistic circuit unless there is a fault condition present in it.

The above table may be used to derive the Four Boolean Equations that are required for all Four Switching Devices Used Across All Single-Phase Legs Of ZSI. The approach known as "sum of product" was applied to deduce these equations, which led to the development of flow diagram Figure 4.18 The following equations are listed below:

Let the following Switches state, $S_1 = A, S_2 = B, S_3 = C$, and $S_4 = D$. This defines that the state of each switch at an active state or zero state (e.g., for S_1 at an active state 1=A or zero state $0 = \bar{A}$), all other switches states will be treated the same way as switch one.

$$S_1 = A\,D + \bar{A}\,\bar{D} \quad \text{(Upper Switch)} \tag{4.20}$$

$$S_2 = A\bar{B} + \bar{A}B \quad \text{(Lower Switch)} \tag{4.21}$$

$$S_3 = D\bar{C} + \bar{D}C \quad \text{(Upper Switch)} \tag{4.22}$$

$$S_4 = \bar{D}\,\bar{A} + DA \quad \text{(Lower Switch)} \tag{4.23}$$

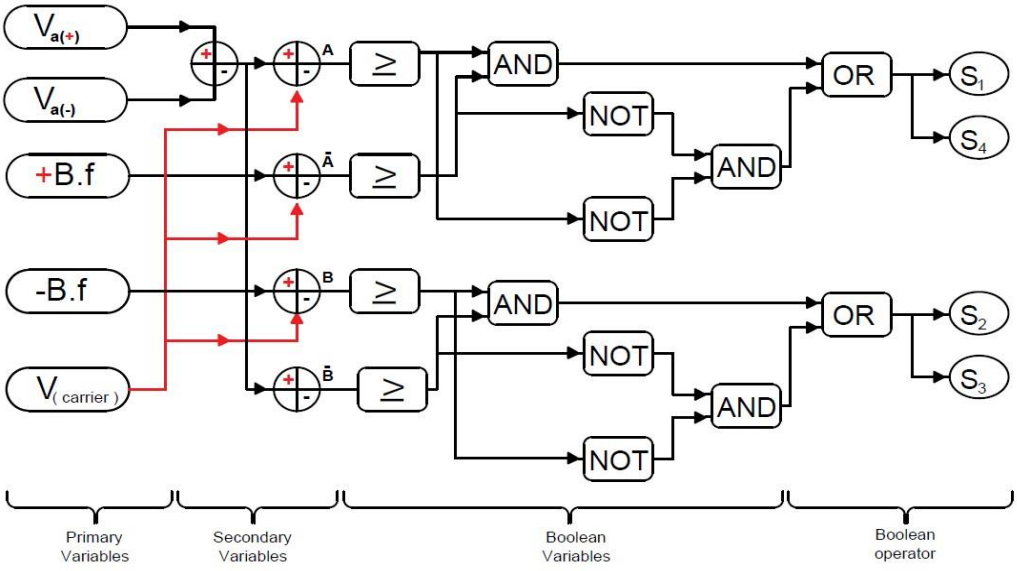

Figure 4. 18: Constant Boost PWM control method

The flow diagram shown in Figure 4.18 illustrates a control circuit for Leg A and Leg B. Switch one (S1) and switch three (S3) are identified as the upper switches, while switch two (S2) and switch four (S4) are recognized as the lower switches. However, the diagram above effectively illustrates the behavioural characteristics of Leg A and Leg B, as defined by equations (4.20), (4.21), (4.22) and (4.23) correspondingly.

The modulation index and shoot-through duty ratio, as well as the boost factor, are adjusted by manipulating the ratio between the peak value of V_{acp} and $V_{carrier}$. The expression (4.11) below provides the output voltage for the CBC PWM technique. Additionally, Figures 4.19 and 4.20 depict a collection of results obtained from the CBC PWM technique when sampled at regular intervals. The voltage, denoted as Vin, was measured to be 200 volts with a corresponding value of 0.65. The remaining outcomes are displayed in Table 4.7.

$$V_{acp} = MB\frac{V_{DC}}{2} \tag{4.24}$$

$$B = \frac{T}{1 - 2T_0/T} \geq 1 \tag{4.25}$$

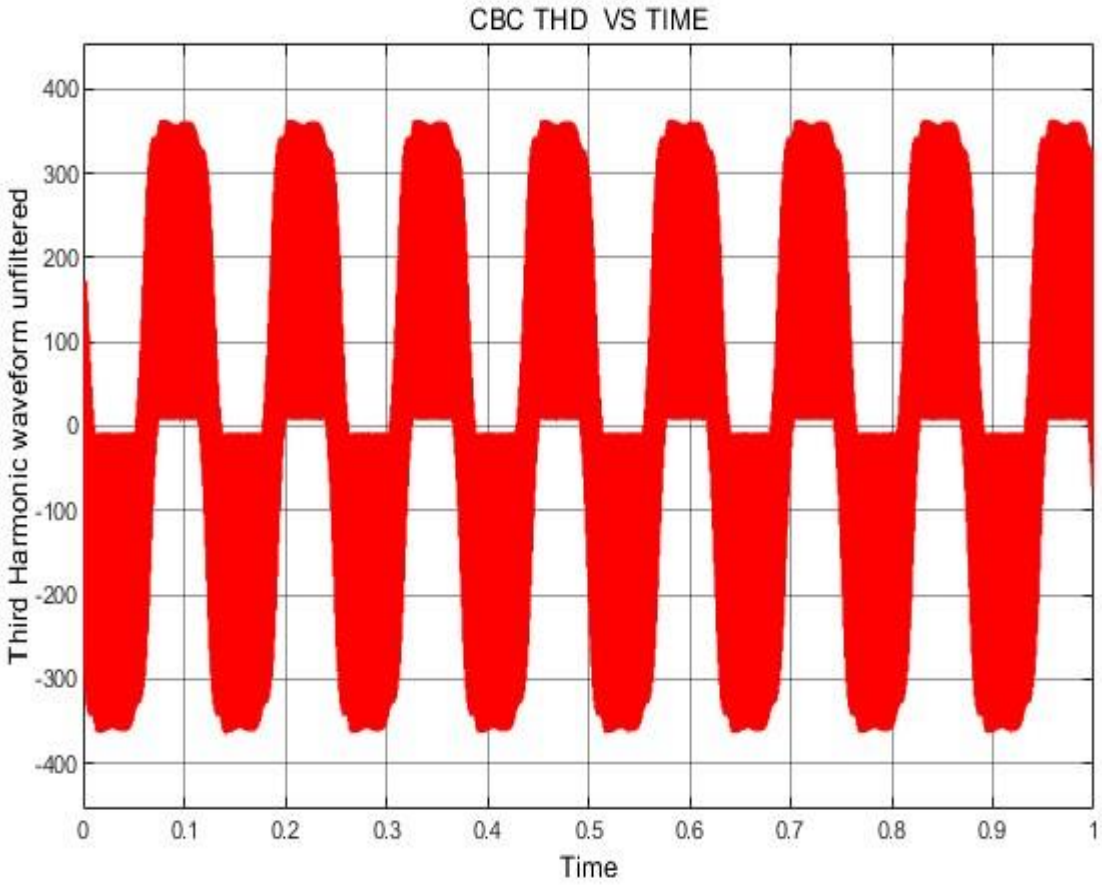

Figure 4. 19: Unfiltered Harmonic at supplied voltage of 200 V and 0.65 Modulation index

Figure 4.19 demonstrates the unfiltered waveform within the Stand-alone PV system, wherein red signifies the presence of danger or higher values of harmonic component in the Circuit. It is imperative to adhere to both the IEEE standard and the SANS 10142 Standard to protect equipment connected to the system.

In Figure 4.20, the filtered waveform showcasing reduced harmonic components is depicted for the Stand-alone Photovoltaic (PV) system. The waveform parameters, crucial for the analysis of output voltage and current harmonic components, are specified as 200V and a Modulation Index of 0.65. In the given waveform, it is solely applicable to LC configurations. However, for LCL and LLCL setups, an analysis will be conducted using data in Table 4.7, considering various conditions in the Stand-alone PV system. This occurrence pertains specifically to the output load of the system or circuit.

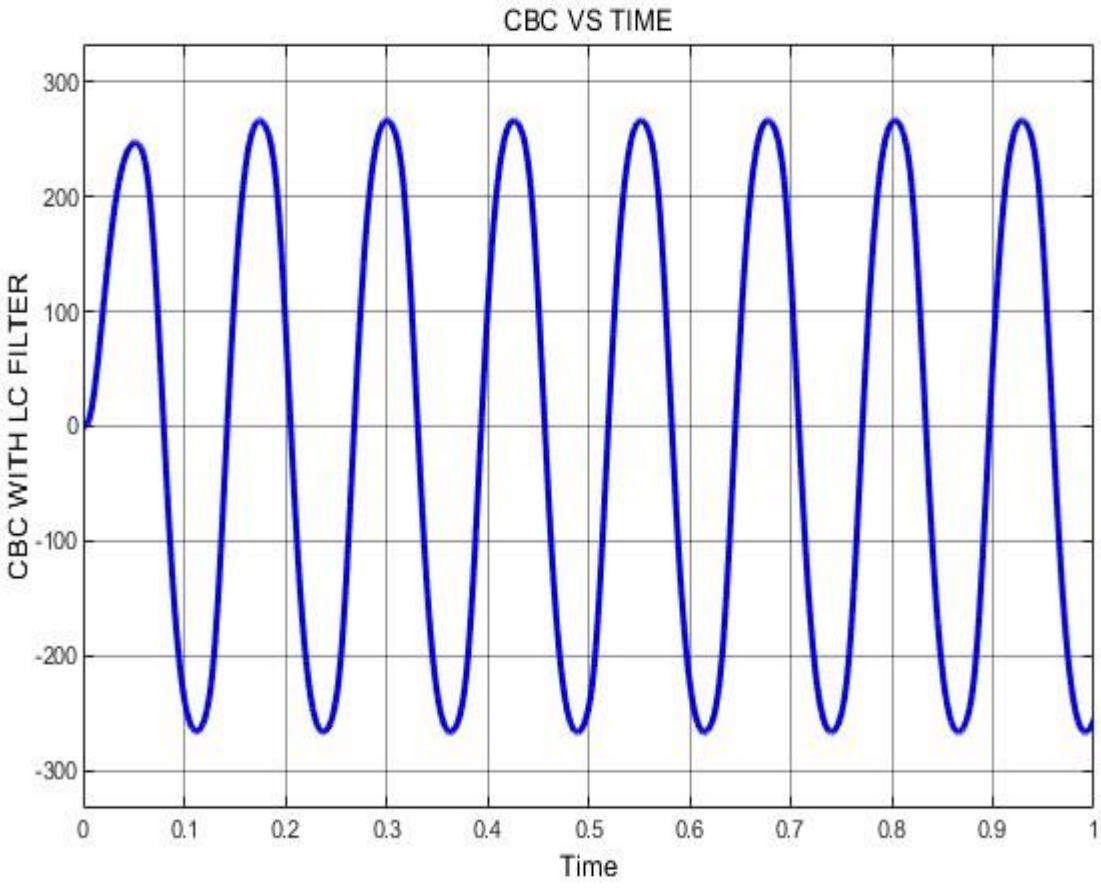

Figure 4. 20: Filter waveform of load voltage at the Modulation index (0.65)

The unfiltered harmonics are visually represented by the colour red, while the filtered harmonics are visually represented by the colour blue. The filtering process involves applying a scale ranging from 0 to 1 to achieve a more distinct and refined waveform. The waveform exclusively pertains to the LC filter in Table 4.7, which will showcase the outcomes for both the LCL and LLCL filters.

Table 4. 7: Analysis of harmonic components and other causes of THD%

Varying the Modulation index and Input Voltage to analysis harmonic components								
V_{IN}	200	300	400	500	200	300	400	500
M	0.65	0.65	0.65	0.65	0.75	0.75	0.75	0.75
V_{Stress}	48.12	72.31	96.43	120.4	40.69	61.12	81.55	102
$V_{DC-LINK}$	89.53	134.5	179.4	224.4	83.33	125.2	167	208.8
$THD\%$	38.85	38.85	38.85	38.85	38.85	38.85	38.85	38.85
$THD_v\%\ with\ LC\ Filter$	4,177	4.29	4.29	4.29	4,177	4,177	4,177	4,177
$THD_I\%\ with\ LC\ Filter$	2.958	3.00	3.00	3.00	2.958	2.958	2.958	2.958
$THDv\%\ with\ LCL\ Filter$	2.457	2.556	2.556	2.556	2.457	2.457	2.457	2.457
$THD_I\%\ with\ LCL\ Filter$	2.00	2.05	2.05	2.05	2.00	2.00	2.00	2.00
$THDv\%\ with\ LLCL\ Filter$	1.901	1.931	1.931	1.931	1.901	1.901	1.901	1.901
$THD_I\%\ with\ LLCL\ Filter$	1.234	1.345	1.345	1.345	1.234	1.234	1.234	1.234
Table 4.7: Continues below from 0.85 to 0.95 of Modulation index and Input Voltage								
V_{IN}	200	300	400	500	200	300	400	500
M	0.85	0.85	0.85	0.85	0.95	0.95	0.95	0.95
V_{Stress}	33.33	50.06	66.81	83.53	27.94	41.99	56.02	70.01
$V_{DC-LINK}$	85.16	127.9	170.7	213.4	105.6	158.7	211.7	264.7
$THD\%$	38.85	38.85	38.85	38.85	38.85	38.85	38.85	38.85
$THDv\%\ with\ LC\ Filter$	4.812	4.812	4.812	4.812	5.01	5.01	5.01	5.01
$THD_I\%\ with\ LC\ Filter$	2.916	2.916	2.916	2.916	3.00	3.00	3.00	3.00
$THDv\%\ with\ LCL\ Filter$	2.655	2.655	2.655	2.655	2.655	2.655	2.655	2.655
$THD_I\%\ with\ LCL\ Filter$	2.05	2.06	2.06	2.06	2.09	2.09	2.09	2.09
$THDv\%\ with\ LLCL\ Filter$	1.951	1.994	1.994	1.994	1.951	1.951	1.951	1.951
$THD_I\%\ with\ LLCL\ Filter$	1.324	1.365	1.365	1.365	1.465	1.465	1.465	1.465

4.4.2.1. Results and analysis of Constant boost PWM

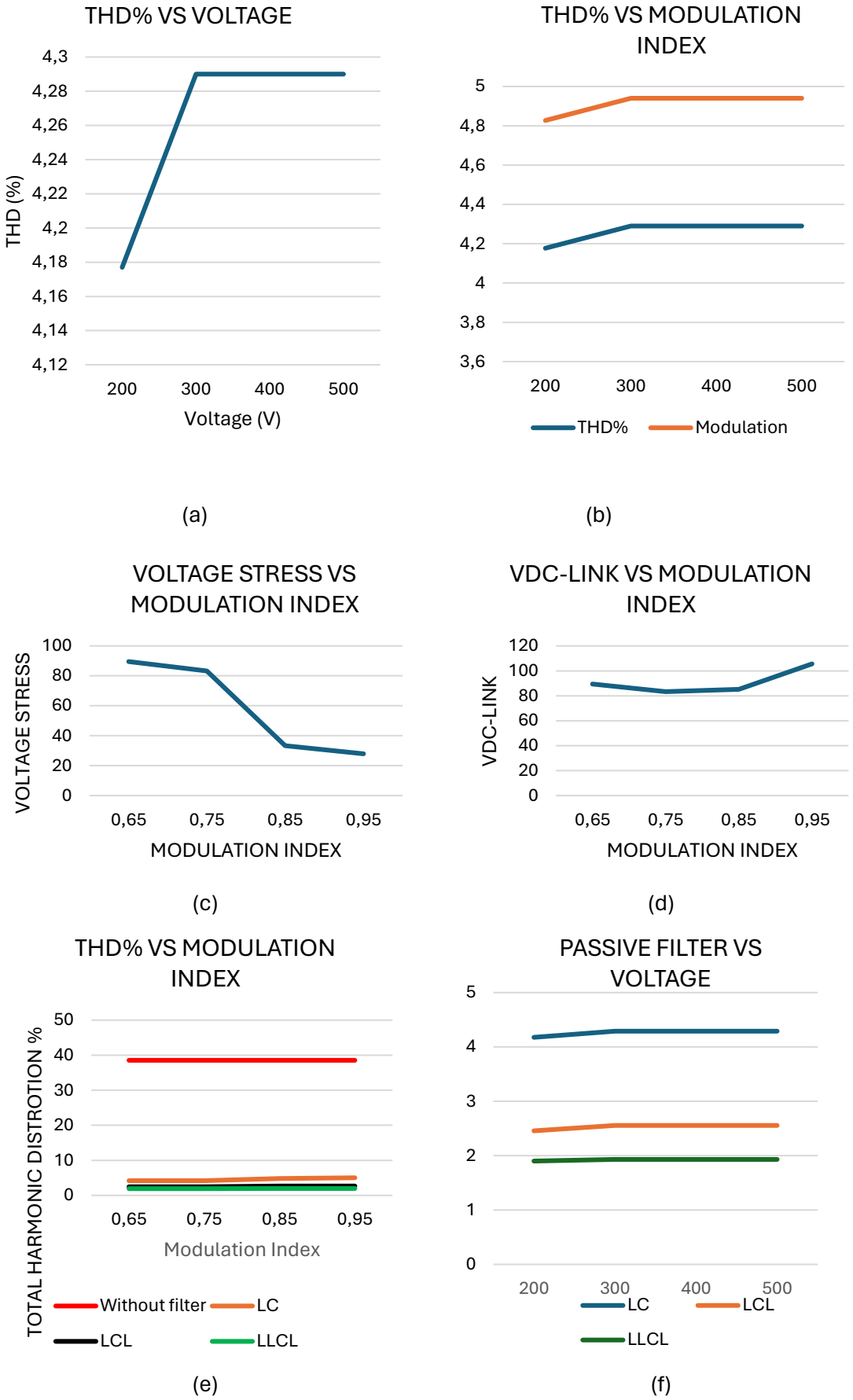

Figure 4.21: result of different conditions to analysis THD% and performance of the off-grid PV system

Figures 4.21:(a) and (b): The total harmonic distortion percentage (THD%) of an LC circuit is a crucial parameter that characterizes the level of distortion present in the circuit's output waveform. The study implements a voltage filter with a specified 200 V to 500 V range. The data illustrates a positive relationship between voltage and the total harmonic distortion percentage (THD%) of voltage, whereas the current demonstrates a direct proportionality to voltage. The modulation index remains constant in this situation. Figure 4.21: (c) displays the voltage stress experienced by the switching devices within the circuit, which consequently contributes to the failure of the network. However, it is crucial to conduct an analysis of the switches and choose the most efficient switches. The relationship between voltage stress and total harmonic distortion should also be taken into consideration. When the modulation index is increased, the voltage stress is eventually decreased, resulting in a reduction of the overall voltage stress.

Figure 4.21: (d): depicts the relationship between the DC Voltage link and the Modulation index is being investigated. Values are being selected from a table with increments of 200 V, while the modulation index is varied. The observed phenomenon illustrates a direct proportionality between the DC Voltage and modulation index, indicating that the DC Voltage is directly proportional to the modulation index. Figure 4.21: (e): shows the total harmonic distortion (THD) in the absence of a filter, using the colour red for a graphical representation. The orange colour is indicative of an LC filter, while the black colour represents an LCL filter. The green colour, on the other hand, corresponds to the LLCL filter, which has demonstrated superior performance in this research study. The graphical representation illustrates the comparative analysis of a Passive filter across various modulation indices.

In Figure 4.21: (f), the graphical representation depicts the total harmonic distortion when filters are applied. The blue colour is indicative of the LC filter, while the orange colour represents the LCL filter. The grey colour, on the other hand, corresponds to the LLCL filter, which has exhibited superior performance in the context of this research study. The graphical representation illustrates the comparative analysis of a Passive filter across varying voltage levels while maintaining a constant modulation index.

To conduct a comprehensive analysis of harmonics, it is imperative to manipulate the modulation index and voltage in a variable manner. This approach allows for a systematic exploration of the impact of these parameters on the harmonics present in the system under investigation. By varying the modulation index and voltage, one can observe how changes in these factors influence the amplitude and frequency distribution of harmonics.

4.4.3 The Simple Boost Control Method (SBC)

The objective is to devise a simple boost pulse width modulation (PWM) control circuit and subsequently present the obtained outcomes.

In addition to the two modulating signals, Vac(φ) and Vcarrier, as described in sub-section 4.4.1, the simple boost PWM technique introduces two additional linear functions that enclose the primary single-phase signal at its positive and negative peaks (as described in Chapter 2) and can be mathematically defined as follows:

$$V_{constant} = \begin{cases} C \\ -C \end{cases} \tag{4.26}$$

Where $V_M \leq C \leq 1$ and $-1 \leq -C \leq V_M$

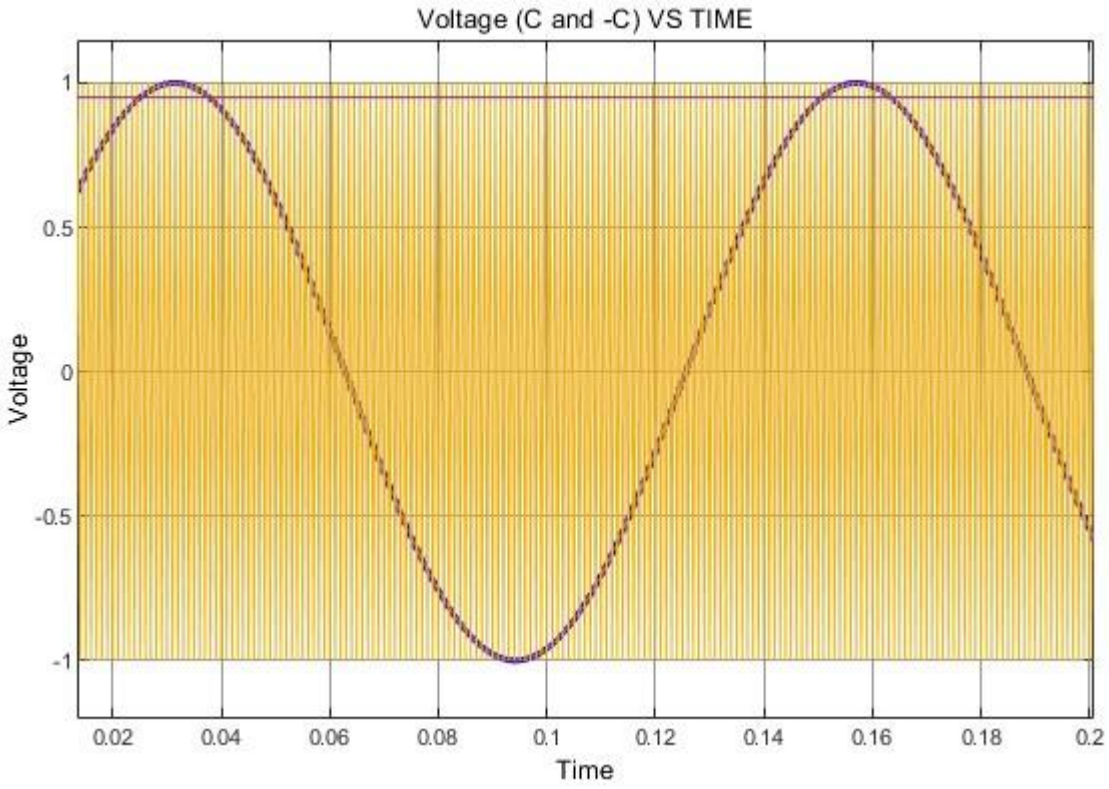

Figure 4.22: Single-phase waveform for Simple Boost Control

Source Inverter (ZSI) of the desired switching behaviour of the simple boost PWM generator, which controls the clocking of the switching devices in the Impedance Source Inverter (ZSI), can

be achieved by formulating four secondary variables based on the three modulating signals: Vac(φ), Vcarrier, and Vconstant. Therefore, consider:

$$\mathrm{A} = V_{A(\varphi)} - V_{(carrier)} \tag{4.27}$$

$$\mathrm{B} = V_{A(\varphi)} - V_{(carrier)} \tag{4.28}$$

$$\mathrm{C} = C - V_{(carrier)} \tag{4.29}$$

$$\mathrm{D} = V_{(carrier)} - (-C) = C + V_{(carrier)} \tag{4.30}$$

The complete definition of the desired switching pattern for the SBC PWM generator, which controls the impedance source inverter (ZSI), can be achieved by utilizing the secondary variables A, B, C and D, as well as the switching states S1 - S4 of the switching devices. Hence, presented in Table 4.8 is a truth table that illustrates the states of every switching device for all potential secondary variable states. This comprehensive representation establishes the complete operational characteristics of the SBC PWM controller, which is necessary to generate the desired Single-phase signal (4.3.1).

Table 4. 8: Truth table for switching state in the Simple boost control PMW Method

Switching State	Switch One S_1	Switch Two S_2	Switch Three S_3	Switch Four S_4	Output Voltage
Active State (1)	1	0	0	1	Finite Voltage
	0	1	1	0	
Zero State (0)	1	0	1	0	Zero
	0	1	0	1	
Shoot-Through State	1	1	S_3	S_4	Zero
	S_1	S_2	1	1	
	1	1	1	1	

One significant difference between the simple boost control and constant boost control PWM technique is due to the formulation of a single-phase fundamental reference shape of the waveform. The above truth table does the same thing as explained in Table 4.6.

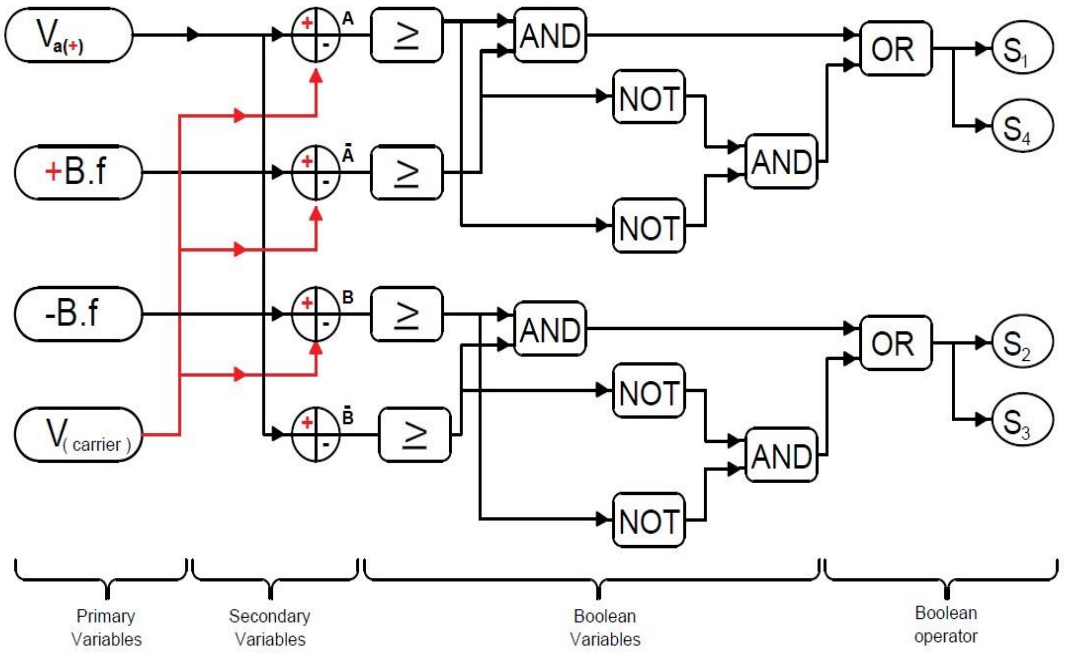

Figure 4.23: Simple boost control method

Figure 4.23 depicts the simple boost control network comprising primary variables, secondary variables, Boolean variables and Boolean operators that constitute the network. This network can be classified as a digital system and control system.

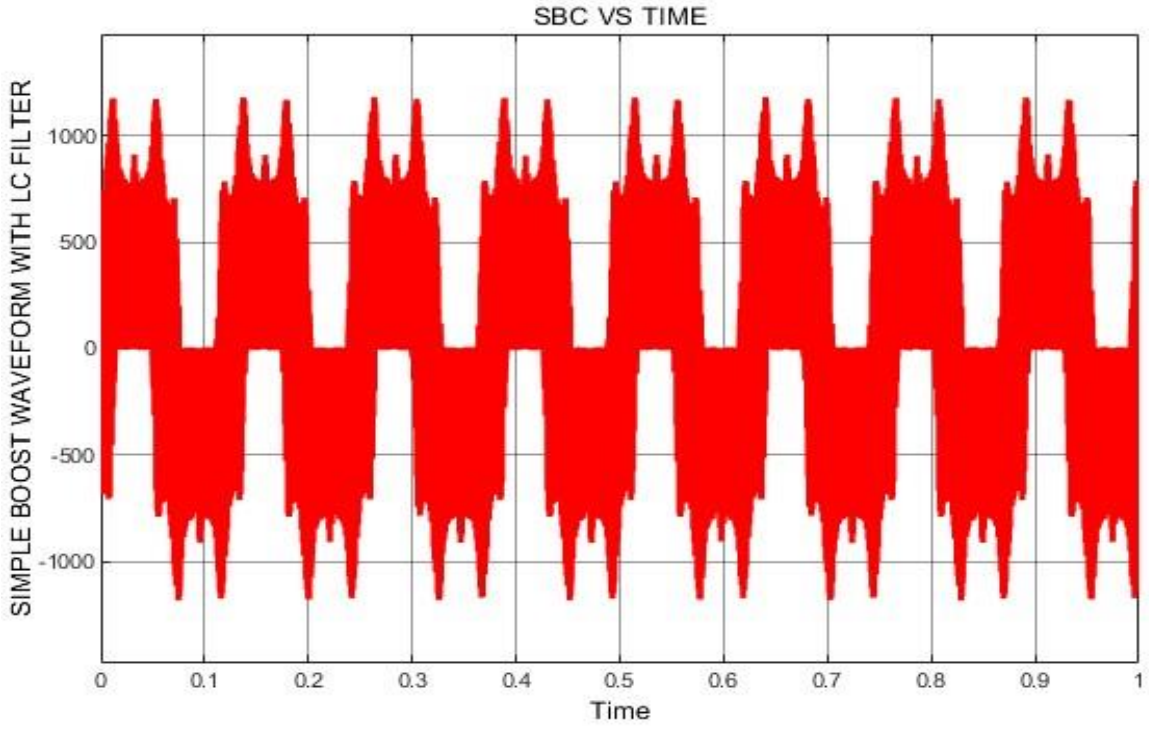

Figure 4.24: Unfiltered waveform of simple boost control method

Figure 4.24 depicts the comprehensive representation of total harmonic distortion in the absence of a filter within the single-phase Z-Source inverter photovoltaic network, specifically pertaining to the simple boost control method.

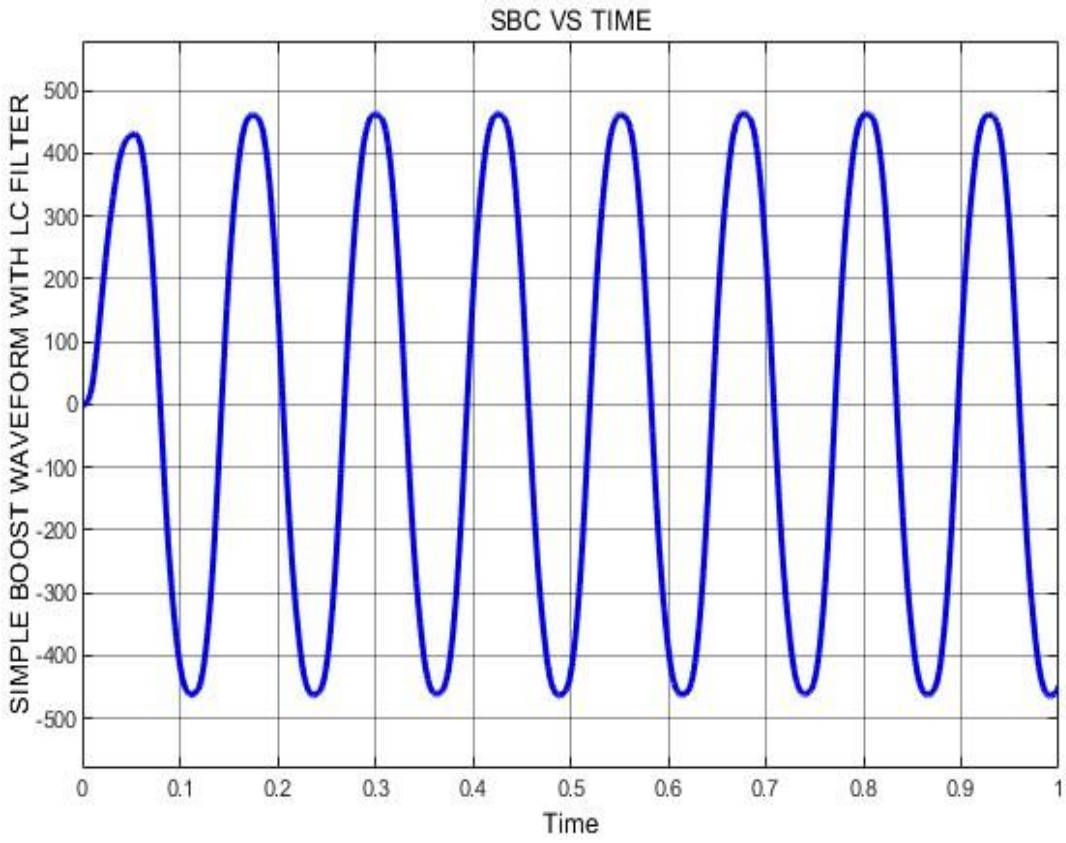

Figure 4.25: Filtered Waveform of Simple Boost Control Method

Figure 4.25 depicts the total harmonic distortion observed in the single-phase Z-Source inverter PV network when implementing the simple boost control method, as indicated by the filter. The health of the waveform surpasses that of Figure 4.24. In this section, the filters were meticulously designed in accordance with the rigorous specifications outlined by the esteemed IEEE Standard 519 of both 1992 and 2014. Table 4.9 below presents additional findings from this study, where various relationships were analysed.

Table 4. 9: Analysis of harmonic components and other causes of the % for the simple boost control method

Varying Modulation index and input Voltage to analysis Harmonic Component								
V_{IN}	200	300	400	500	200	300	400	500
M	0.65	0.65	0.65	0.65	0.75	0.75	0.75	0.75
$Voltage_{stress}$	22.37	33.66	44.91	56.16	19.19	28.86	38.46	48.15
$V_{DC-LINK}$	45.14	67.93	90.62	113.3	38.75	58.26	77.66	97.21
$THD\%\ without\ Filter$	44.98	44.98	44.98	44.98	44.98	44.98	44.98	44.98
$THD_v\%\ with\ LC\ Filter$	4.011	4.013	4.014	4.016	2.345	2.345	2.345	2.345
$THD_i\%\ with\ LC\ Filter$	4.012	4.012	4.012	4.012	2.346	2.346	2.346	2.346
$THD_v\%\ with\ LCL\ Filter$	3.321	3.323	3.323	3.323	1.920	1.920	1.920	1.920
$THD_i\%\ with\ LCL\ Filter$	3.321	3.322	3.322	3.322	1.921	1.921	1.921	1.921
$THD_v\%\ with\ LLCL\ Filter$	1.550	1.551	1.551	1.551	0.921	0.912	0.910	0.910
$THD_i\%\ with\ LLCL\ Filter$	1.401	1.401	1.401	1.401	0.201	0.201	0.201	0.201
Table 4.8: Continuous below from 0.85 to 0.95 of modulation index								
M	0.85	0.85	0.85	0.85	0.95	0.95	0.95	0.95
V_{IN}	200	300	400	500	200	300	400	500
$Voltage_{stress}$	19.49	29.25	39.04	48.77	5.331	4.301	3.195	2.115
$V_{DC-LINK}$	39.34	59.03	78.82	98.47	128.4	192.9	257.3	128.4
$THD\%\ without\ Filter$	44.98	44.98	44.98	44.98	44.98	44.98	44.98	44.98
$THD_v\%\ with\ LC\ Filter$	2.345	2.345	2.345	2.345	2.345	2.345	2.345	2.345
$THD_i\%\ with\ LC\ Filter$	2.346	2.346	2.346	2.346	2.346	2.346	2.346	2.346
$THD_v\%\ with\ LCL\ Filter$	1.920	1.920	1.920	1.920	1.920	1.920	1.920	1.920
$THD_i\%\ with\ LCL\ Filter$	1.921	1.921	1.921	1.921	1.921	1.921	1.921	1.921
$THD_v\%\ with\ LLCL\ Filter$	0.211	0.211	0.211	0.211	0.211	0.211	0.211	0.211
$THD_i\%\ with\ LLCL\ Filter$	0.201	0.201	0.201	0.201	0.201	0.201	0.201	0.201

4.4.3.1 Results and Analysis of the Simple boost PWM Method

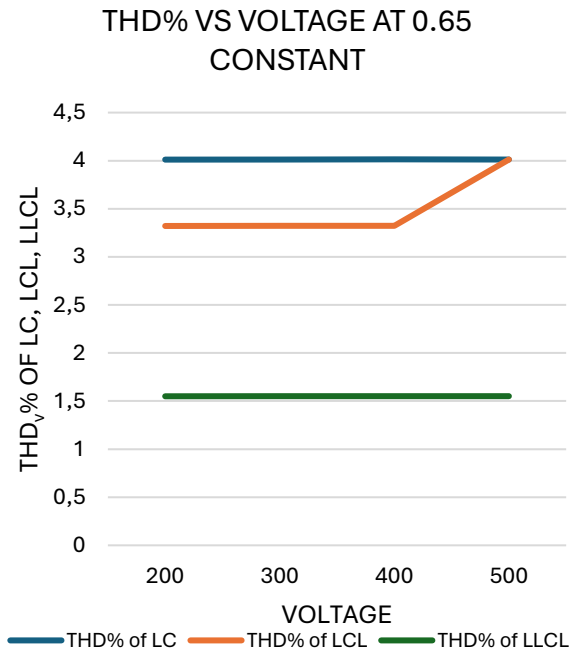

(a)

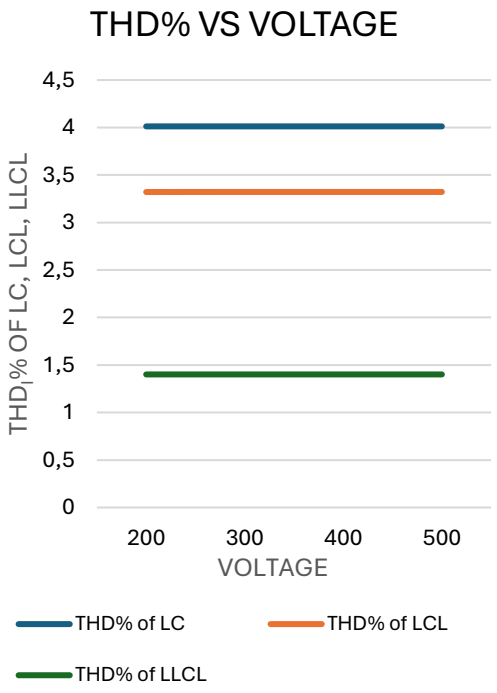

(b)

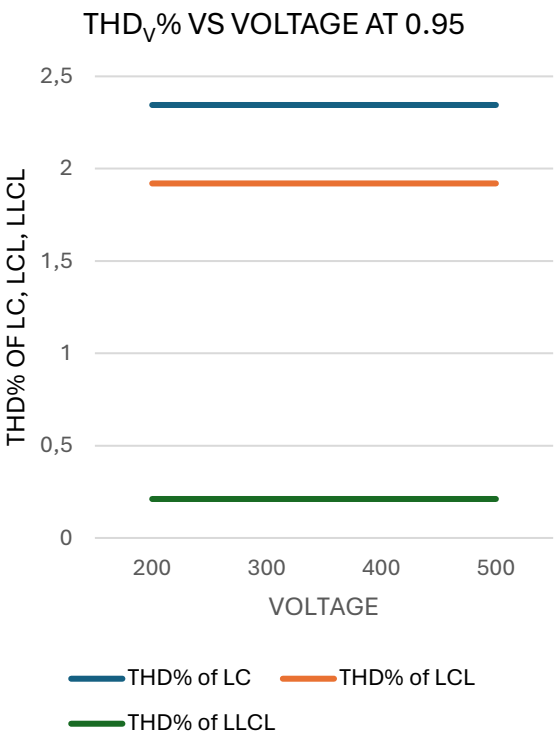

(c)

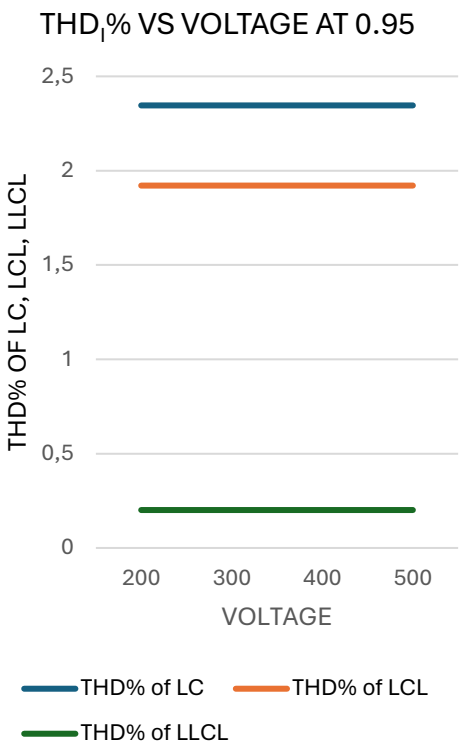

(d)

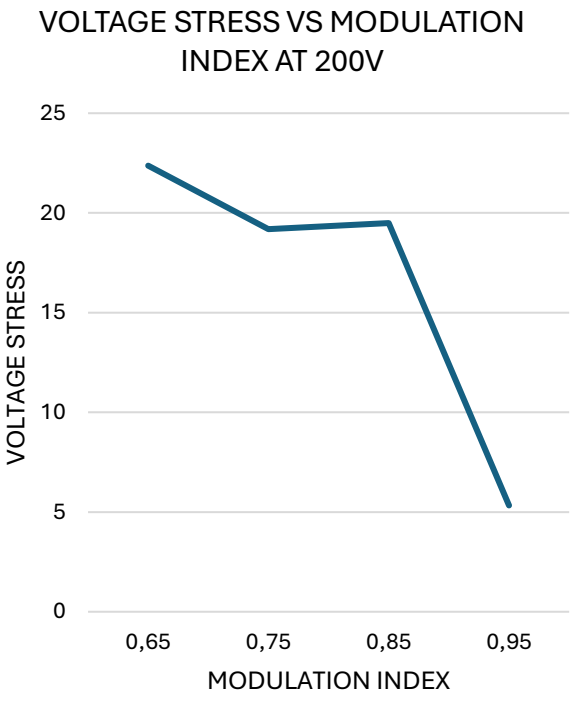

(e)

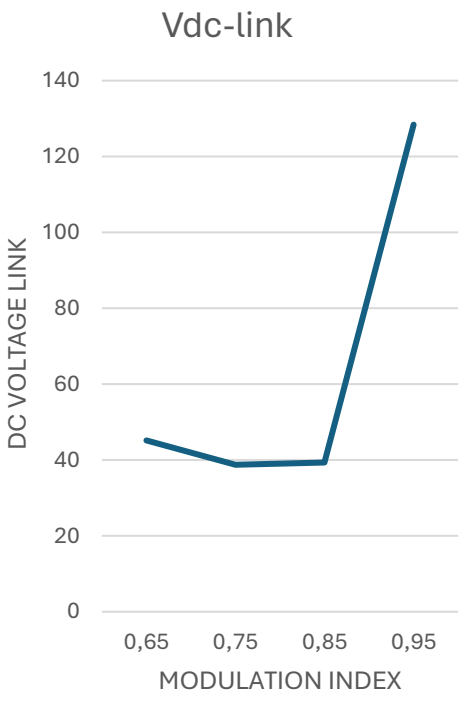

(f)

Figure 4.26: Analysis of Simple Results of THD% and Performance

Figure 4.26: (a): The total harmonic distortion percentage of passive filters is found to be higher than the specified threshold when considering LC filters, specifically at a modulation index of 0.65. The observational data proves the relationship between the voltage and modulation index. The LCL filter operating at a modulation index of 0.65 has experienced improvements. However, as the modulation index is increased, it is observed that the LCL filter successfully meets the prescribed THD% threshold as specified by the IEEE Standard. On the contrary, the LLCL filter demonstrates consistent behaviour even as the modulation index is increased. However, it is worth noting that the LLCL filter demonstrates greater improvement in performance. Figure (b): At the current parameters of the LC passive filter, it is observed that the filter's performance remains constant, although not meeting the required Total Harmonic Distortion (THD%) percentage of current as per the IEEE Standard. However, it is noteworthy that the filter's performance improves with an increase in the modulation index. The LCL filter demonstrates constant behaviour and satisfies the specifications outlined in the IEEE Standard. Furthermore, it demonstrates improved performance as the modulation index is increased. The LLCL filter demonstrates optimal performance, with significant improvements observed when the modulation index has been increased or decreased.

Figures 4.26: (c) and (d): The voltage and current results, at a modulation index of 0.95, demonstrate compliance with the IEEE Standard. Figure (e): The phenomenon of voltage stress displays a reduction in magnitude when the modulation index is increased, as opposed to when it is decreased. This observation corresponds to the findings illustrated in Figures 4.26: (c) and (d), specifically in relation to the Total Harmonic Distortion percentage. Figure (f): The observed phenomenon is that the DC voltage displays a decline in magnitude as the modulation index decreases, and inversely, it also experiences a decline when the modulation index is augmented.

4.5 Comparison analysis of the LLCL Filter in the Single-phase off-grid PV System and Single-phase Z-Source inverter off-grid PV System

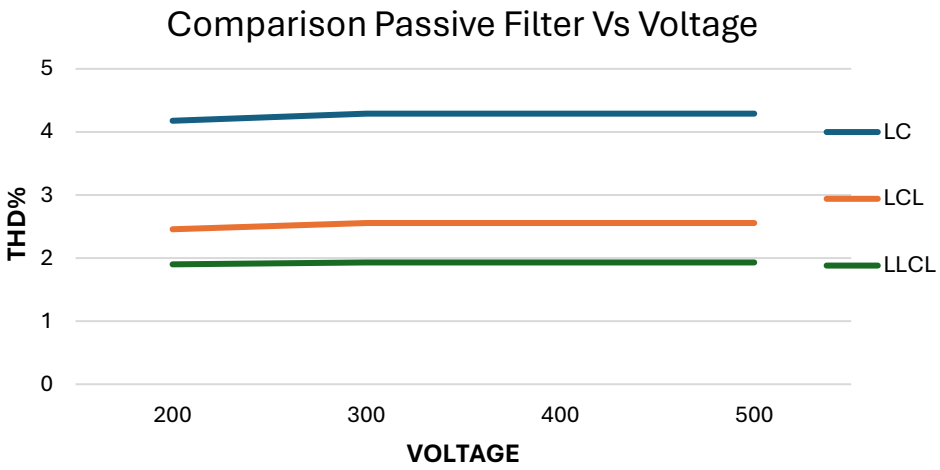

Figure 4.27 (a): Comparison of LLCL filters under different networks for voltage

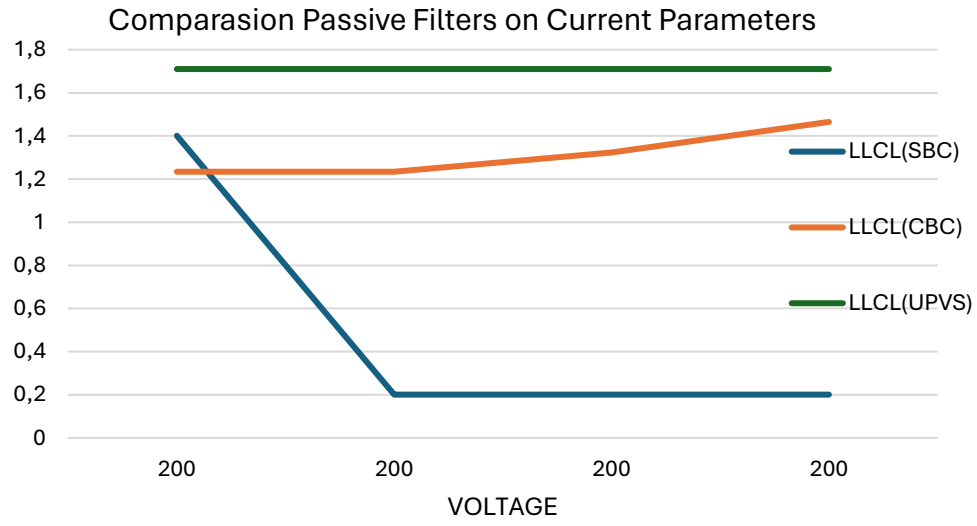

Figure 4.27 (b): Comparison of LLCL Filters Under different networks for current

Figures 4.27 (a) and (b): The Z-Source inverter in the single-phase off-grid PV network is designated by using the orange colour. It is integrated with a simple boost control method and is interconnected to the LLCL filter. The colour grey is designated for the single-phase off-grid PV network equipped with an LLCL filter. The Z-Source inverter in a single-phase off-grid PV network with a constant boost control method is associated with the use of the blue colour. This is specifically applicable when connected to the LLCL filter.

Figure 4.27 (a): The graphical representation depicts the total harmonic distortion of voltage, wherein it is evident that the orange line (CBC) indicates a higher magnitude in the graph. The grey line in the graph represents the second lowest value of total harmonic distortion of voltage. This data point corresponds to the first circuit that was specifically designed for this study. The circuit in question is a Stand-alone PV Network that applied a universal inverter to generate the observed results. The optimal outcome is achieved through the implementation of a simple boost control methodology, denoted by the blue line. The voltage's total harmonic distortion of all three components complies with both the IEEE Standard and the SANS 10142 Standard, ensuring the protection of equipment connected to the system. Figure 4.27 (b): The graphical representation of the total harmonic distortion of current is used to determine the optimal current within a network. In this study, it is observed that the stand-alone system with a universal inverter indicates a greater current compared to the other networks designed. The grey line indicates a higher magnitude compared to the orange line in this case. Consequently, the Constant Boost Control method ranks as the second most optimal approach. However, the blue line continues to demonstrate superior outcomes, indicating that the Simple Boost Control method remains the most effective in protecting applications.

Chapter Five: Conclusion and Recommendation

5.1 Conclusion

The primary focus and purpose of this research covered the comprehensive examination and evaluation of the total harmonic distortion characteristics within an off-grid photovoltaic (PV) system. Total harmonic distortions arise due to various factors within the electronic circuit or network. In order to effectively mitigate harmonic components, it is imperative to implement measures that safeguard both the circuit and the alternating current (AC) load.

The research presented herein satisfactorily fulfils all the stipulations outlined in the IEEE Standard (519) and SANS 10142 Standard, thereby ensuring the safeguarding of equipment interconnected with the PV system. The present study additionally investigated the enhancement of power quality through the implementation of passive filters. The harmonic components, surpassing the prescribed standards, were effectively mitigated, resulting in notable improvements in both power quality and power factor.

During the research, an analysis was conducted on the characteristics of voltage and current, primarily due to the direct proportionality between current and voltage. The graphical representation on an off-grid PV network illustrates the relationship between current and voltage. This relationship is observed by varying the Irradiance and temperature conditions to analyse the impact of each condition. Additionally, different conditions are examined to analysis the Total Harmonic Distortion of Voltage and Current characteristics.

Two circuits were designed to analysis the total harmonic distortion for single-phase systems, such as the single-phase off-grid PV circuit and single-phase impedance source inverter circuit (off-grid). The analysis was conducted on a single-phase off-grid photovoltaic (PV) system, which includes a step-up booster connected to a universal inverter. The universal inverter is further connected to a filter, while other components remain unconnected to the filter. The purpose of this analysis was to evaluate the total harmonic distortion present in the network. The observed results indicate a THD of 89.05% in current and voltage. In section 4.1.3.1, figures 4.4 (a) and 4.4 (b) depict waveforms exhibiting a total harmonic distortion (THD) of 89.05%. These waveforms were effectively mitigated through the implementation of designed filters as outlined in section 4.1.4.1. These filters aim to reduce the total harmonic distortion to meet the specified standard set by the Institute of Electrical and Electronics Engineers (IEEE).

The single-phase z-source inverter exhibits a reduced level of total harmonic distortion in comparison to the single-phase photovoltaic network. The ZSI comprises two controllers, namely the constant boost control method and the simple boost control method. These controllers are interconnected with the ZSI off-network to enhance harmonics and elevate the output voltage to the desired level. The implementation of a constant boost control system is required. The integration of the Pulse Width Modulation (PWM) technique in conjunction with a simple boost control structure has been considered. The total harmonic distortion values of the PWM method without the implementation of passive filters on the impedance Source Inverter (ZSI) circuit have been measured to be 38.85% and 44.96% respectively.

Impedance source inverters have the advantage of being able to increase voltage indefinitely because of the PWM technique stated above. Sections 4.3.1 and 4.3.2 provided more details on the PWM approach that was used in this study, along with the literature review. This study additionally encompassed various subjects combined to provide information for this research, which are described as follows: The study was made possible by the integration of digital systems, control systems, electronic protection systems, and power electronics into the design of the renewable network.

The LC, LCL and LLCL were subjected to various conditions for the purpose of design and analysis. The assessment of total harmonic performance has been conducted at the designated testing establishment. The tables presented in Chapter 4 have been meticulously developed to efficiently gather data across various filters. However, it is important to note that the analysis did not solely focus on harmonic components. The stress distribution across the switches was analysed, and the DC voltage was investigated using the PWM method to accurately determine the various relationships that were discovered.

The graphical figures in Chapter 4 depict the comparison of results obtained from tables under various conditions. Waveforms were generated from a circuit incorporating passive filters (LC, LCL and LLCL). The results indicate that the LLCL Filter outperforms other conditions and circuit designs presented in Chapter 4, specifically in sections 4.2 and 4.3. The network or circuit of the Single-phase off-grid PV System and Single-phase ZSI off-grid PV demonstrate significant improvements in the total harmonic distortion. The voltage stress across the switching devices, boost factor and percentage of total harmonic distortion were found to be purely independent of the modulation index. Furthermore, it was observed that all these parameters decrease as the modulation index increases.

5.2 Recommendation

In order to facilitate the automation of this system, it would be advantageous to implement certain measures. The consideration of integrating with a digital system may be necessary for improving the performance of various characteristics. Communication protocols are a set of rules and standards that govern the exchange of information between two or more devices or systems [131]. These protocols define the format, timing, sequencing and error control. Developing and integrating a robust communication protocol, such as Modbus, Profibus or Ethernet/IP, establishes a seamless and efficient data interchange mechanism between the impedance source inverter and the digital control system. This facilitates the implementation of real-time monitoring, control and automation functionalities for the inverter.

Sensor Integration: Facilitates the seamless integration of diverse sensors into the impedance source inverter system, enabling the acquisition of crucial data pertaining to voltage, current, temperature and fault conditions. The sensors possess the capability of furnishing feedback to the digital control system, thereby empowering it to make judicious determinations and execute suitable measures.

The development of advanced digital control algorithms is required to optimize the performance of the impedance source inverter. The algorithms have the capability of being engineered for the purpose of regulating output voltage, current, or frequency. Additionally, they possess the ability to incorporate functionalities such as maximum power point tracking specifically tailored for photovoltaic-based inverters. The implementation of fault detection and diagnostics algorithms in the digital control system enhanced performance and reliability. The automation system can detect and address faults or abnormalities in the impedance source inverter, thereby enhancing the reliability of the entire system, and minimizing operational downtime.

References

[1] L. Jackson, S. Soliman, and M. Srinath, "Electrical Filters: Fundamentals and System Applications 55," *The Froehlich/Kent Encyclopedia of Telecommunications: Volume 7-Electrical Filters: Fundamentals and System Applications to Federal Communications Commission of the United States,* p. 55, 2021.

[2] W. Wu, S. Feng, J. Ji, M. Huang, and F. Blaabjerg, "LLCL-filter based single-phase grid-tied Aalborg inverter," in *2014 International Power Electronics and Application Conference and Exposition*, 2014: IEEE, pp. 658-663.

[3] V. Kuitenbrouwer, A. Luscombe, and H. Wijfjes, "Developing Radio Histories," *TMG Journal for Media History,* vol. 22, no. 2, 2019.

[4] V. Kureichik and V. Bova, "Hybryd approach for computer-aided design problems," in *2019 International Seminar on Electron Devices Design and Production (SED)*, 2019: IEEE, pp. 1-5.

[5] A. K. Pandey, S. Anshari, and J. VITS, "DESIGN OF NEW HARMONIC FILTER FOR RENEWABLE ENERGY SOURCE WITH HIGH ATTENUATION AND LESS DAMPING."

[6] J. M. Guerrero, P. C. Loh, T.-L. Lee, and M. Chandorkar, "Advanced control architectures for intelligent microgrids—Part II: Power quality, energy storage, and AC/DC microgrids," *IEEE Transactions on industrial electronics,* vol. 60, no. 4, pp. 1263-1270, 2012.

[7] Z. B. Duranay and H. Guldemir, "Modelling and simulation of a single phase standalone PV system," in *2019 11th International Conference on Electronics, Computers and Artificial Intelligence (ECAI)*, 2019: IEEE, pp. 1-6.

[8] A. A. Khamisani, "Design methodology of off-grid PV solar powered system (A case study of solar powered bus shelter)," *Goolincoln Avenue Charleston, IL: Eastern Illinois University,* 2019.

[9] P. Shaw, P. K. Sahu, S. Maity, and P. Kumar, "Modeling and control of a battery connected standalone photovoltaic system," in *2016 IEEE 1st International Conference on Power Electronics, Intelligent Control and Energy Systems (ICPEICES)*, 2016: IEEE, pp. 1-6.

[10] S. Lyden, M. Haque, A. Gargoom, and M. Negnevitsky, "Modelling photovoltaic cell: Issues and operational constraints," in *2012 IEEE International Conference on Power System Technology (POWERCON)*, 2012: IEEE, pp. 1-6.

[11] C. W. Lander, *Power electronics*. McGraw-Hill, Inc., 1987.

[12] Y. Djeghader, L. Zellouma, A. Lakehal, and Z. Chelli, "Harmonic Mitigation in Electrical Radial Distribution System Using Photovoltaic Unified Power Quality Conditioner (PV-UPQC)," in *2019 8th International Conference on Systems and Control (ICSC)*, 2019: IEEE, pp. 94-99.

[13] M. El-Sayed, A. Abou El-Ela, and R. A. El-Sehiemy, "Effect of photovoltaic system on power quality in electrical distribution networks," in *2016 Eighteenth International Middle East Power Systems Conference (MEPCON)*, 2016: IEEE, pp. 1005-1012.

[14] A. Srivastav, "Energy Dynamics and Climate Mitigation: An Indian Perspective," 2020.

[15] O. M. Akinbami, S. R. Oke, and M. O. Bodunrin, "The state of renewable energy development in South Africa: An overview," *Alexandria Engineering Journal,* vol. 60, no. 6, pp. 5077-5093, 2021.

[16] H.-L. Tsai, C.-S. Tu, and Y.-J. Su, "Development of generalized photovoltaic model using MATLAB/SIMULINK," in *Proceedings of the world congress on Engineering and computer science*, 2008, vol. 2008: San Francisco, USA, pp. 1-6.

[17] I. Altas and A. Sharaf, "A photovoltaic array simulation model for Matlab-Simulink GUI environment," in *2007 International Conference on Clean Electrical Power*, 2007: IEEE, pp. 341-345.

[18] C.-T. Pan, J.-Y. Chen, C.-P. Chu, and Y.-S. Huang, "A fast maximum power point tracker for photovoltaic power systems," in *IECON'99. Conference Proceedings. 25th Annual Conference of the IEEE Industrial Electronics Society (Cat. No. 99CH37029)*, 1999, vol. 1: IEEE, pp. 390-393.

[19] T. Ahmad and D. Zhang, "A critical review of comparative global historical energy consumption and future demand: The story told so far," *Energy Reports,* vol. 6, pp. 1973-1991, 2020.

[20] L. Richardson, "Solar electricity vs. fossil fuels: how do they compare," ed: Retrieved from Energsage: https://news. energysage. com/solar-energy-vs …, 2017.

[21] U. Vargas, G. C. Lazaroiu, E. Tironi, and A. Ramirez, "Harmonic modeling and simulation of a stand-alone photovoltaic-battery-supercapacitor hybrid system," *International Journal of Electrical Power & Energy Systems,* vol. 105, pp. 70-78, 2019.

[22] D. Murillo-Yarce *et al.*, "A review of control techniques in photovoltaic systems," *Sustainability,* vol. 12, no. 24, p. 10598, 2020.

[23] A. Sinha and S. B. Singh, "Modelling and Simulation of Grid Connected PV System for Harmonic Reduction by Using Digital Filter," in *2020 First IEEE International Conference on Measurement, Instrumentation, Control and Automation (ICMICA)*, 2020: IEEE, pp. 1-5.

[24] N. H. Baharudin, T. Mansur, F. A. Hamid, R. Ali, and M. I. Misrun, "Topologies of DC-DC converter in solar PV applications," *Indonesian Journal of Electrical Engineering and Computer Science,* vol. 8, no. 2, pp. 368-374, 2017.

[25] S. Sumathi, L. A. Kumar, and P. Surekha, *Solar PV and wind energy conversion systems: an introduction to theory, modeling with MATLAB/SIMULINK, and the role of soft computing techniques*. Springer, 2015.

[26] J. Das, *Power system harmonics and passive filter designs*. John Wiley & Sons, 2015.

[27] S. Adak, "Harmonics Mitigation of Stand-Alone Photovoltaic System Using LC Passive Filter," *Journal of Electrical Engineering & Technology,* vol. 16, no. 5, pp. 2389-2396, 2021.

[28] M. A. Vitorino and M. B. de Rossiter Corrêa, "Compensation of DC link oscillation in single-phase VSI and CSI converters for photovoltaic grid connection," in *2011 IEEE energy conversion congress and exposition*, 2011: IEEE, pp. 2007-2014.

[29] S. A. Singh, G. Carli, N. A. Azeez, and S. S. Williamson, "Modeling, design, control, and implementation of a modified Z-source integrated PV/grid/EV DC charger/inverter," *IEEE Transactions on Industrial Electronics,* vol. 65, no. 6, pp. 5213-5220, 2017.

[30] M. A. Razak, N. Islam, M. A. U. Zaman, M. J. J. Fahim, and R. S. Dhar, "Design and Simulation of PV Based Harmonic Compensator for Three Phase load," in *2019 International Conference on Computer, Communication, Chemical, Materials and Electronic Engineering (IC4ME2)*, 2019: IEEE, pp. 1-6.

[31] K. Ding, X. Bian, H. Liu, and T. Peng, "A MATLAB-simulink-based PV module model and its application under conditions of nonuniform irradiance," *IEEE Transactions on energy conversion,* vol. 27, no. 4, pp. 864-872, 2012.

[32] A. Suleyman and H. Cangi, "ELIMINATION OF HARMONIC COMPONENTS IN SOLAR SYSTEM WITH L AND LC PASSIVE FILTERS," *International Journal of Energy and Smart Grid,* vol. 6, no. 1-2, pp. 14-27.

[33] S. Khomfoi and L. M. Tolbert, "Power electronics handbook," *University of Tennessee,* p. 2, 2007.

[34] A. R. Jordehi, "Maximum power point tracking in photovoltaic (PV) systems: A review of different approaches," *Renewable and Sustainable Energy Reviews,* vol. 65, pp. 1127-1138, 2016.

[35] F. Liu, Y. Kang, Y. Zhang, and S. Duan, "Comparison of P&O and hill climbing MPPT methods for grid-connected PV converter," in *2008 3rd IEEE Conference on Industrial Electronics and Applications*, 2008: IEEE, pp. 804-807.

[36] Y. H. Lim and D. Hamill, "Simple maximum power point tracker for photovoltaic arrays," *Electronics letters,* vol. 36, no. 11, p. 1, 2000.

[37] S. A. Rizzo and G. Scelba, "ANN based MPPT method for rapidly variable shading conditions," *Applied Energy,* vol. 145, pp. 124-132, 2015.

[38] G. Chen and S. Zheng, "Study on Wind Speed Frequency Distribution and Wind Energy Density Distribution in Complex Mountainous Areas," *Sol. Energy,* vol. 7, pp. 53-57, 2016.

[39] I. T. Papaioannou, A. S. Bouhouras, A. G. Marinopoulos, M. C. Alexiadis, C. S. Demoulias, and D. P. Labridis, "Harmonic impact of small photovoltaic systems connected to the LV distribution network," in *2008 5th International Conference on the European Electricity Market*, 2008: IEEE, pp. 1-6.

[40] M. K. M. Zambri, M. S. M. Aras, and A. Khamis, "Investigating the impact of photovoltaic connection to the malaysian distribution system," *Journal of Telecommunication, Electronic and Computer Engineering (JTEC),* vol. 8, no. 7, pp. 23-28, 2016.

[41] M. Ali, S. Kamarudin, M. Masdar, and A. Mohamed, "An overview of power electronics applications in fuel cell systems: DC and AC converters," *The Scientific World Journal,* vol. 2014, 2014.

[42] O. Deveci and C. Kasnakoğlu, "Performance improvement of a photovoltaic system using a controller redesign based on numerical modeling," *International Journal of Hydrogen Energy,* vol. 41, no. 29, pp. 12634-12649, 2016.

[43] L. Alhafadhi, J. Teh, C.-M. Lai, and M. Salem, "Predictive adaptive filter for reducing total harmonics distortion in PV systems," *Energies,* vol. 13, no. 12, p. 3286, 2020.

[44] D. Galzina, "Voltage quality improvement using solar photovoltaic system," *Journal of Sustainable Development of Energy, Water and Environment Systems,* vol. 3, no. 2, pp. 140-150, 2015.

[45] N. A. Yusof, N. M. Sapari, H. Mokhlis, and J. Selvaraj, "A comparative study of 5-level and 7-level multilevel inverter connected to the grid," in *2012 IEEE International Conference on Power and Energy (PECon)*, 2012: IEEE, pp. 542-547.

[46] L. Alhafadhi and J. Teh, "Advances in reduction of total harmonic distortion in solar photovoltaic systems: A literature review," *International Journal of Energy Research,* vol. 44, no. 4, pp. 2455-2470, 2020.

[47] B. Ge *et al.*, "An energy-stored quasi-Z-source inverter for application to photovoltaic power system," *IEEE transactions on industrial electronics,* vol. 60, no. 10, pp. 4468-4481, 2012.

[48] M. Shen, J. Wang, A. Joseph, F. Z. Peng, L. M. Tolbert, and D. J. Adams, "Constant boost control of the Z-source inverter to minimize current ripple and voltage stress," *IEEE transactions on industry applications,* vol. 42, no. 3, pp. 770-778, 2006.

[49] C. V. Deshpande and S. A. Deokar, "Enhancement of power quality using dynamic voltage restorer based on EZ source inverter," *International Journal of Advance Research in Electrical, Electronics & Instrumentation Engineering,* vol. 4, no. 2, 2015.

[50] A.-V. Ho, T.-W. Chun, H.-H. Lee, H.-G. Kim, and E.-C. Nho, "Active switched-capacitor and switched-inductor Z-source inverters," in *2014 IEEE International Conference on Industrial Technology (ICIT)*, 2014: IEEE, pp. 330-335.

[51] A. Ravindranath, S. K. Mishra, and A. Joshi, "Analysis and PWM control of switched boost inverter," *IEEE Transactions on industrial electronics,* vol. 60, no. 12, pp. 5593-5602, 2012.

[52] S. M. Dehghan, M. Mohamadian, A. Yazdian, and F. Ashrafzadeh, "A dual-input–dual-output Z-source inverter," *IEEE Transactions on power electronics,* vol. 25, no. 2, pp. 360-368, 2009.

[53] D. Jovcic, "Offshore wind farm with a series multiterminal CSI HVDC," *Electric Power Systems Research,* vol. 78, no. 4, pp. 747-755, 2008.

[54] M. A. Memon, S. Mekhilef, M. Mubin, and M. Aamir, "Selective harmonic elimination in inverters using bio-inspired intelligent algorithms for renewable energy conversion applications: A review," *Renewable and Sustainable Energy Reviews,* vol. 82, pp. 2235-2253, 2018.

[55] M. Ahmad and S. Kirmani, "Performance Analysis of a Solar PV based Grid Tied Multilevel Inverter Scheme for Linear and Non Linear Load," *International Journal of Recent Technology and Engineering,* vol. 8, no. 3, pp. 400-405, 2019.

[56] N. Saeed, A. Ibrar, and A. Saeed, "A review on industrial applications of Z-source inverter," *Journal of Power and Energy Engineering,* vol. 5, no. 9, pp. 14-31, 2017.

[57] R. Senthilkumar, R. Bharanikumar, and J. Jerom, "Z-source inverter for UPS application," in *2007 International Conference on Intelligent and Advanced Systems*, 2007: IEEE, pp. 835-839.

[58] L. Suresh, G. N. Kumar, M. Sudarsan, and K. Rajesh, "Simulation of Z-source inverter using maximum boost control PWM technique," *International Journal of Simulation Systems,* vol. 7, no. 2, pp. 49-59, 2013.

[59] M. S. P. Ngongoma, "Impact of different pulse width modulation (PWM) techniques on the performance of a three phase Z-Source inverter (ZSI)," 2019.

[60] M. Zhu, K. Yu, and F. L. Luo, "Switched inductor Z-source inverter," *IEEE Transactions on Power Electronics,* vol. 25, no. 8, pp. 2150-2158, 2010.
[61] F. Z. Peng, X. Yuan, X. Fang, and Z. Qian, "Z-source inverter for adjustable speed drives," *IEEE power electronics letters,* vol. 1, no. 2, pp. 33-35, 2003.
[62] S. Thangaprakash and A. Krishnan, "Comparative evaluation of modified pulse width modulation schemes of Z-source inverter for various applications and demands," *International Journal of Engineering, Science and Technology,* vol. 2, no. 1, pp. 103-115, 2010.
[63] Y. Yu, Q. Zhang, B. Liang, and S. Cui, "Single-phase Z-source inverter: Analysis and low-frequency harmonics elimination pulse width modulation," in *2011 IEEE Energy Conversion Congress and Exposition*, 2011: IEEE, pp. 2260-2267.
[64] C. M. Wang, C. H. Lin, S. Y. Hsu, C. M. Lu, and J. C. Li, "Analysis, design and performance of a zero-current-switching pulse-width-modulation interleaved boost dc/dc converter," *IET Power Electronics,* vol. 7, no. 9, pp. 2437-2445, 2014.
[65] N. Sabeur, S. Mekhilef, and A. Masaoud, "Extended maximum boost control scheme based on single-phase modulator for three-phase Z-source inverter," *IET Power Electronics,* vol. 9, no. 4, pp. 669-679, 2016.
[66] H. A. Mosalam, R. A. Amer, and G. Morsy, "Fuzzy logic control for a grid-connected PV array through Z-source-inverter using maximum constant boost control method," *Ain Shams Engineering Journal,* vol. 9, no. 4, pp. 2931-2941, 2018.
[67] M. M. Elkholy, M. El-Hameed, and A. El-Fergany, "Harmonic analysis of hybrid renewable microgrids comprising optimal design of passive filters and uncertainties," *Electric Power Systems Research,* vol. 163, pp. 491-501, 2018.
[68] Y.-S. Cho and H. Cha, "Single-tuned passive harmonic filter design considering variances of tuning and quality factor," *Journal of International Council on Electrical Engineering,* vol. 1, no. 1, pp. 7-13, 2011.
[69] H. Eroğlu, E. Cuce, P. M. Cuce, F. Gul, and A. Iskenderoğlu, "Harmonic problems in renewable and sustainable energy systems: A comprehensive review," *Sustainable Energy Technologies and Assessments,* vol. 48, p. 101566, 2021.
[70] S. Sagiroglu, R. Terzi, Y. Canbay, and I. Colak, "Big data issues in smart grid systems," in *2016 IEEE international conference on renewable energy research and applications (ICRERA)*, 2016: IEEE, pp. 1007-1012.
[71] S. Malla and C. Bhende, "Voltage control of stand-alone wind and solar energy system," *International Journal of Electrical Power & Energy Systems,* vol. 56, pp. 361-373, 2014.
[72] S. A. A. Shufat, K. Erol, K. M. El Hadad, and A. HANCERLİOGULLARİ, "A numerical model for a Stirling engine," *Journal of Energy Systems,* vol. 2, no. 1, pp. 1-12, 2018.
[73] F. Zhou, A. Luo, Y. Li, Q. Xu, Z. He, and J. M. Guerrero, "Double-carrier phase-disposition pulse width modulation method for modular multilevel converters," *Energies,* vol. 10, no. 4, p. 581, 2017.
[74] O. F. Kececioglu, H. Acikgoz, C. Yildiz, A. Gani, and M. Sekkeli, "Power quality improvement using hybrid passive filter configuration for wind energy systems," *Journal of Electrical Engineering and Technology,* vol. 12, no. 1, pp. 207-216, 2017.
[75] D. Wu, Z. Xiang, X. Zhu, L. Quan, M. Jiang, and Y. Liu, "Optimization Design of Power Factor for an In-Wheel Vernier PM Machine From the Perspective of Air-Gap Harmonic

Modulation," *IEEE Transactions on Industrial Electronics,* vol. 68, no. 10, pp. 9265-9276, 2020.

[76] A. G. Peter and K. A. Saha, "Comparative study of harmonics reduction and power factor enhancement of six and 12-pulses HVDC system using passive and shunt APFs harmonic filters," in *2018 International Conference on the Domestic Use of Energy (DUE)*, 2018: IEEE, pp. 1-10.

[77] X. Bao, F. Zhuo, Y. Tian, and P. Tan, "Simplified feedback linearization control of three-phase photovoltaic inverter with an LCL filter," *IEEE Transactions on Power Electronics,* vol. 28, no. 6, pp. 2739-2752, 2012.

[78] D.-J. Jwo, M.-Y. Chen, C.-H. Tseng, and T.-S. Cho, "Adaptive and nonlinear kalman filtering for GPS navigation processing," *Kalman Filter: Recent Advances and Applications,* vol. 19, 2009.

[79] L. Alhafadhi and J. Teh, "Kalman filter for reducing total harmonics distortion in stand-alone PV system," in *2020 Global Congress on Electrical Engineering (GC-ElecEng)*, 2020: IEEE, pp. 81-87.

[80] S. Swain and B. Subudhi, "A new grid synchronization scheme for a three phase PV system employing Kalman filtering," in *2017 IEEE Region 10 Symposium (TENSYMP)*, 2017: IEEE, pp. 1-5.

[81] S. Gannot, "Speech processing utilizing the Kalman filter," *IEEE Instrumentation & Measurement Magazine,* vol. 15, no. 3, pp. 10-14, 2012.

[82] L. Alhafadhi, J. Asumadu, and A. Alsafi, "Total harmonics distortion reduction using adaptive, Weiner, and Kalman filters," in *2017 IEEE 7th Annual Computing and Communication Workshop and Conference (CCWC)*, 2017: IEEE, pp. 1-8.

[83] L. Alhafadhi, "Total Harmonics Distortion Reduction Using Adaptive, Weiner, and Kalman Filters," 2016.

[84] R. G. Wandhare and V. Agarwa, "A novel technique for THD control in grid connected photovoltaic systems using step variable inductor approach," in *2010 35th IEEE Photovoltaic Specialists Conference*, 2010: IEEE, pp. 002844-002848.

[85] M. Tali, A. Obbadi, A. Elfajri, and Y. Errami, "Passive filter for harmonics mitigation in standalone PV system for non linear load," in *2014 International Renewable and Sustainable Energy Conference (IRSEC)*, 2014: IEEE, pp. 499-504.

[86] M. W. Hussain and M. A. Qureshi, "Analysis and Design of Passive Filters for Power Quality Improvement in 3ϕ Grid-Tied PV Systems," in *2021 4th International Conference on Energy Conservation and Efficiency (ICECE)*, 2021: IEEE, pp. 1-6.

[87] M. Jayaraman, V. Sreedevi, and R. Balakrishnan, "Analysis and design of passive filters for power quality improvement in standalone PV systems," in *2013 Nirma University International Conference on Engineering (NUiCONE)*, 2013: IEEE, pp. 1-6.

[88] K. Kumari and A. K. Jain, "Cascaded control for LCL filter based grid-tied system with reduced sensors," *IET Power Electronics,* 2022.

[89] M. Awal, L. Della Flora, and I. Husain, "Observer based generalized active damping for voltage source converters with LCL filters," *IEEE Transactions on Power Electronics,* vol. 37, no. 1, pp. 125-136, 2021.

[90] K. Sharma and V. K. Sharma, "Single Phase Modeling and Harmonics Compensation of Standalone PV+ SOFC System with SAPF," in *2020 International Conference on Electronics and Sustainable Communication Systems (ICESC)*, 2020: IEEE, pp. 979-983.
[91] N. Sood, "Effects of Harmonics on Power Quality Due to Photovoltaic System," California State University, Northridge, 2018.
[92] A. Süleyman and H. CANGİ, "HARMONIC ANALYSIS OF STAND ALONE PHOTOVOLTAIC SYSTEM AT LOW IRRADIANCE CONDITIONS," *The International Journal of Energy and Engineering Sciences,* vol. 5, no. 1, pp. 1-11, 2020.
[93] S. Adak and H. Cangi, "Analysis and Simulation Total Harmonic Distortion of Output Voltage Three Level Diode Clamped Inverter in Photovoltaic System, Bitlis Eren University," *Fen Bilimleri Dergisi, ISSN,* vol. 2147, p. 3129, 2015.
[94] M. T. Bina and E. Pashajavid, "An efficient procedure to design passive LCL-filters for active power filters," *Electric Power Systems Research,* vol. 79, no. 4, pp. 606-614, 2009.
[95] G. Brando, L. Di Noia, R. Rizzo, D. Lauria, and C. Pisani, "An advanced system for power supply and power quality improvement of isolated AC passive network," in *2015 International Conference on Renewable Energy Research and Applications (ICRERA)*, 2015: IEEE, pp. 1446-1450.
[96] S. Adak, "Mitigation harmonic with LCL passive filter in off-grid PV system," 2018.
[97] M. Liserre, F. Blaabjerg, and S. Hansen, "Design and control of an LCL-filter-based three-phase active rectifier," *IEEE Transactions on industry applications,* vol. 41, no. 5, pp. 1281-1291, 2005.
[98] A. Süleyman, "Mitigation Harmonic with LCL Passive Fitler in off-Grid PV System," *Journal of Engineering and Technology,* vol. 2, no. 1, pp. 9-20, 2018.
[99] W. Wu, Y. He, T. Tang, and F. Blaabjerg, "A new design method for the passive damped LCL and LLCL filter-based single-phase grid-tied inverter," *IEEE transactions on industrial electronics,* vol. 60, no. 10, pp. 4339-4350, 2012.
[100] M. Huang, X. Wang, P. C. Loh, F. Blaabjerg, and W. Wu, "Stability analysis and active damping for llcl-filter-based grid-connected inverters," *IEEJ Journal of Industry Applications,* vol. 4, no. 3, pp. 187-195, 2015.
[101] A. Suleyman, H. Cangi, and A. S. Yilmaz, "Design of an LLCL type filter for stand-alone PV systems' harmonics," *Journal of Energy Systems,* vol. 3, no. 1, pp. 36-50, 2019.
[102] A. H. Patel, "Power quality of stand-alone "Photovoltaic (PV) and Wind" energy based system."
[103] K. Prabha, T. Malathi, and M. Muruganandam, "Power Quality Features Improvement In Single-Phase Grid-Connected Inverter With Non-Linear Loads."
[104] P. K. Gayen, "A novel control approach for two-stage power converters in stand-alone solar photovoltaic system," *International Journal of Electronics,* vol. 109, no. 2, pp. 221-245, 2022.
[105] Y. W. Kean, P. S. Yong, A. Ramasamy, and V. K. Ramachandaramurthy, "Comparison of the effect of filter designs on the total harmonic distortion in three-phase stand-alone photovoltaic systems," *ARPN Journal of Engineering and Applied Sciences,* vol. 10, no. 21, pp. 9919-9925, 2015.

[106] K. K. Srivastava, S. Shakil, and A. V. Pandey, "Harmonics & its mitigation technique by passive shunt filter," *International Journal of Soft Computing and Engineering (IJSCE) ISSN,* pp. 2231-2307, 2013.
[107] N. B. Lai and K.-H. Kim, "An improved current control strategy for a grid-connected inverter under distorted grid conditions," *Energies,* vol. 9, no. 3, p. 190, 2016.
[108] I. J. Gabe, V. F. Montagner, and H. Pinheiro, "Design and implementation of a robust current controller for VSI connected to the grid through an LCL filter," *IEEE Transactions on Power Electronics,* vol. 24, no. 6, pp. 1444-1452, 2009.
[109] Y. Yu, H. Li, Z. Li, and Z. Zhao, "Modeling and analysis of resonance in LCL-type grid-connected inverters under different control schemes," *Energies,* vol. 10, no. 1, p. 104, 2017.
[110] N. Zhang, H. Tang, and C. Yao, "Analysis of active damping of LCL filter used in single-phase PV system in discrete domain," *International Journal of Electronics,* vol. 102, no. 6, pp. 1022-1043, 2015.
[111] N. Zhang, H. Tang, and C. Yao, "A systematic method for designing a PR controller and active damping of the LCL filter for single-phase grid-connected PV inverters," *Energies,* vol. 7, no. 6, pp. 3934-3954, 2014.
[112] A. Anzalchi, M. Moghaddami, A. Moghaddasi, A. I. Sarwat, and A. K. Rathore, "A new topology of higher order power filter for single-phase grid-tied voltage-source inverters," *IEEE transactions on industrial electronics,* vol. 63, no. 12, pp. 7511-7522, 2016.
[113] Z. Li, A. Jiang, P. Shen, Y. Han, and J. M. Guerrero, "Resonance damping and parameter design method for LCL-LC filter interfaced grid-connected photovoltaic inverters," in *2016 IEEE 8th International Power Electronics and Motion Control Conference (IPEMC-ECCE Asia)*, 2016: IEEE, pp. 1581-1586.
[114] Y. Liu, W. Wu, Y. He, Z. Lin, F. Blaabjerg, and H. S.-H. Chung, "An efficient and robust hybrid damper for $ LCL $-or $ LLCL $-based grid-tied inverter with strong grid-side harmonic voltage effect rejection," *IEEE Transactions on Industrial Electronics,* vol. 63, no. 2, pp. 926-936, 2015.
[115] H. Bai, X. Wang, P. C. Loh, and F. Blaabjerg, "Harmonic analysis and mitigation of low-frequency switching voltage source inverter with series LC filtered VSI," in *2017 IEEE Applied Power Electronics Conference and Exposition (APEC)*, 2017: IEEE, pp. 3299-3306.
[116] F. Li, X. Zhang, H. Zhu, H. Li, and C. Yu, "An LCL-LC filter for grid-connected converter: topology, parameter, and analysis," *IEEE Transactions on Power Electronics,* vol. 30, no. 9, pp. 5067-5077, 2014.
[117] C. Sahana, "Study on Mitigation of Harmonics by Using Passive Filter and Active Filter," in *International Conference On Advances in Computer & Communication Engineering (ACCE-2015)*, 2015, vol. 3.
[118] S. Jiang, Y. Liu, W. Liang, J. Peng, and H. Jiang, "Active EMI filter design with a modified LCL-LC filter for single-phase grid-connected inverter in vehicle-to-grid application," *IEEE Transactions on Vehicular Technology,* vol. 68, no. 11, pp. 10639-10650, 2019.

[119] J. Fang, X. Li, X. Yang, and Y. Tang, "An integrated trap-LCL filter with reduced current harmonics for grid-connected converters under weak grid conditions," *IEEE Transactions on Power Electronics,* vol. 32, no. 11, pp. 8446-8457, 2017.

[120] S. Jiang and Y. Liu, "EMI noise reduction for the single-phase grid-connected inverter with a modified harmonic filter design," *IEEE Transactions on Electromagnetic Compatibility,* vol. 63, no. 3, pp. 739-751, 2020.

[121] S. Murugan, "Harmonics elimination in grid connected single phase PV inverter," *Int. J. Innovative Research in Science, Engineering and Technology,* vol. 3, pp. 1473-1480, 2014.

[122] I. Wallace, "Key Changes and Differences between the New IEEE 519-2014 Standard and IEEE 519-1992," *Alcatel Telecommunications Review,* vol. 11, no. 1, 2014.

[123] K. Arulkumar, K. Palanisamy, and D. Vijayakumar, "Recent advances and control techniques in grid connected PV system–A review," *International Journal of Renewable Energy Research,* vol. 6, no. 3, pp. 1037-1049, 2016.

[124] J. Ji, W. Wu, Y. He, Z. Lin, F. Blaabjerg, and H. S.-H. Chung, "A simple differential mode EMI Suppressor for the $ LLCL $-filter-based single-phase grid-tied transformerless inverter," *IEEE Transactions on Industrial Electronics,* vol. 62, no. 7, pp. 4141-4147, 2014.

[125] K. Arulkumar, P. Manojbharath, S. Meikandasivam, and D. Vijayakumar, "Robust control design of Grid power converters in improving Power Quality," in *2015 International Conference on Technological Advancements in Power and Energy (TAP Energy)*, 2015: IEEE, pp. 460-465.

[126] S. Parthasarathy and N. Anandkumar, "Effect of Fluctuating Solar Irradiance on the Quality of Power Generated by Solar Photovoltaic System," *International Journal of Advanced Engineering Research and Technology (IJAERT) Volume,* vol. 5, 2017.

[127] J. M. Malof, R. Hou, L. M. Collins, K. Bradbury, and R. Newell, "Automatic solar photovoltaic panel detection in satellite imagery," in *2015 International Conference on Renewable Energy Research and Applications (ICRERA)*, 2015: IEEE, pp. 1428-1431.

[128] O. Ellabban and H. Abu-Rub, "Z-source inverter: Topology improvements review," *IEEE Industrial Electronics Magazine,* vol. 10, no. 1, pp. 6-24, 2016.

[129] D. Cao, S. Jiang, X. Yu, and F. Z. Peng, "Low-cost semi-Z-source inverter for single-phase photovoltaic systems," *IEEE Transactions on Power electronics,* vol. 26, no. 12, pp. 3514-3523, 2011.

[130] S. Fathi, S. M. J. Mousavi, and E. Babaei, "A high-frequency isolated four-switch single-phase quasi-Z-source AC–AC converter with inherent commutation and step-changed frequency operation," *IEEE Transactions on Power Electronics,* vol. 38, no. 4, pp. 4937-4944, 2022.

[131] J. Dizdarević, F. Carpio, A. Jukan, and X. Masip-Bruin, "A survey of communication protocols for internet of things and related challenges of fog and cloud computing integration," *ACM Computing Surveys (CSUR),* vol. 51, no. 6, pp. 1-29, 2019.

Appendices

A1. Designed Stand-alone PV circuit without filters on MATLAB/SIMULK Model

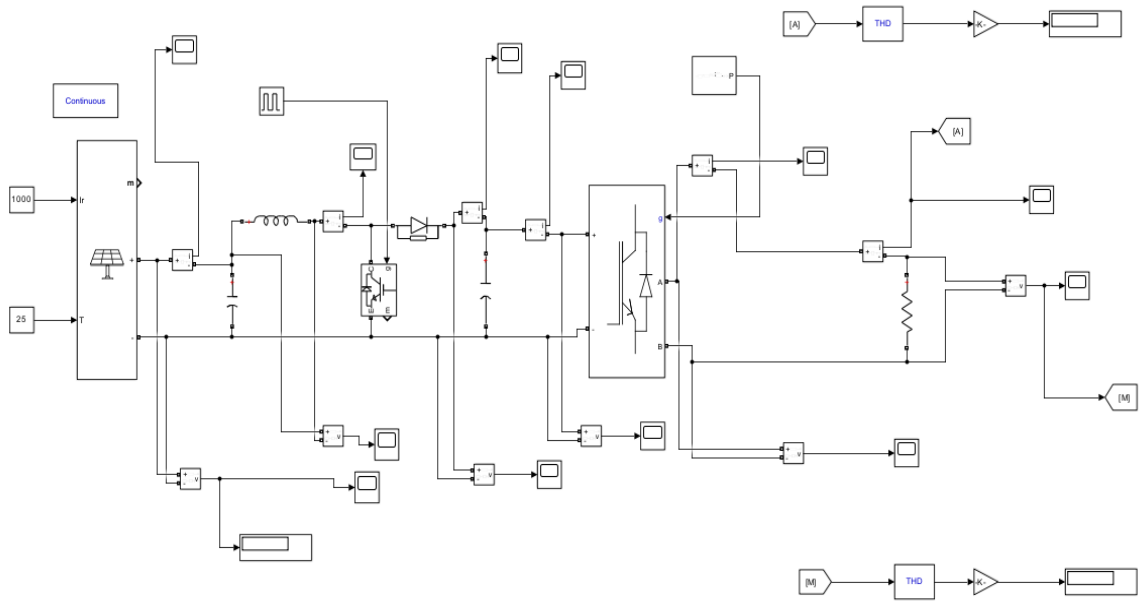

A2. Photovoltage Parameters on MATLAB/SIMULK Model

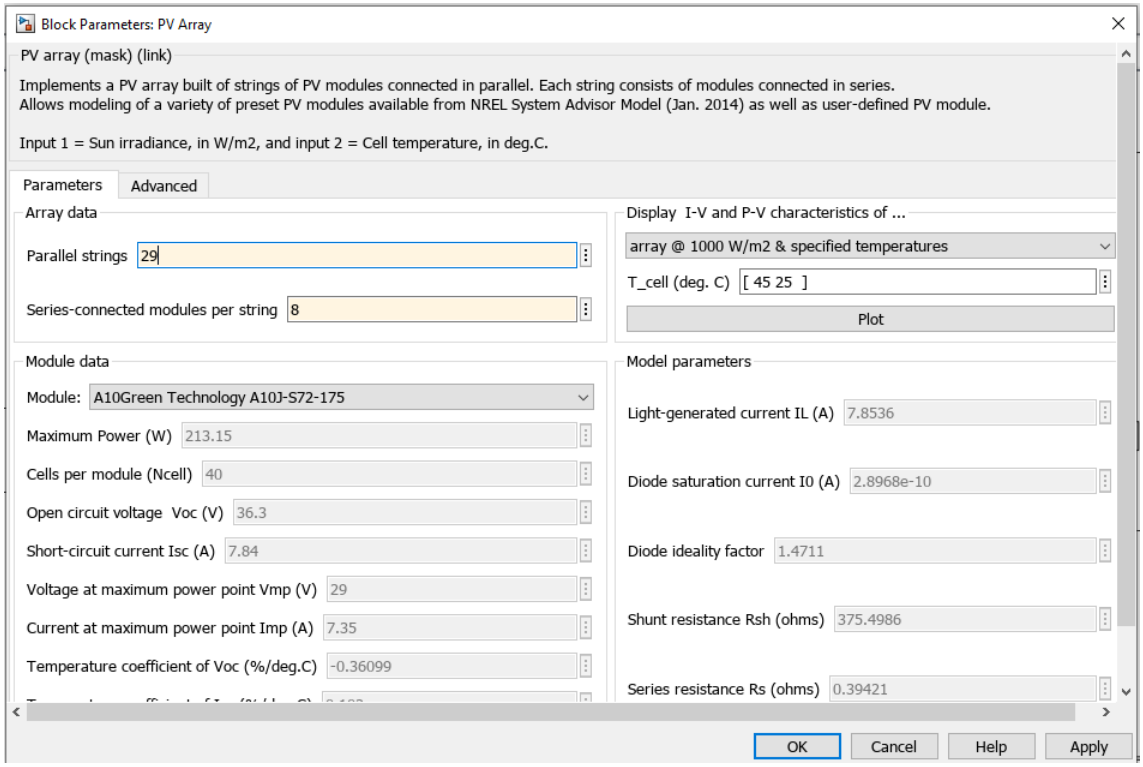

A3. Array type: A0J-S72-175, 1 Series modules and 1 Parallel Strings

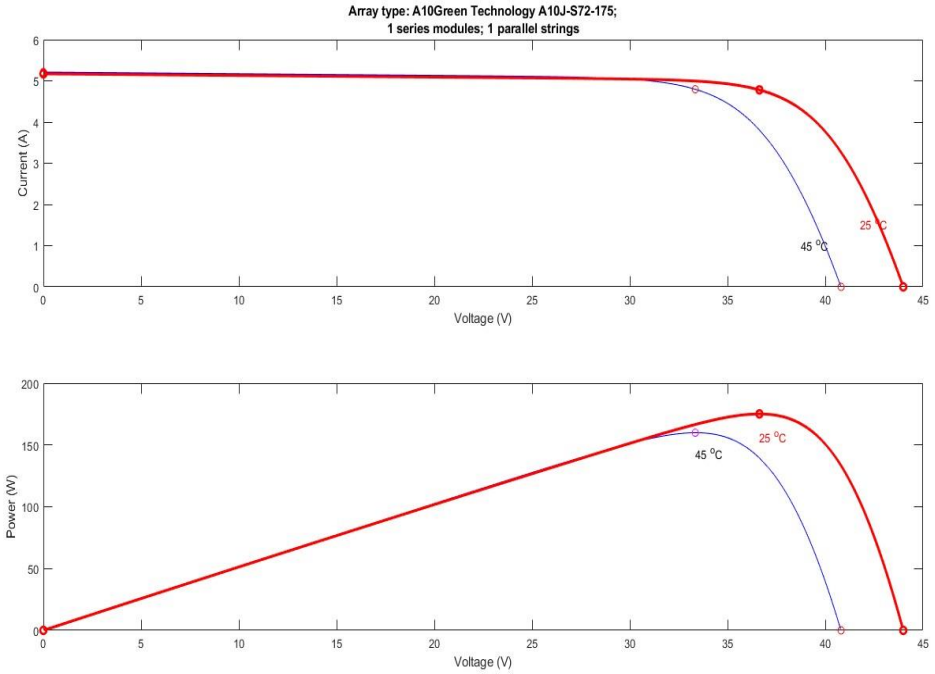

A4. Array type A0J-S72-175, 8 Series modules and 29 Parallel Strings

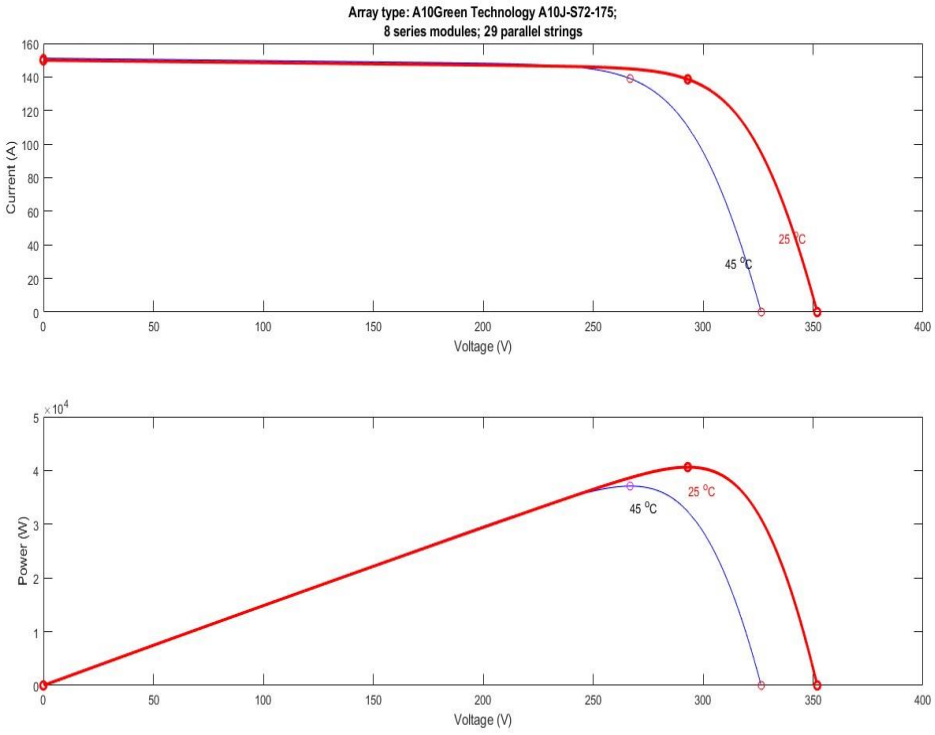

A5. The different Solar Penals to produce unlimited DC Voltage

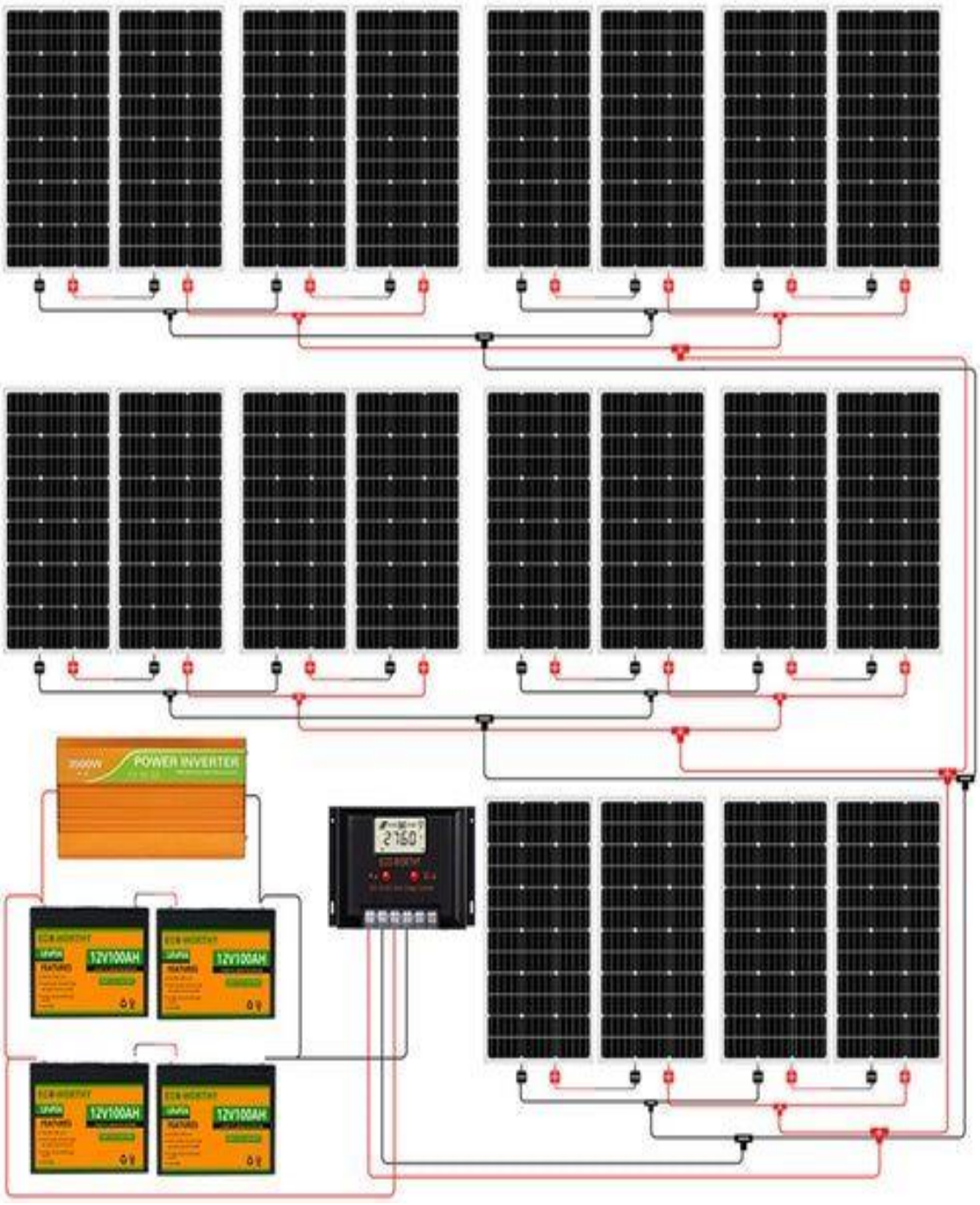

A6. Designed Single-phase off-grid PV network with LC Filter on MATLAB/SIMULK Model

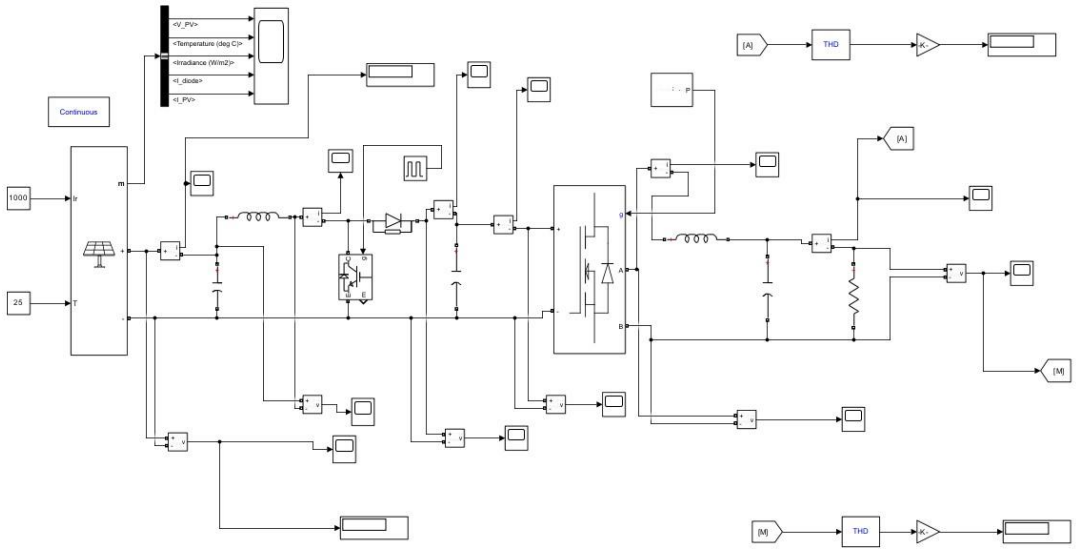

A7. Designed Single-phase off-grid PV network with LCL Filter on MATLAB/SIMULK Model

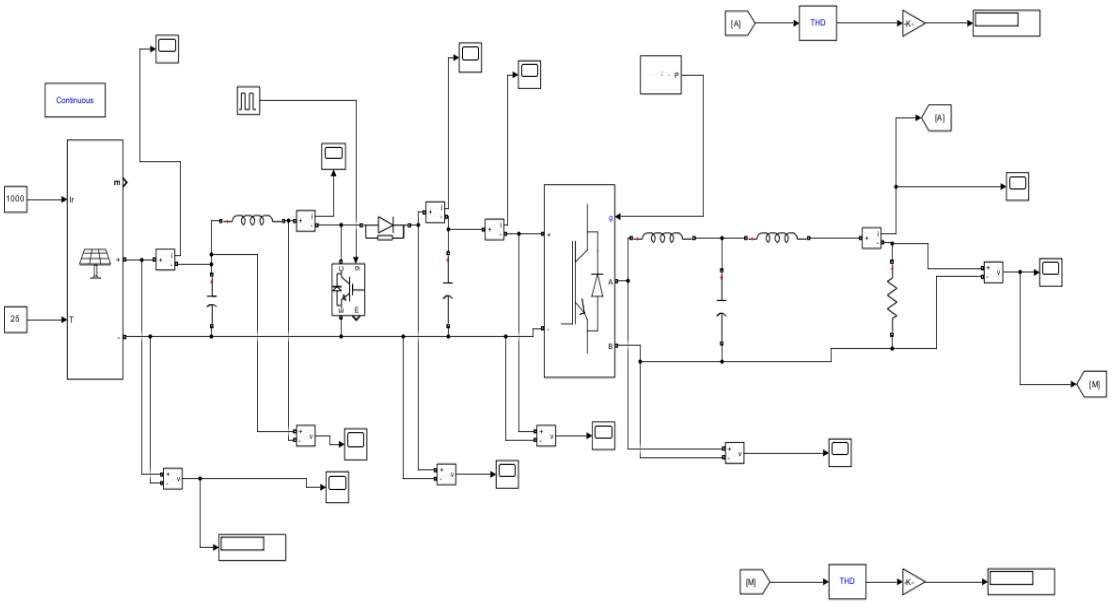

A8. Designed Single-phase off-grid PV network with LLCL Filter on MATLAB/SIMULK Model

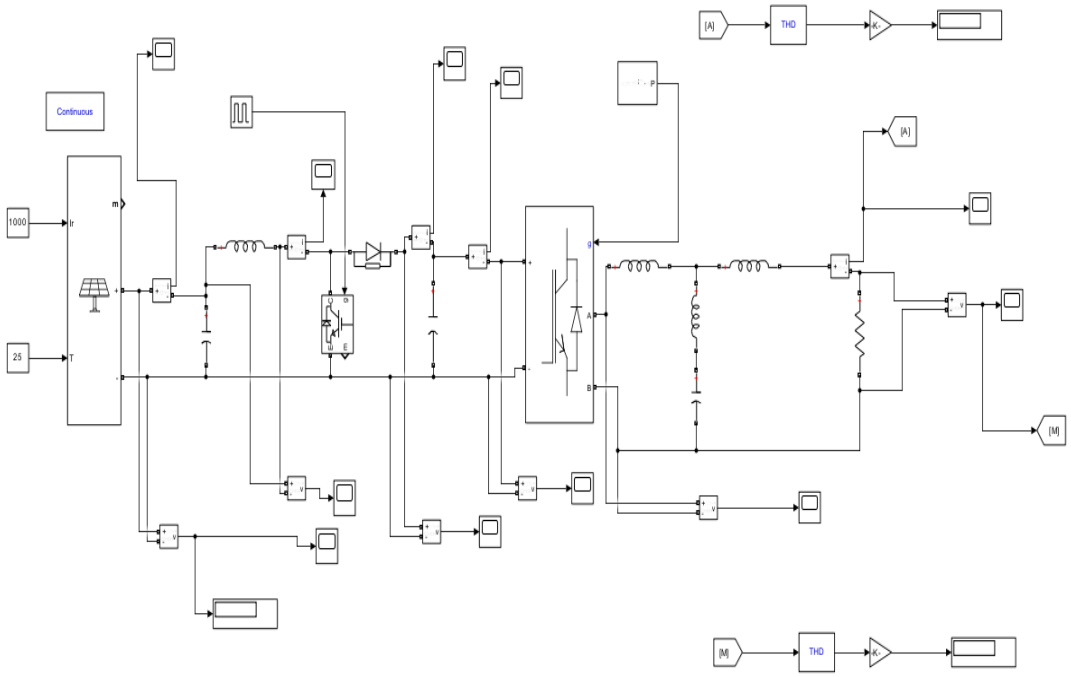

A9. Designed Z-Source Inverter network without filter and PWM Control Method on MATLAB/SIMULK Model

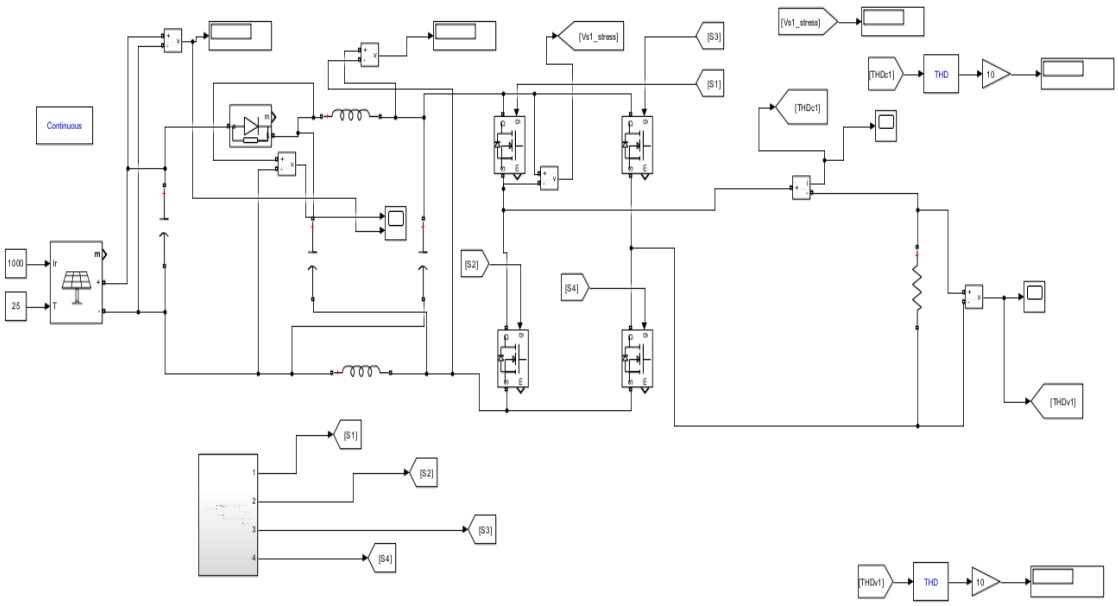

A10. Constant Boost control method on MATLAB

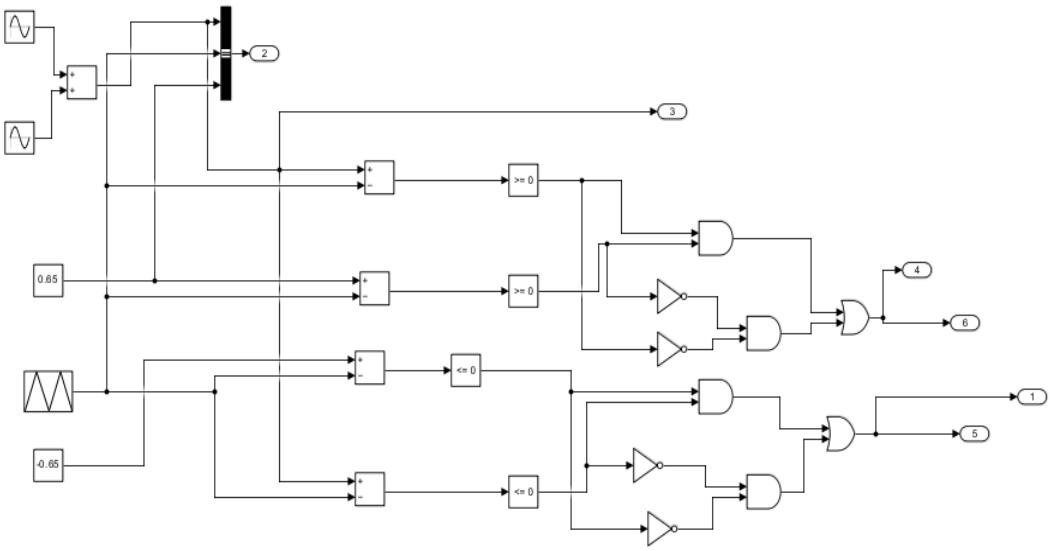

A11. Simple Boost Control Method on MATLAB

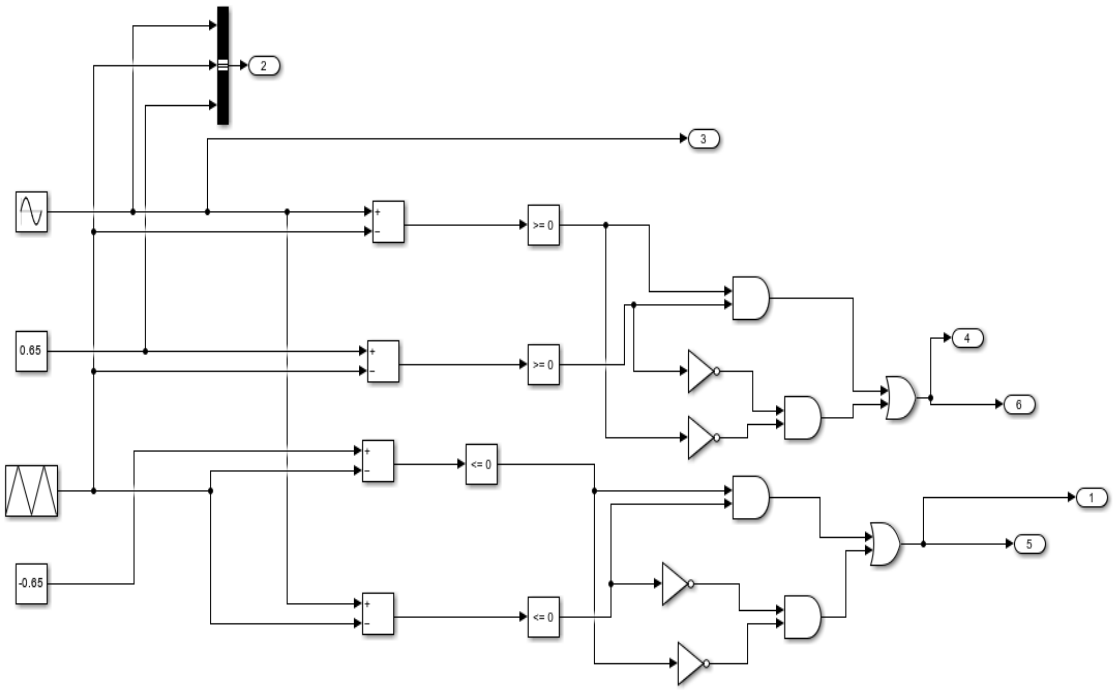

A12. Designed Z-Source Inverter Network with an LC filter to reduce total harmonics distortion on MATLAB.

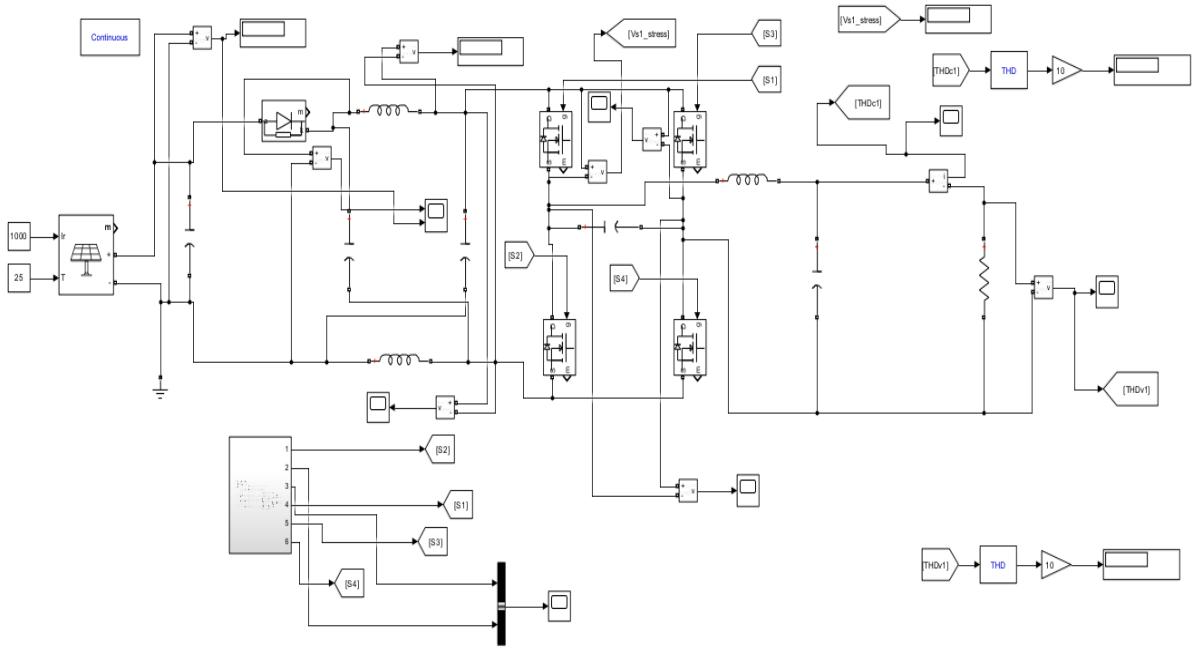

A13. Designed Z-Source Inverter Network with an LCL Filter to reduce THD on MATLAB

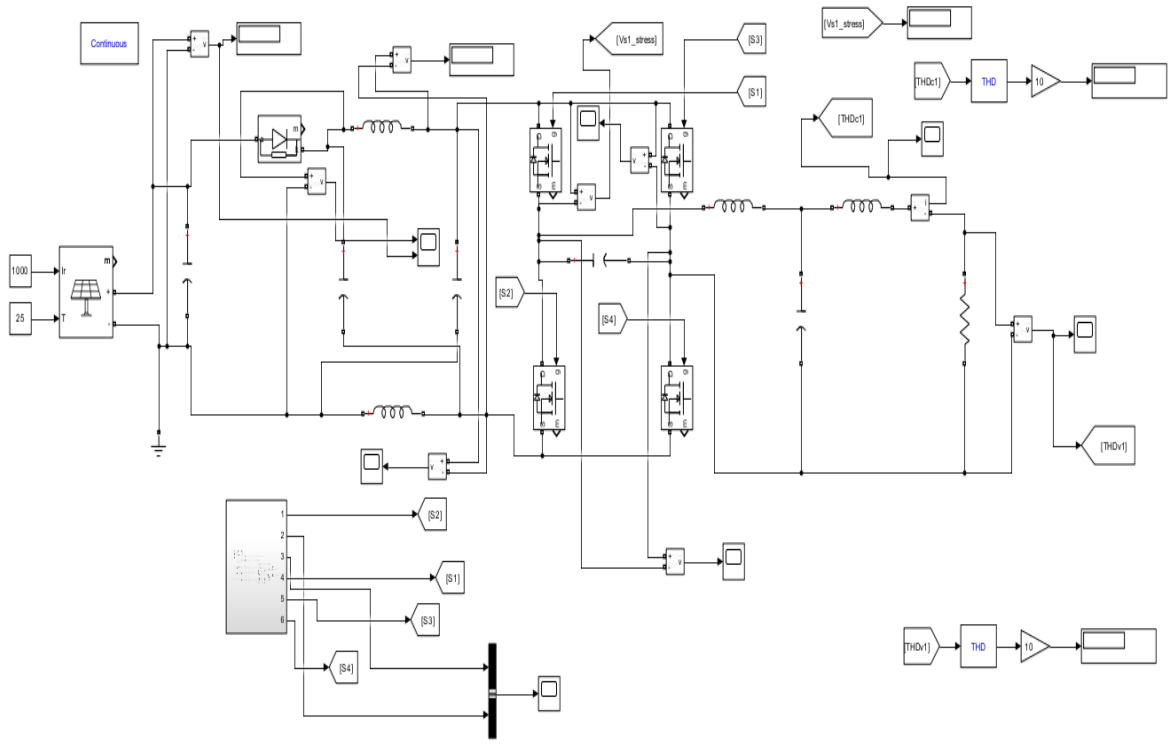

A14. Designed Z-Source Inverter with LLCL Filter to reduce THD on MATLAB